CYCLOTRON LABORATORY

Department of Physics

The University of Michigan

Annual Report

June 15, 1973 - June 15, 1974

U.S. Atomic Energy Commission

Contract No. AT(11-1)-2167

DISCLAIMER

CONTENTS

INTRODUCTION

This report contains a summary of the research and technical development carried on in the Cyclotron Laboratory of the Department of Physics at The University of Michigan during the period June 15, 1973 to June 15, 1974.

The bulk of the experimental effort during the past year has been devoted to experiments utilizing the neutron time-of-flight system, to a continuation of the investigations of rare-earth nuclei using single-proton transfer reactions, and to studies of a number of light nuclei.

The major technical effort was devoted to the construction and initial operation of the total instrumentation necessary for the study of heavy-ion induced reactions. This instrumentation includes a new ion source designed to produce beams of heavy ions and a new focal plane detection system based upon a position-sensitive proportional counter.

As in years past, it is a pleasure for the research staff to acknowledge their indebtedness to Professor K. T. Hecht for his theoretical help and guidance.

A. EXPERIMENTAL PROGRAM

A1. $(d,^6Li)$ Reactions on Light and Heavy Nuclei

A. VanderMolen, F. D. Becchetti and J. Janecke

Alpha particle pickup reactions on nuclei ranging from carbon to lead have been studied using 35-MeV deuterons. Spectra and angular distributions have been obtained using a ΔE-E counter telescope system in the scattering chamber and a position-sensitive detector in the focal plane of the analyzer magnet. Figure A1-1 shows angular distributions obtained from the $^{12}C(d,^6Li)^8Be$ reaction for the transitions to the 0^+ ground state, the 2^+ state at 2.9 MeV, and the 4^+ state at 11.4 MeV in ^8Be. The solid lines represent preliminary DWBA fits using a simple cluster transfer mechanism. While the transition to the 0^+ state is well represented by the calculated curve, the lack of agreement for the 2^+ state may indicate the presence of a more complicated reaction mechanism.

Complete angular distributions have been obtained for the target nuclei ^{12}C, ^{16}O, ^{18}O, ^{20}Ne, and ^{22}Ne. Spectra and/or ground state cross sections have been measured for ^{40}Ca, $^{58,60}Ni$, $^{112,116,120,124}Sn$, ^{160}Dy, ^{166}Er and ^{208}Pb. The cross sections for the alpha-particle pickup reactions decrease with increasing atomic number A of the target in agreement with theoretical predictions. For the $^{208}Pb(d,^6Li)^{204}Hg$ reaction, the cross section is reduced by a factor of 5×10^{-4} compared to the corresponding cross sections in the $^{12}C(d,^6Li)^8Be$ reaction.

The 5-nucleon $(d,^7Li)$ transfer reactions on ^{12}C, $^{16,18}O$ and $^{20,22}Ne$

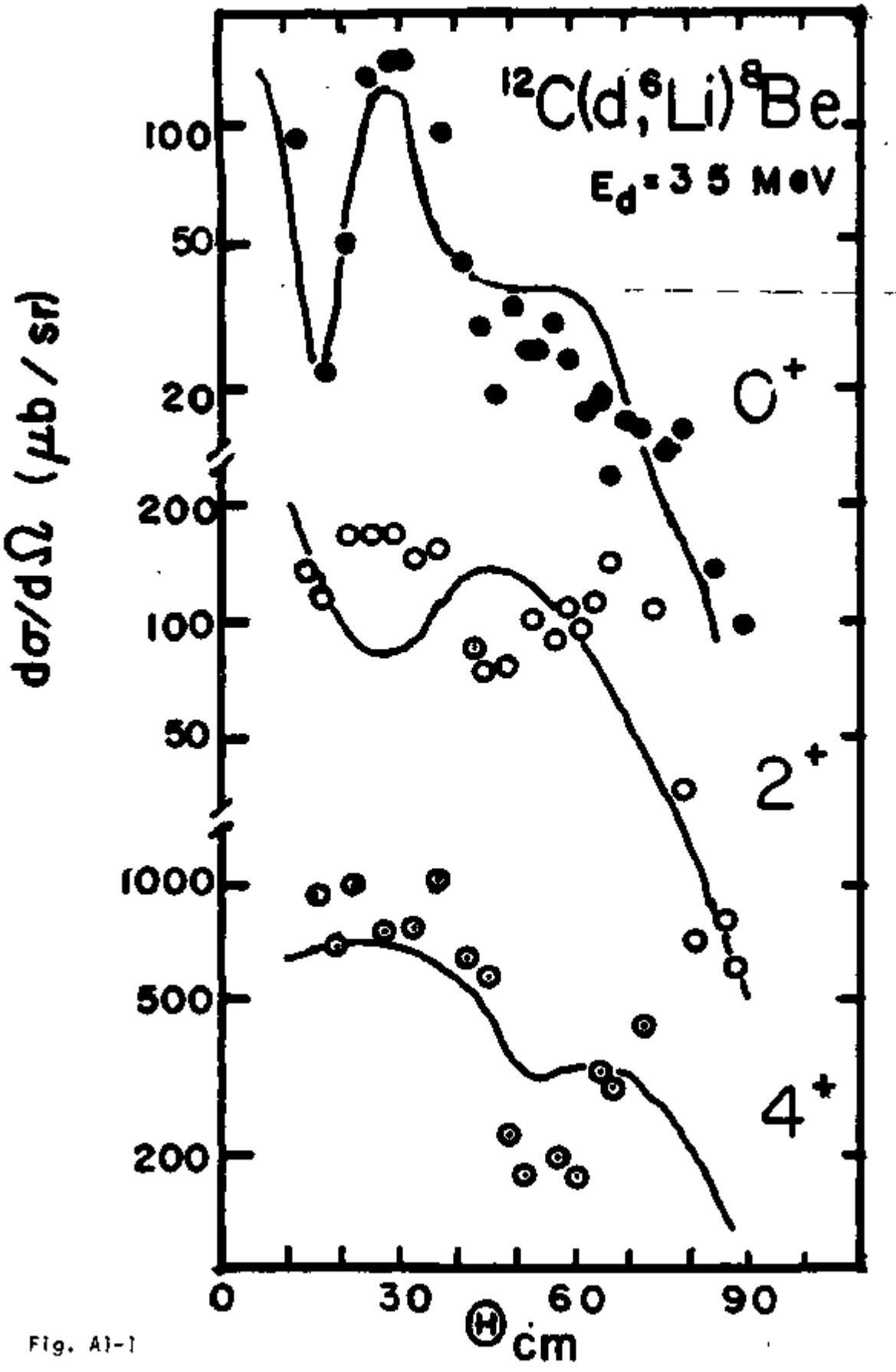
$^{12}C(d,^{6}Li)^{8}Be$
$E_d = 35$ MeV
0^+
2^+
4^+
$d\sigma/d\Omega$ (μb / sr)
100
50
20
200
100
50
1000
500
200
0
30
60
90
Θ_{cm}

Fig. A1-1

leading to the respective ground states or ground state doublets have cross sections comparable to those of (d,^{6}Li) reactions and the angular distributions are also characteristic for a direct reaction mechanism.

A2. The Isospin-violating Reaction $^{12}C(\alpha,d)^{14}N_{0^+,T=1}$

J. Janecke

Isospin-violating (d,α) and (α,d) reactions on light nuclei have been observed in the past by many authors. They are generally believed to be due to isospin mixing in the compound nucleus. However, experiments at higher bombarding energies such as the observation [1] of the 0^+,T=1 state in ^{10}B from the (d,α) reaction on ^{12}C at 29 MeV suggest the possibility of direct or semi-direct reaction mechanisms. A controversy [2,3] concerning this possibility is not yet resolved.

Attempts have been made to observe transitions to the 0^+,T=1 state in ^{14}N at 2.313 MeV using the (α,d) reaction on ^{12}C at 69 MeV. Compound nucleus contributions to the cross section should essentially be absent at this bombarding energy. All T=0 states in ^{14}N up to an excitation energy of 6 MeV have been observed with cross sections ranging from 0.3 to 1.3 mb/sr at θ_{cm} = 15°. Transitions to the 0^+,T=1 state could not be seen even though θ_{cm} = 15° is a favored angle for observing such a transition. [1] An upper limit of 0.4 μb/sr can be placed on the cross section. This result is similar to that of Zafiratos et al. [4] obtained at a bombarding energy of 42 MeV.

Further work is planned. Much longer exposure times and even more careful considerations for eliminating background are necessary.

References

1) J. Janecke, T. F. Yang, W. S. Gray, and R. M. Pollichar, Phys. Rev. C3, 79 (1971).

2) D. von Ehrenstein, L. Meyer-Schutzmeister, J. E. Monahan, A. Richter, and J. C. Stolzfus, Phys. Rev. Lett. 27, 107 (1971).

3) H. T. Richards and H. V. Smith, Phys. Rev. Lett. 27, 1735 (1971).

4) C. D. Zafiratos, J. S. Lilley, and F. W. Slee, Phys. Rev. 154, 887 (1967).

A3. Study of the $(\alpha, {}^{8}He)$ Reaction

F. Becchetti, L. Chua, J. Janecke, and A. VanderMolen

We have begun a study of the $(\alpha, {}^{8}He)$ reaction [1] on nuclei having $A < 70$. The purpose of this investigation is to make an accurate re-determination of the mass of ^{8}He and to establish the mechanism for this reaction. When this work is completed, it will be possible to use the $(\alpha, {}^{8}He)$ reaction to make precise mass measurements for many proton-rich nuclei.

Preliminary data have been obtained for the reaction $^{18}O(\alpha, {}^{8}He)^{14}O$ at $\theta_L = 8°$ and $E_\alpha = 58$ MeV. The target was nickel-oxide consisting of 140 $\mu g/cm^2$ of ^{18}O and 450 $\mu g/cm^2$ of Ni (see Section B6 for the details of the target preparation). Reaction products were detected in the focal plane of the first analyzing magnet using a double proportional counter backed by a solid-state position sensitive detector (PSD) used to measure the total energy. At this bombarding energy (58 MeV), the ^{8}He particles ($Q = -38$ MeV) must be identified in the midst of an intense inelastic α^{++} and $^{3}He^{++}$ background, e.g., typically $\sim 10^7$ alpha and ^{3}He events per ^{8}He event. Thus, in addition to the double proportional counter, pile-up rejection was also used

to minimize mis-identification. In spite of these efforts the background was not completely suppressed. As a means of further identification, the depletion depth of the PSD was varied ∿ 40 μm by changing the bias voltage. The background particles, which are sufficiently energetic to pass through the position sensitive detector, then shift in the "E" spectrum whereas stopped particles such as ^{8}He do not shift.

A composite position (i.e., Bρ) spectrum obtained from five runs (three different frequency settings for the spectrograph and two different PSD biases) is shown in Fig. A3-1. The gates on E1, E2 and E3 (see Section B3) have been set for calculated ^{8}He signals based on E1, E2 and E3 calibration curves determined emperically from α^{++}, α^{+}, $^{3}He^{++}$ and $^{6}He^{++}$ data. The position spectra from each run have been shifted by appropriate amounts depending on the spectrograph frequency and then added to form the composite spectrum shown.

The group seen near channel 360 would correspond to a Q = -37.97 MeV for the (α,^{8}He) reaction and a mass excess for ^{8}He of 31.60 ± 0.03 MeV. The cross section at 8° (lab) for this group is ≈ 40 nb/sr (lab). These preliminary results are to be compared with the mass excess (31.65 ± 0.12 MeV) and cross section (≈ 35 nb/sr (lab) at 14° and 80 MeV) for the ^{26}Mg(α,^{8}He) reaction reported in Ref. 1.

It is planned to extend these measurements to heavier nuclei, e.g., the nickel isotopes in order to verify the results obtained for ^{18}O and to improve the accuracy of the mass determination of ^{8}He.

References

1) J. Cerny, et al., Phys. Rev. Lett. 16, 469 (1966).

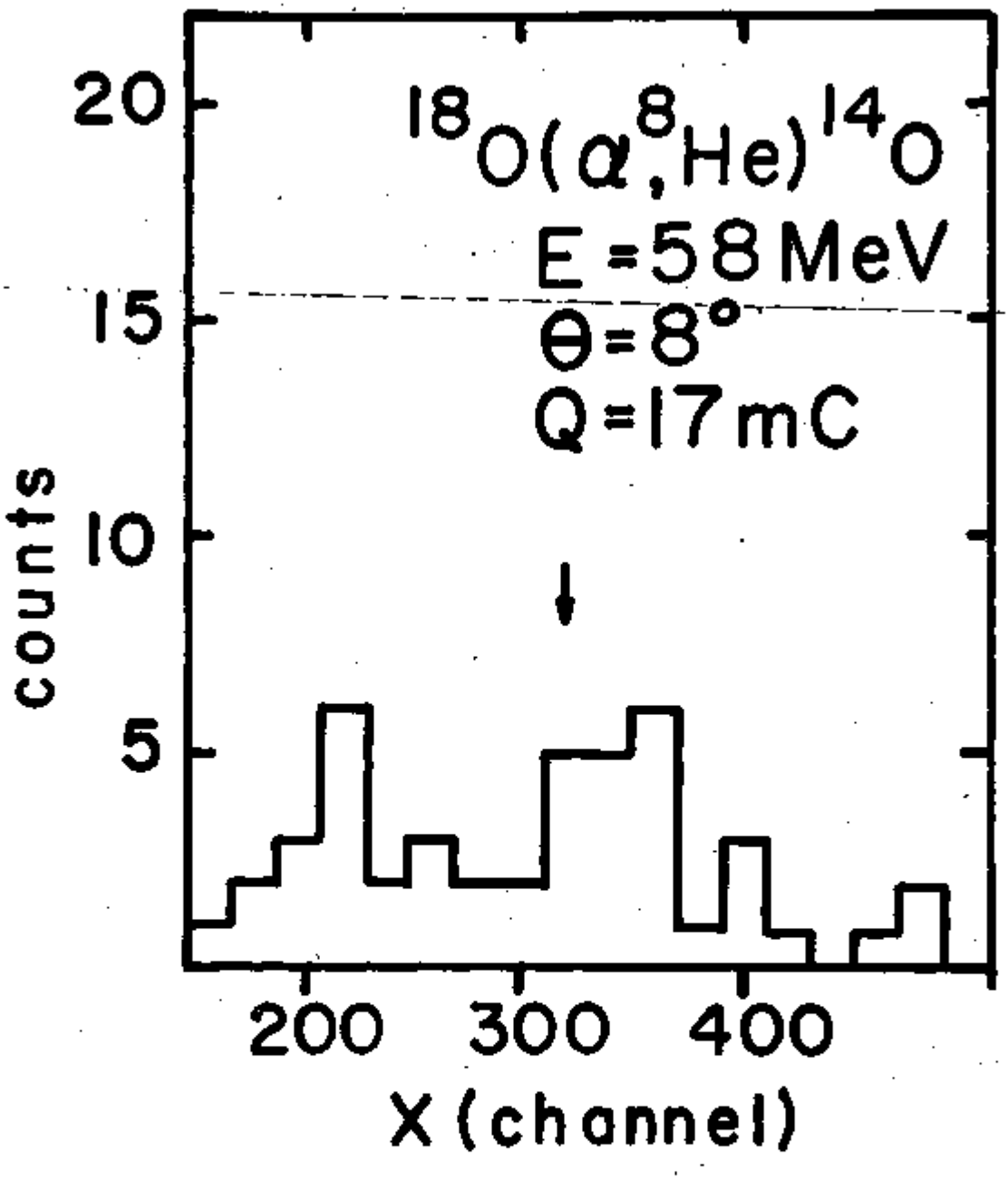

Fig. A3-1. A composite position (Bρ) spectrum obtained for the $^{18}O(\alpha,^{8}He)$ reaction. The energy range shown is about 300 keV. The predicted ^{14}O g.s., based on the previous ^{8}He mass (± 120 keV), is indicated by the arrow.

28770

A4. The Reaction $^{18}O(\alpha,^3He)^{19}O$

F. L. Milder, A. VanderMolen, F. D. Becchetti, J. Janecke, L. Chua

9,10

The nuclear structure of ^{19}O for which shell model calculations are available is of particular interest because of its simple structure with three neutrons outside the doubly-magic ^{16}O core. To study the structure of ^{19}O, the neutron transfer reaction $^{18}O(\alpha,^3He)^{19}O$ is being used with an alpha bombarding energy of 58 MeV. The reaction products are detected with a ΔE-E counter telescope mounted in the scattering chamber. Preliminary data have been obtained with a self-supporting Ni ^{18}O target.

The angular distribution for the transition to the ground-state doublet in ^{19}O is shown in Fig. A4-1 together with two calculated curves from a DWBA analysis for the transition to the ground state (the transition to the state at 96 keV is weak). There exists reasonable agreement. The preliminary spectroscopic factors C^2S of 0.85 and 1.30 are somewhat bigger than the simple shell model estimate of 0.67. The analysis has shown a strong dependence on the details of the optical potential parameters. Future measurements will require the use of an ^{18}O gas target or a different oxide because of strong interference from the $(\alpha,^3He)$ reactions on ^{58}Ni and ^{60}Ni.

28771

A5. The $^{18,16}O(^4He,^6He)^{16,14}O$ Reactions

9,11-14

A. VanderMolen, J. Janecke, F. B. Becchetti and L. Chua

The $(^4He,^6He)$ reactions on ^{18}O and ^{16}O have been studied using a

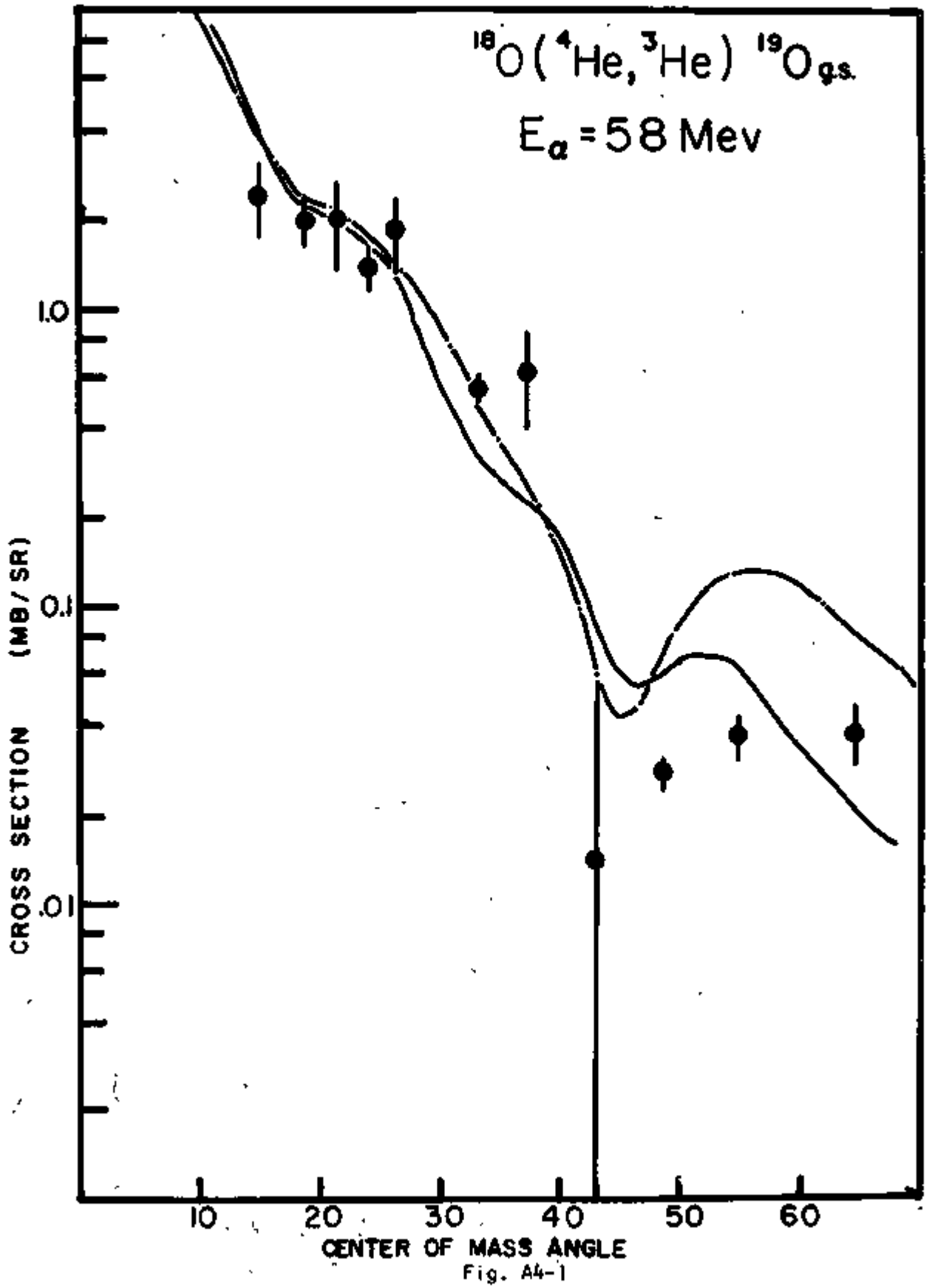
$^{18}O(^4He, ^3He)\ ^{19}O_{g.s.}$
$E_\alpha = 58$ Mev
1.0
0.1
.01
CROSS SECTION (MB/SR)
10
20
30
40
50
60
CENTER OF MASS ANGLE

Fig. A4-1

bombarding energy of 58 MeV and self-supporting Ni ^{18}O and Ni ^{16}O targets. Energy spectra and angular distributions have been obtained with a ΔE-E counter telescope in the scattering chamber. Additional measurements have been made using magnetic analysis with position-sensitive detectors mounted along the focal plane to obtain forward angle points in the angular distributions including measurements at $\theta_{lab} = 0°$. Special attention was given to the transitions to some of the extremely weak 0^+ states in both ^{16}O and ^{14}O.

Figure A5-1 shows an energy spectrum obtained for the (^4He,^6He) reaction on ^{18}O. Only the transition to the ^{16}O ground state is seen strongly. This transition has a center-of-mass cross section of 40 - 50 μb/sr at the secondary maximum near $\theta_{cm} = 27°$. The experimental angular distribution for this transition is shown in Fig. A5-2. Angular distributions were also obtained for the 0^+ 6.05 MeV/3^- 6.13 MeV doublet and the 2^+ 6.92 MeV/1^- 7.12 MeV doublet. The cross sections are about 5 - 10 μb/sr and the angular distributions are quite structureless. Additional states at higher excitation energies may be present with cross sections < 3 μb/sr, but the presence of ^{58}Ni and ^{60}Ni in the target makes their identification difficult. Several long exposures at different angles were taken on a Ni ^{16}O target. Background from reactions on Ni is seen and an upper limit of 1 μb/sr can be placed on the (^4He,^6He) transition to the ^{14}O ground state.

The magnitudes of the observed (^4He,^6He) cross sections are comparable to (^3He,^6He) cross sections in this mass region which are typically 1 μb/sr. However, they are substantially less (by one to two orders of magnitude) than the corresponding (p,t) cross sections. This fact probably reflects the strong absorption of the projectiles and the structure of ^6He. Magnitudes

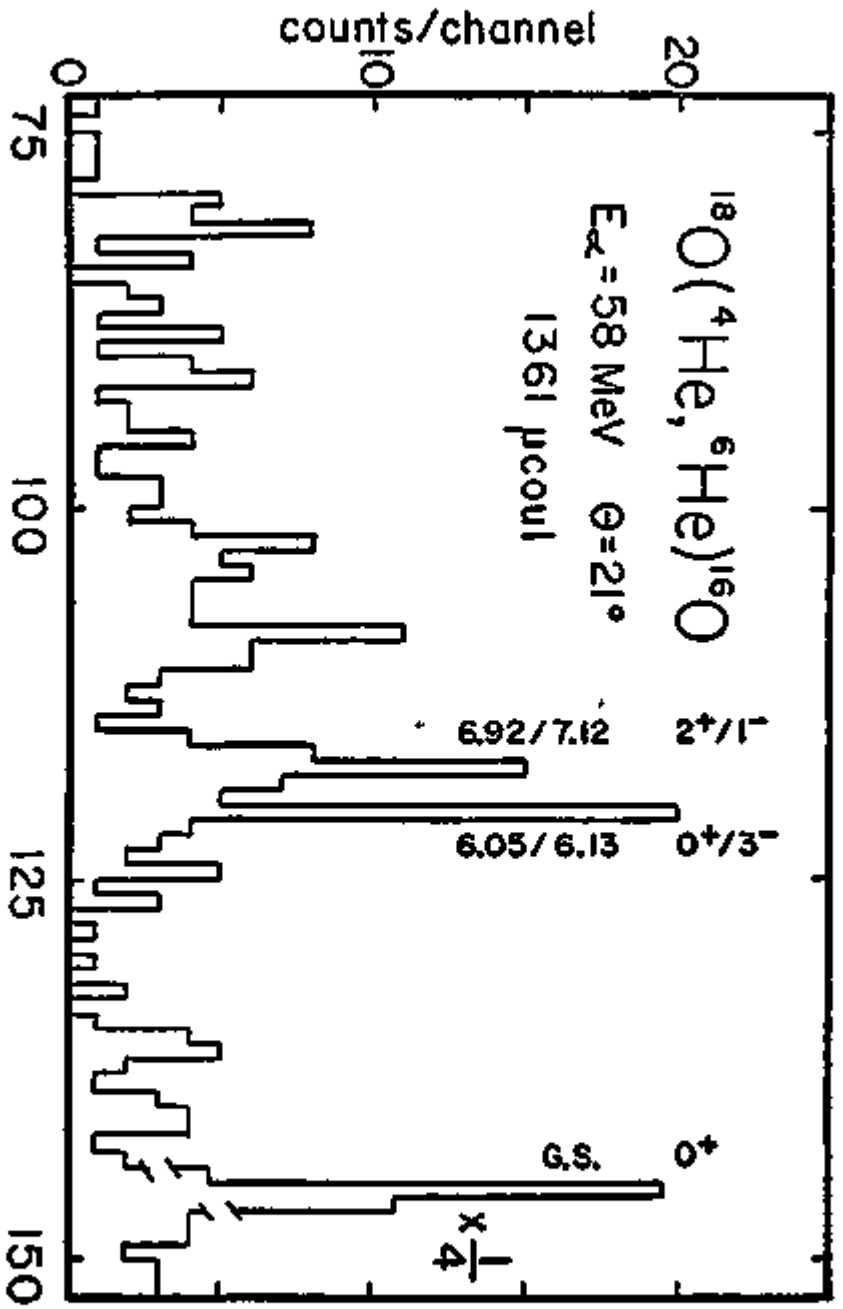
counts/channel
0
10
20
75
100
125
150
channel no.
$^{18}O(^4He,^6He)^{16}O$
E_α=58 MeV Θ=21°
1361 μcoul
6.92/7.12 2⁺/1⁻
6.05/6.13 0⁺/3⁻
G.S. 0⁺
x 1/4

Fig. A5-1.

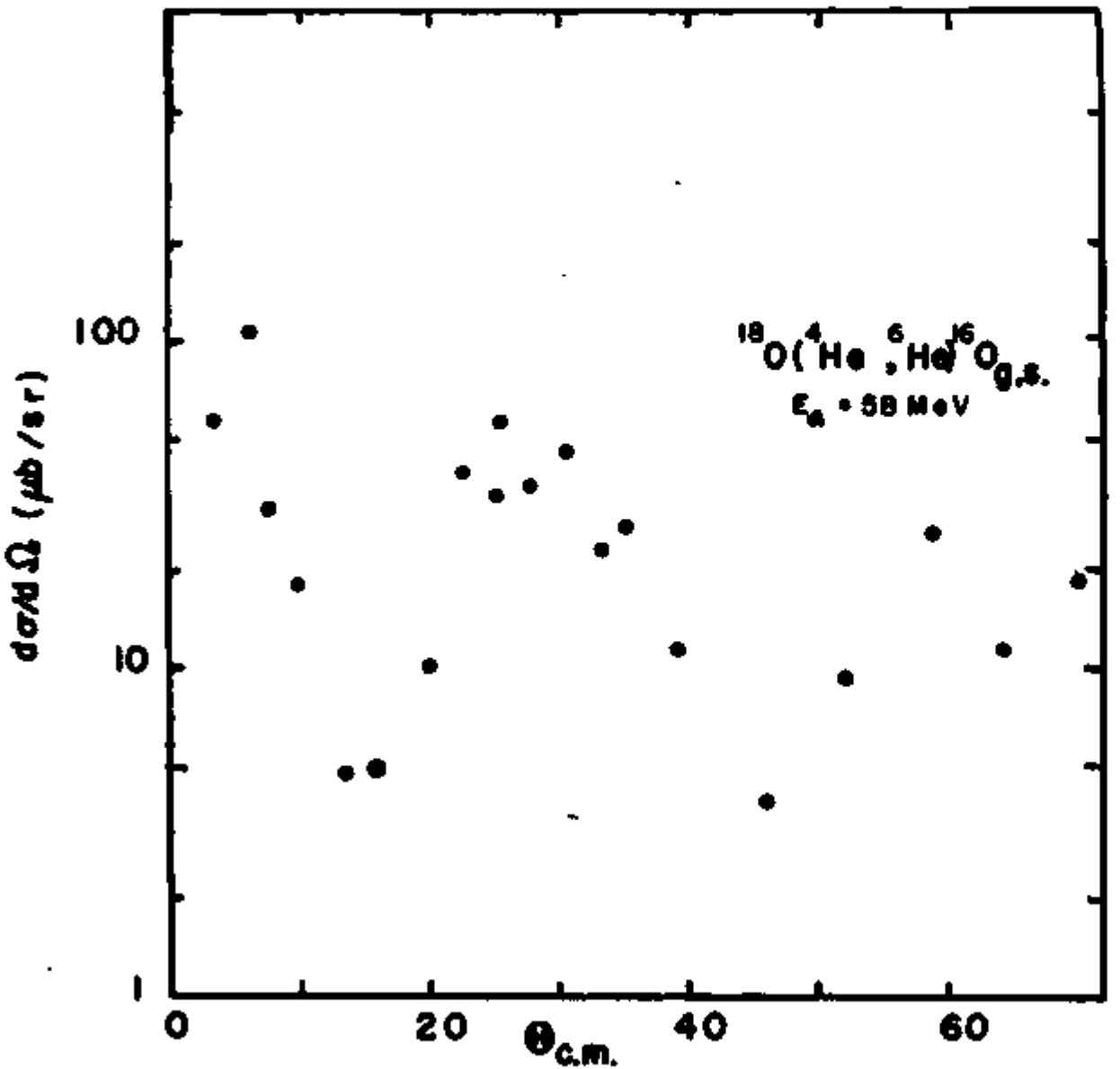
100
10
1
0
20
40
60
$\theta_{c.m.}$
$d\sigma/d\Omega$ (μb/sr)
$^{18}O(^{4}He, ^{6}He)^{16}O_{g.s.}$
E_α = 58 MeV

Fig. A5-2.

of the relative (^{4}He,^{6}He) cross sections also are not yet fully understood but probably can be explained by a strongly reduced cross section for pickup of a J=0 coupled neutron pair from a lower oscillator shell.

The analysis of the data will concentrate on the transitions to the various 0^+ states in ^{16}O and ^{14}O since their structure in terms of zero-particle--zero-hole, two-particle--two-hole, and four-particle--four-hole configurations is of particular interest.

28772

A6. The Reaction ^{16}O(d,^{3}He)^{15}N at 29.0 MeV

M. A. Firestone and J. Janecke

The present experiment was motivated by recent theoretical calculations which suggest that the ^{16}O ground state configuration contains 20-40% core excitations. The single-proton pickup reaction ^{16}O(d,^{3}He)^{15}N was used to determine the two-particle--two-hole and the four-particle--four-hole contributions to ^{16}O ground state. Most of the data have been presented in previous reports, with the conclusion that only the strong $1p_{1/2}$ and $1p_{3/2}$ pickup transitions were well described by DWBA. The importance of compound nucleus effects on the weak transitions was described in last year's report. Less than 5-35% (depending on the state) of the total cross section was estimated to result from compound nucleus formation. The weak transitions must therefore be due to a more complicated direct-reaction mechanism. This report will show the remaining data required for the analysis, review the previous data and its DWBA analysis, and present a CCBA (Coupled Channels Born Approximation) analysis for three of the weak

transitions.

Most of the data were taken with a gas cell--counter telescope arrangement which did not resolve the important $5/2^+$ 5.27 MeV, $1/2^+$ 5.30 MeV doublet. Using a solid Al_2O_3 target and the magnetic spectrograph, these states were separated and angular distributions obtained. Figure A6-1 shows the resolved spectrum at $\theta_{lab} = 15°$. The angular distributions were extracted from the resolved spectra with the help of the peak-fitting program AUTOFIT. [1)]

Figures A6-2 and A6-3 show the angular distributions and DWBA curves for the $^{16}O(d,^3He)^{15}N$ transitions. Three different sets of optical-model parameters were used. Sets A and B [2)] fit the two strong transitions best while set C [3)] was used for the CCBA analysis. The d and ^3He optical model parameters of set C are more consistent than the others. However, there is very little difference among the three sets in the quality of fit or extracted spectroscopic factors. The transitions to the $1/2^-$ ground state and $3/2^-$ 6.32 MeV state are well reproduced. The 8.31 MeV $1/2^+$ distribution is also reasonably well fitted. The other weak transitions, however, are either not fit at all or have very little structure. Table A6-1 is a comparison of theoretical and extracted spectroscopic factors. The ratio of the spectroscopic factors for the 6.32 MeV state and the ground state is 1.93, which is very close to the closed-shell estimate of 2.00. The 8.31 MeV transition also has a reasonable strength. The shapes of the $1/2^+$ and $3/2^+$ angular distributions which are relatively structureless are reproduced by DWBA but yield unreasonably large spectroscopic factors. Thus, even when an adequate fit is obtained from a DWBA analysis, a direct one-step reaction mechanism may not always be assumed.

A CCBA analysis of the $1/2^-$ ground state, $5/2^+$ 5.27 MeV, $5/2^+$ 7.16 MeV,

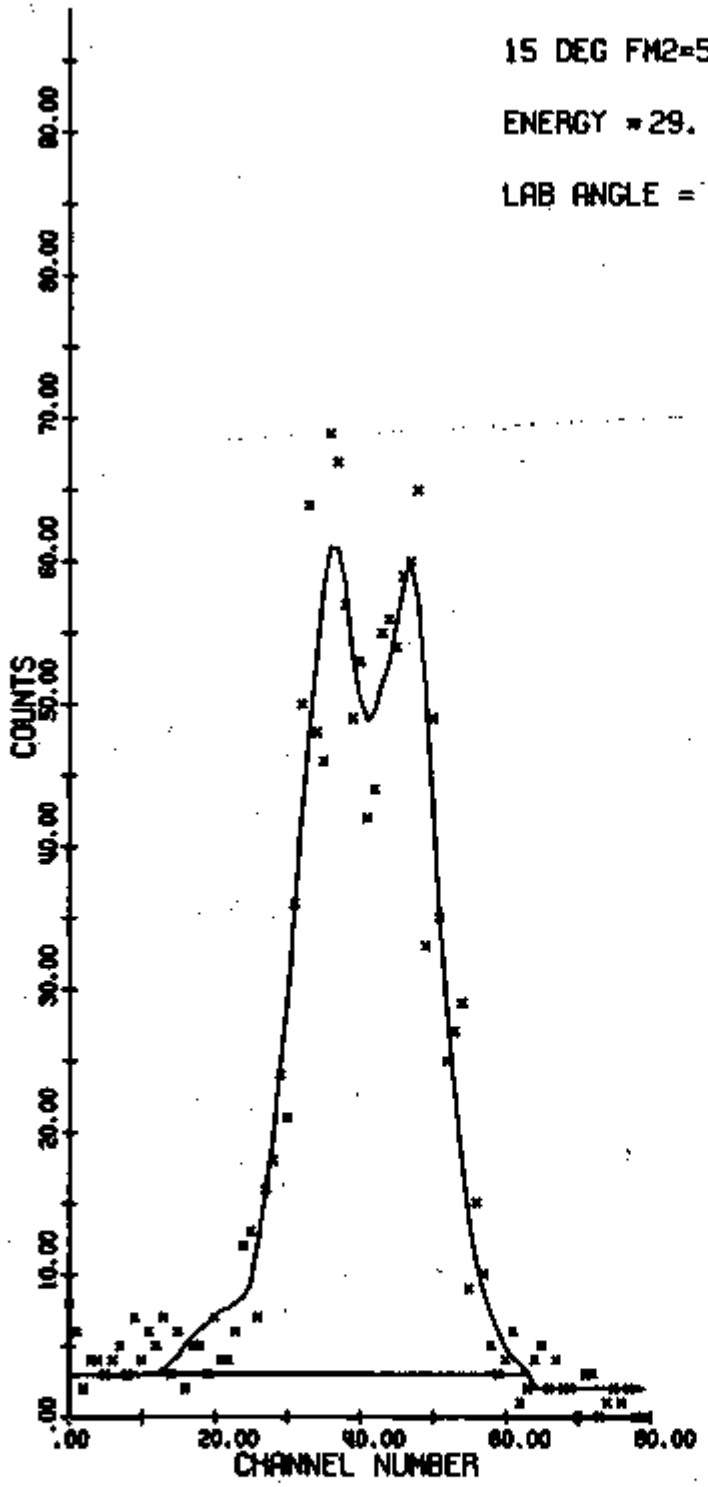
15 DEG FM2=5MM #1=1MM
ENERGY = 29. MEV
LAB ANGLE = 15. DEGREES. LOAD 15 5
COUNTS
CHANNEL NUMBER
.00
10.00
20.00
30.00
40.00
50.00
60.00
70.00
80.00
90.00
.00
20.00
40.00
60.00
80.00

Fig. A6-1.

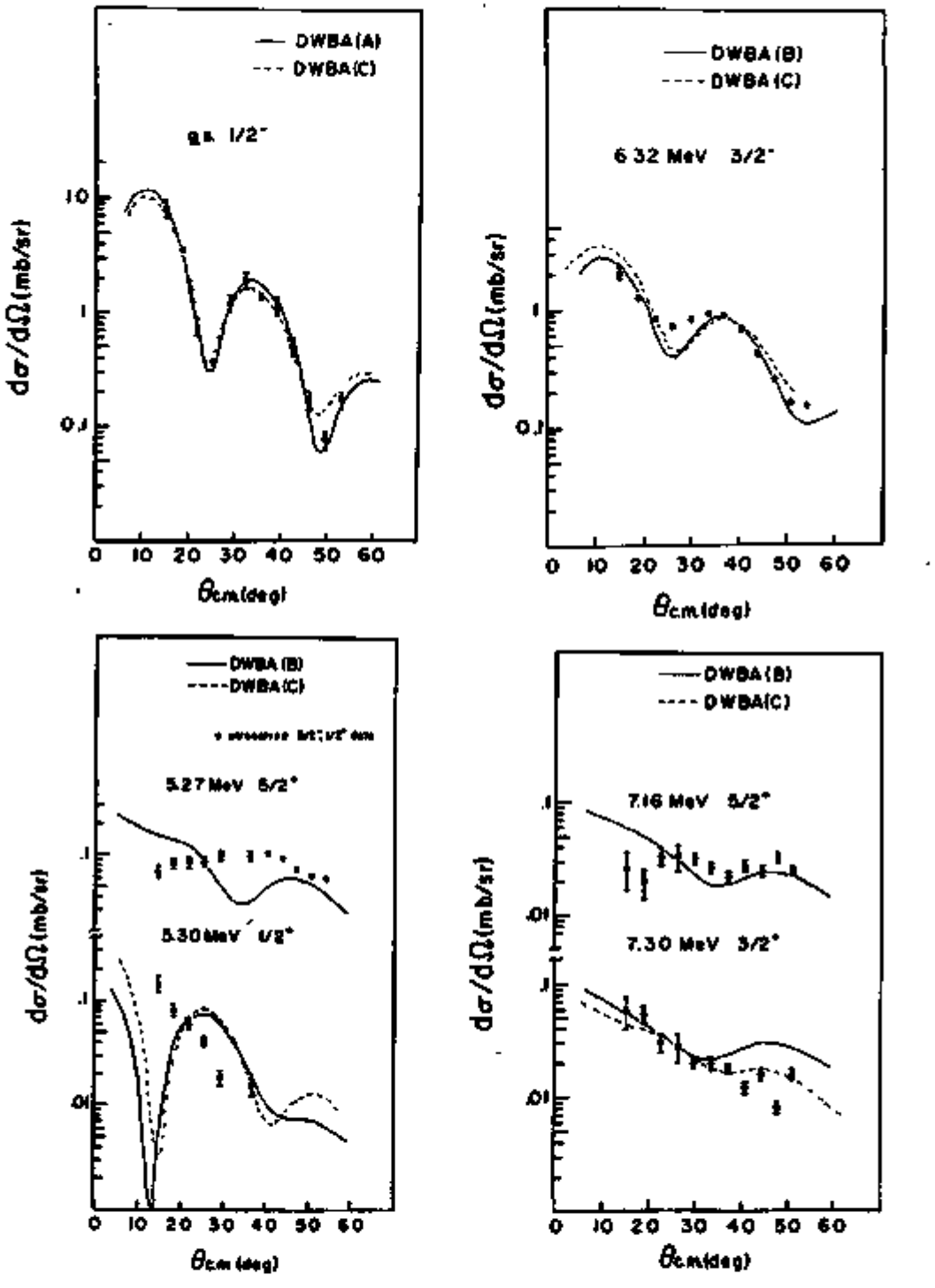
DWBA(A)
DWBA(C)
g.s. 1/2⁺
6.32 MeV 3/2⁺
DWBA(B)
DWBA(C)
5.27 MeV 5/2⁺
5.30 MeV 1/2⁺
7.16 MeV 5/2⁺
7.30 MeV 3/2⁺
dσ/dΩ(mb/sr)
θcm(deg)

Fig. A6-2.

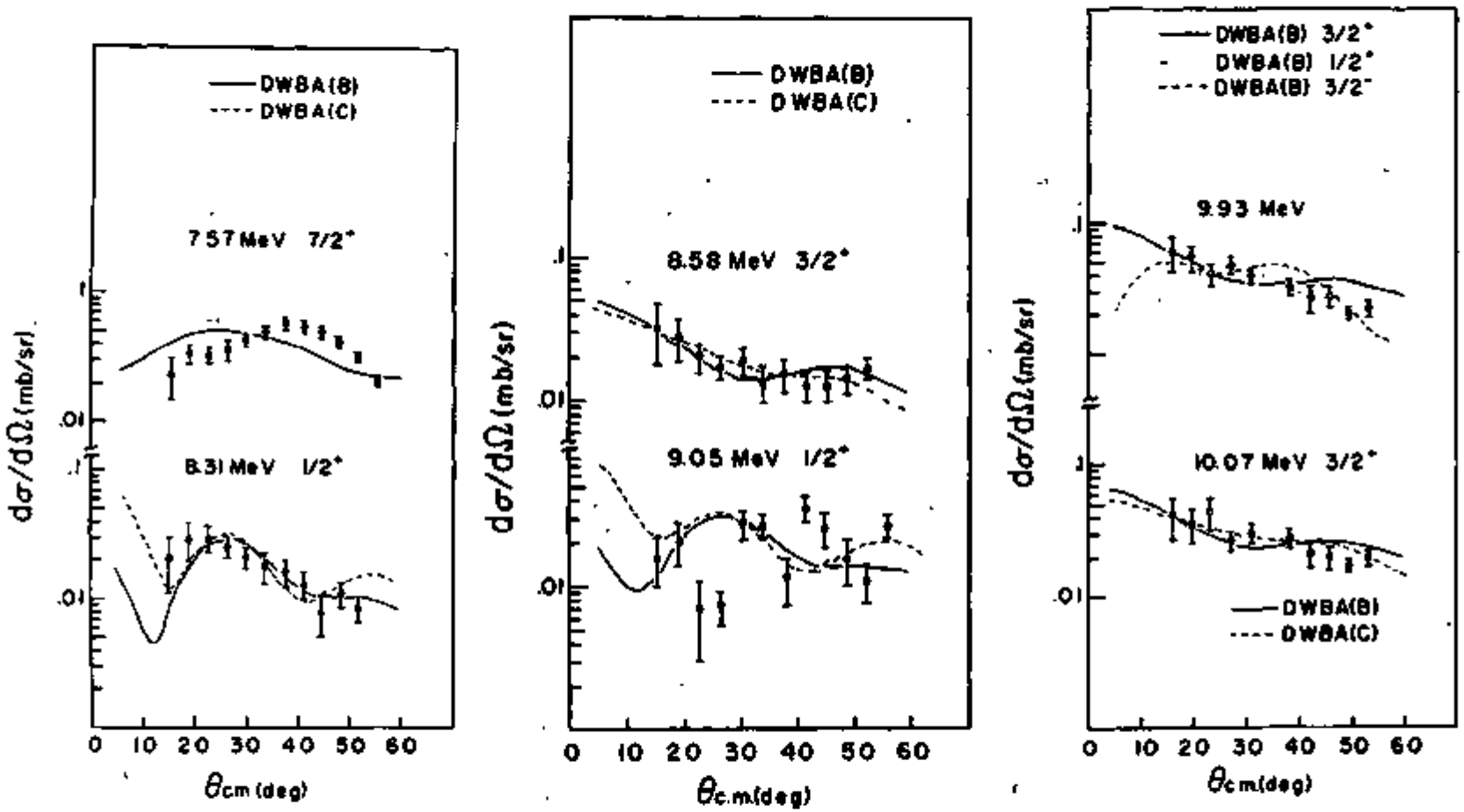
DWBA(B)
DWBA(C)
7.57 MeV 7/2⁺
8.31 MeV 1/2⁺
dσ/dΩ (mb/sr)
θcm (deg)
8.58 MeV 3/2⁺
9.05 MeV 1/2⁺
θc.m.(deg)
DWBA(B) 3/2⁺
DWBA(B) 1/2⁺
DWBA(B) 3/2⁻
9.93 MeV
10.07 MeV 3/2⁺

Fig. A6-3.

TABLE A6-1 - C^2S

^{15}N level		BZM[a] (theory)	WONG[b] (theory)	Ellis, Engeland[c] (theory)	Present Exp. (DWBA)
0	$1/2^-$	1.60	$\Sigma 1p_{1/2} = 1.85$	1.51	2.85
5.27	$5/2^+$	.35	$\Sigma 1d_{5/2} = .20$	.17	.29
5.30	$1/2^+$	.04	$\Sigma 2s_{1/2} = 0.0$	.004	.034
6.32	$3/2^-$		$\Sigma 1p_{3/2} = 2.95$		5.45
7.16	$5/2^+$			.014	.15
7.30	$3/2^+$		$\Sigma 1d_{3/2} = .07$	.0074	.19
7.57	$7/2^+$			0.0	.54
8.31	$1/2^+$			.01	.036
8.58	$3/2^+$			.013	.13
9.05	$1/2^+$			0.0	.05
10.07	$3/2^+$			.0007	.25

(a) Ref. 4

(b) Ref. 5

(c) Ref. 6

and $7/2^+$ 7.57 MeV ^{15}N angular distributions was performed by A. Dudek-Ellis and P. J. Ellis at Oxford University. [7] Inelastic scattering in the d and ^3He channels was analyzed in a coupled-channels framework to extract the strength of the collective potential. Spectroscopic amplitudes were obtained

from the "weak coupling" model wavefunctions of Ellis and Engeland, so the calculation did not include any normalization. The theoretical CCBA and DWBA predictions together with the experimental angular distributions, are shown in Figs. A6-4 through A6-7. The agreement between the CCBA predictions and the data is remarkable, especially for the $7/2^+$ 7.57 MeV transition. The latter transition cannot be attributed to a one-step pickup reaction mechanism due to the absence of $(g_{7/2})^2$ components in the ground state configuration of ^{16}O. The DWBA analysis describes the ground-state transition well, as previously discussed. The two $5/2^+$ transitions do not resemble the DWBA predictions, and a direct component is not even considered for the $7/2^+$ distribution. Also note from the figures that the strengths of some of the two-step contributions are comparable to the strength of the direct one-step contributions. This result explains the failure of the DWBA analysis to describe these angular distributions and points to the necessity of considering a multistep mechanism which has been done successfully for three characteristic transitions. The conclusion is that a complete CCBA analysis is required to understand all the weak transitions populated in this experiment, and that spectroscopic information obtained by other authors for these transitions is subject to criticism.

References

1) J. R. Comfort, Argonne National Laboratory Informal Report PHY-1970B (1970).

2) J. C. Hiebert, E. Newman, and R. H. Bassel, Phys. Rev. 154, 898 (1967).

3) G. C. Ball and J. Cerny, Phys. Rev. 177, 1466 (1969); F. Hinterberger, G. Mairle, U. Schmidt-Rohr, G. J. Wagner, and P. Turek, Nucl. Phys. A111, 265 (1968).

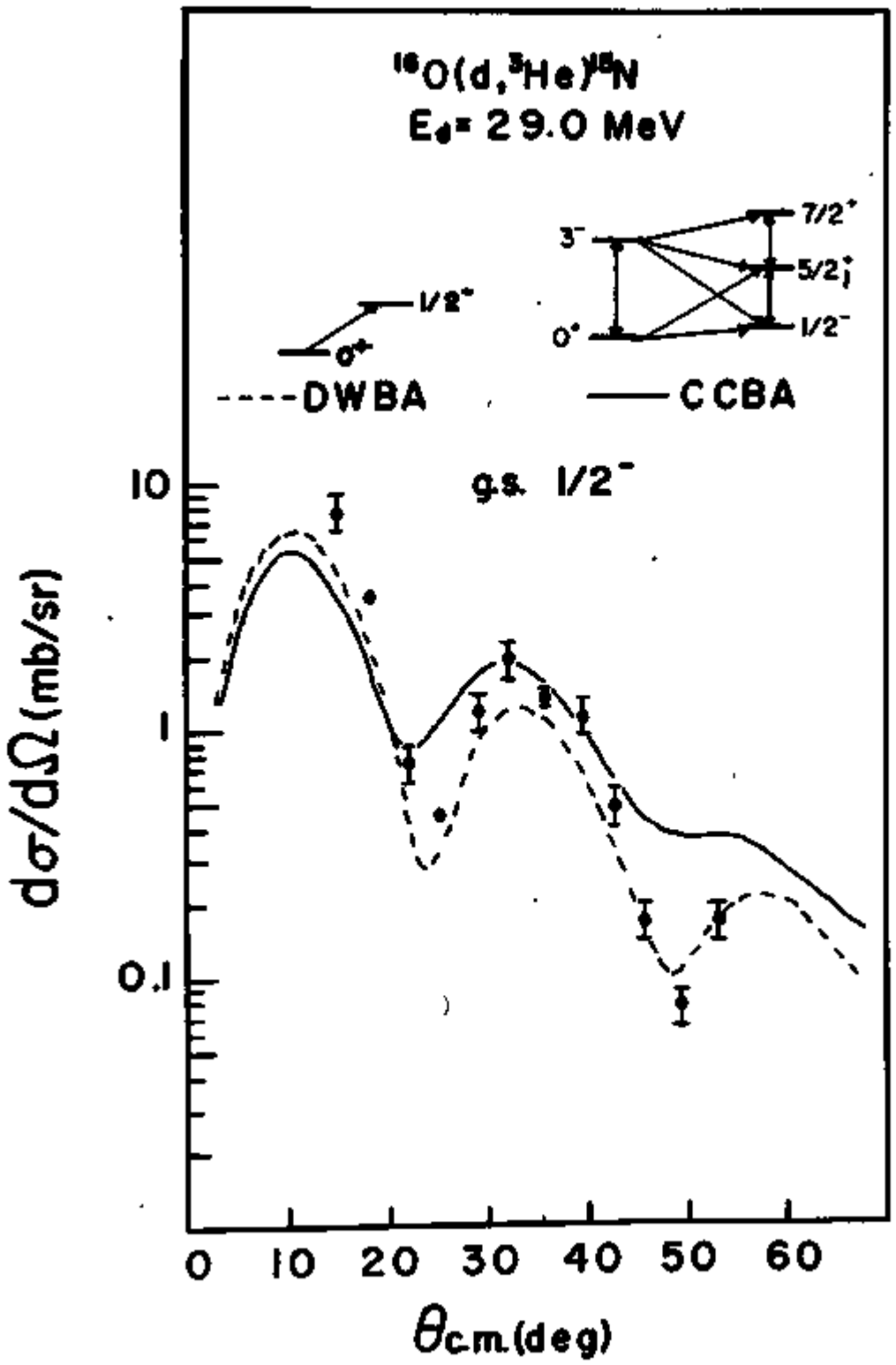
$^{16}O(d,^3He)^{15}N$
E_d= 29.0 MeV
7/2⁺
3⁻
5/2⁺
1/2⁻
0⁺
1/2⁻
0⁺
----DWBA
—— CCBA
g.s. 1/2⁻
10
1
0.1
dσ/dΩ(mb/sr)
0
10
20
30
40
50
60
θc.m.(deg)

Fig. A6-4.

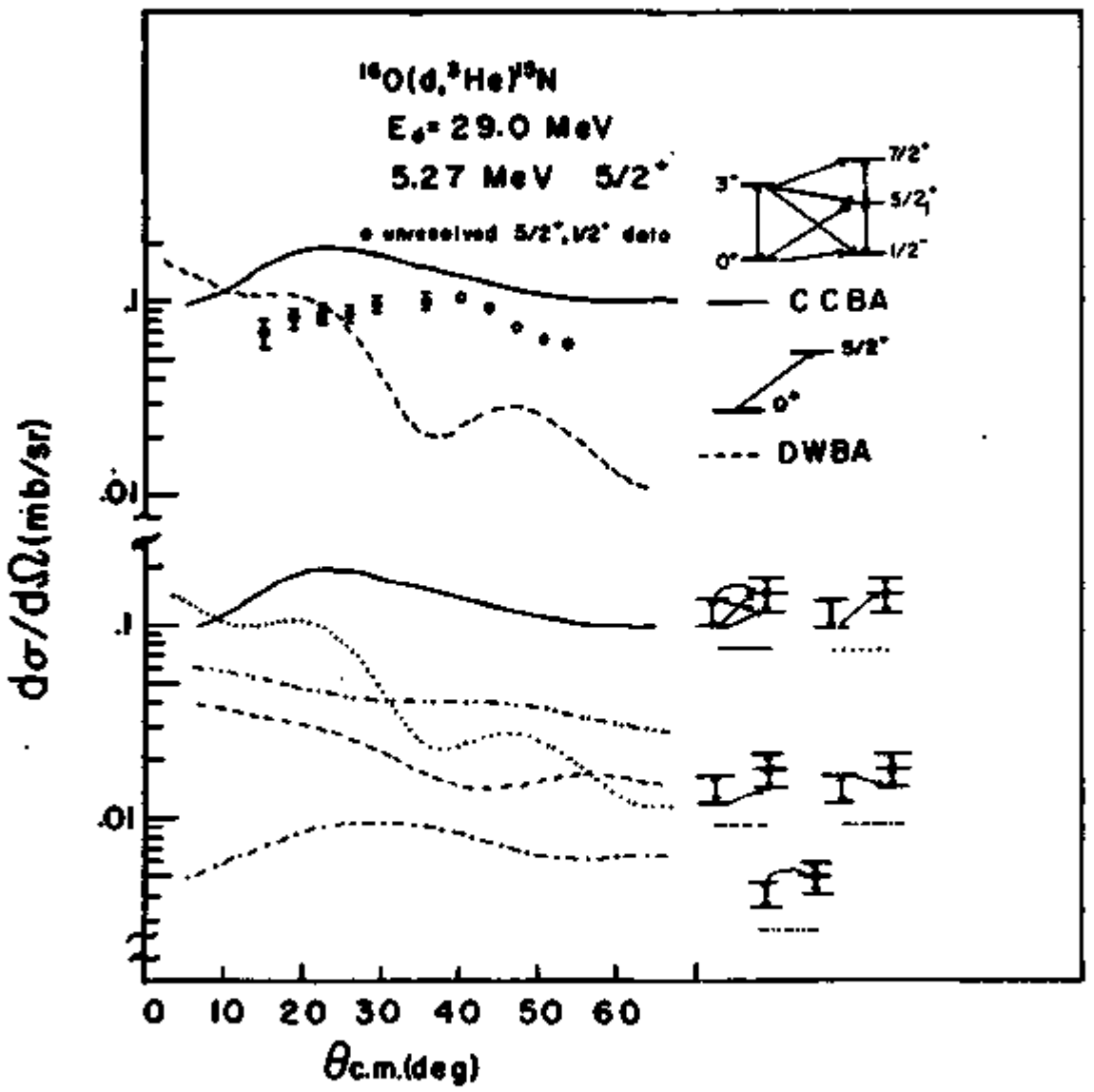
$^{16}O(d,^3He)^{15}N$
E_d= 29.0 MeV
5.27 MeV 5/2$^+$
unresolved 5/2$^+$,1/2$^+$ data
7/2$^+$
3$^+$
5/2$^+_1$
0$^+$
1/2$^-$
CCBA
5/2$^+$
0$^+$
DWBA
1
.1
.01
0 10 20 30 40 50 60
$\theta_{c.m.}$(deg)
$d\sigma/d\Omega$(mb/sr)

Fig. A6-5.

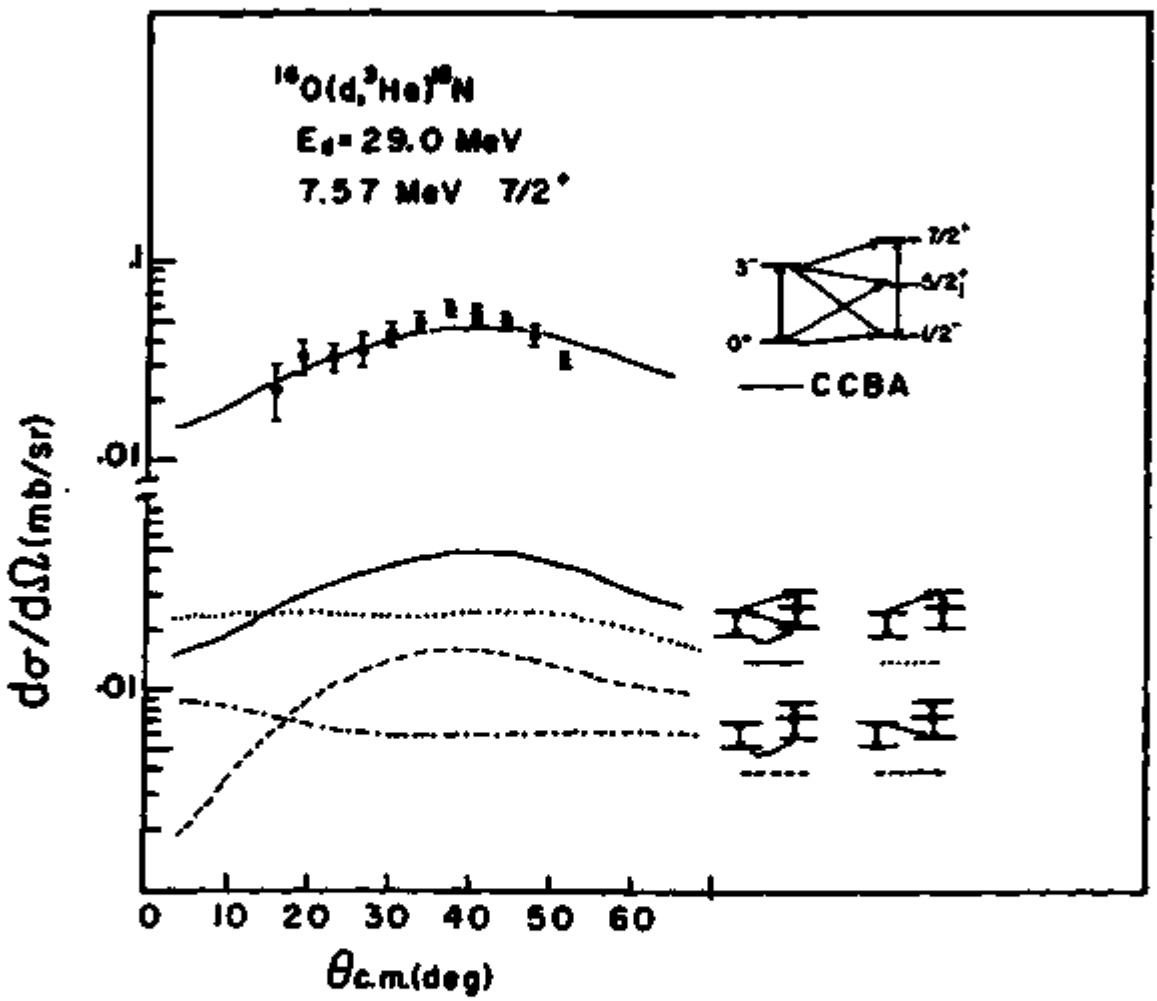
$^{16}O(d,^3He)^{15}N$
E_d = 29.0 MeV
7.57 MeV 7/2°
CCBA
$d\sigma/d\Omega$ (mb/sr)
$\theta_{c.m.}$ (deg)
0 10 20 30 40 50 60

Fig. A6-6.

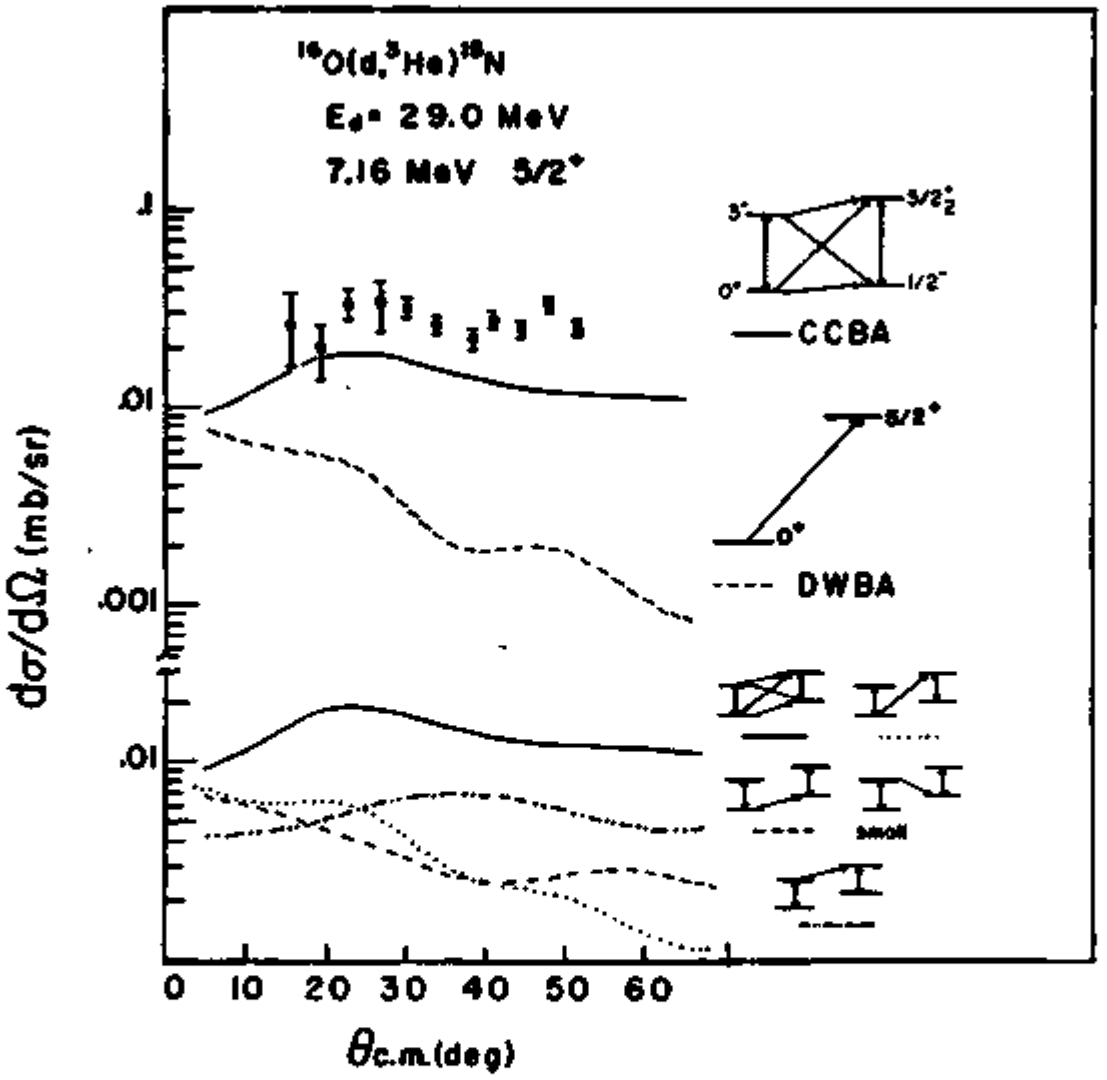
$^{16}O(d,^3He)^{15}N$
E_d= 29.0 MeV
7.16 MeV 5/2+
CCBA
DWBA
small
1
.01
.001
.01
$d\sigma/d\Omega$ (mb/sr)
0 10 20 30 40 50 60
$\theta_{c.m.}$(deg)

Fig. A6-7.

4) D. Hartwig, Unpublished Thesis, Karlsruhe (1971).

5) S. S. M. Wong, Nucl. Phys. A120, 625 (1968).

6) T. Engeland, private communication, 1973.

7) M. A. Firestone, J. Janecke, A. Dudek-Ellis, P. J. Ellis, and T. Engeland, Bull. Am. Phys. Soc. 19, 454 (1974); and to be published.

A7. The $^{40}Ca(d,p)^{41}Ca$ Reaction as a Test of the Johnson-Soper Model of Deuteron Stripping

W. S. Gray, W. C. Parkinson, and R. S. Tickle

The (d,p) reaction on ^{40}Ca is being studied in order to test the adiabatic breakup model proposed by Johnson and Soper [1] for deuteron stripping in a new energy regime. This study is being made in conjunction with G. R. Satchler of Oak Ridge National Laboratory. Thus far angular distributions have been measured at E_d = 29 and 35 MeV for a number of levels up to 4.1 MeV excitation in ^{41}Ca. This excitation range includes the levels having most of the $1f_{7/2}$, $2p_{3/2}$, and $2p_{1/2}$ strength, as well as several positive-parity levels arising from (2s-1d) hole configurations. A sample spectrum is shown in Fig. A7-1. The proton spectra were recorded on nuclear track plates and the angular distributions have not yet been completely analyzed. Preliminary calculations indicate large differences between the angular distributions predicted by the conventional DWBA and the Johnson-Soper model at these bombarding energies. It is therefore hoped that the experiments will provide a sensitive test of the model.

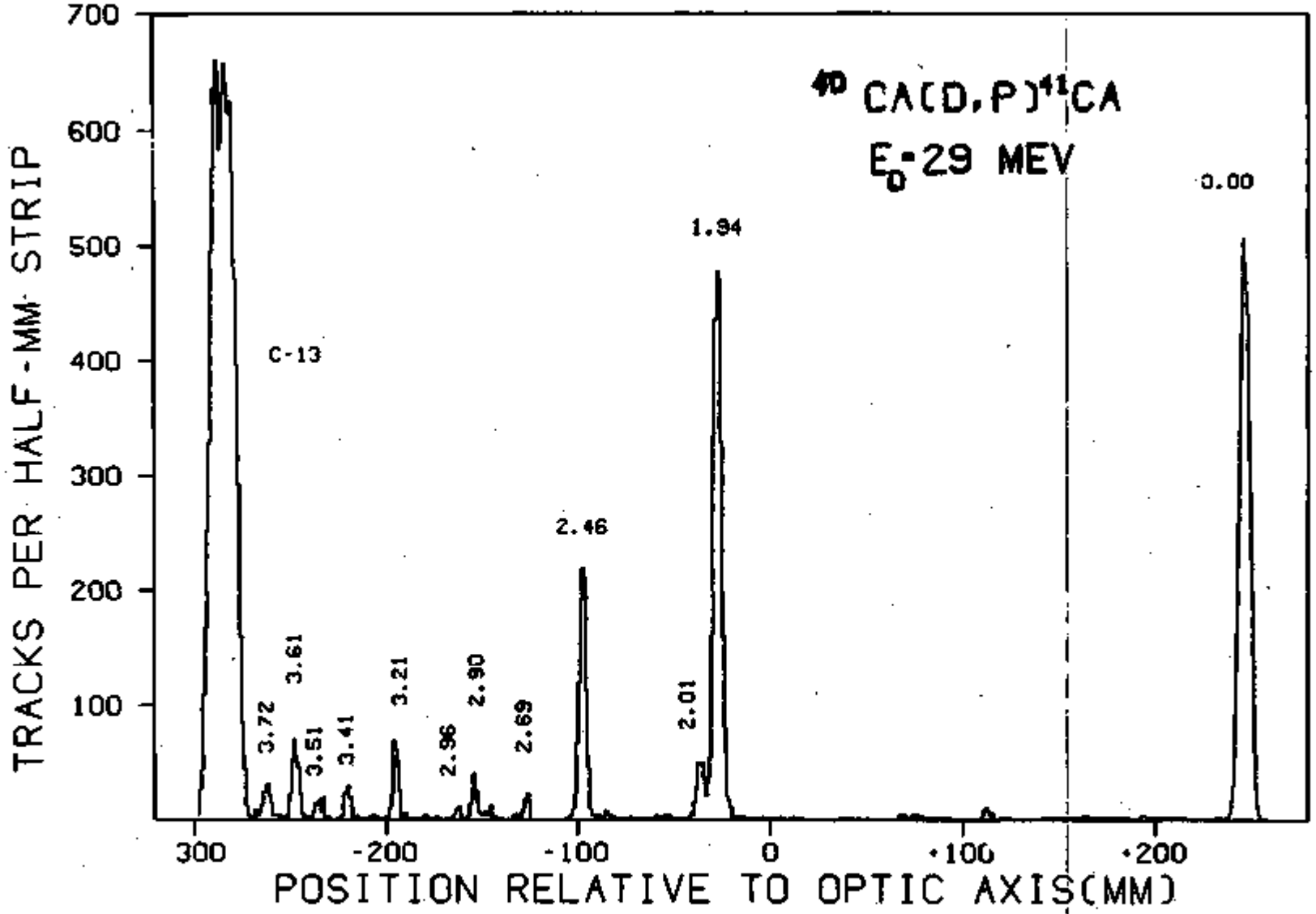
^{40}CA(D,P)^{41}CA
E_0=29 MEV
TRACKS PER HALF-MM STRIP
POSITION RELATIVE TO OPTIC AXIS(MM)
700
600
500
400
300
200
100
300
-200
-100
0
•100
•200
C-13
3.72
3.61
3.51
3.41
3.21
2.96
2.90
2.69
2.46
2.01
1.94
0.00

Fig. A7-1.

References

1) R. C. Johnson and P. J. R. Soper, Phys. Rev. C1, 976 (1970).

A8. The $^{40}Ar(^{3}He,n)^{42}Ca$ Reaction

J. F. Petersen and W. C. Parkinson

The energy spectrum of ^{42}Ca is known to contain low-lying states which cannot be described by the two valence neutrons in the $1f_{7/2}$ shell alone. The extra 0^+ and 2^+ states at 1.84 and 2.42 MeV, respectively, have been attributed to 4p-2h states, with the four particles (two protons and two neutrons) assumed to be in a low-lying deformed state projected from the #14 Nilsson orbital. The $(^{3}He,n)$ reaction leading to ^{42}Ca from an ^{40}Ar target should selectively populate 4p-2h excited states. Thus in an attempt to verify the nature of these extra levels in ^{42}Ca, the $^{40}Ar(^{3}He,n)^{42}Ca$ reaction has been studied using the neutron time-of-flight spectrometer. Measurements were made at eight angles with an 18.65 MeV ^{3}He beam incident on a natural gas target. A typical neutron time-of-flight spectrum is shown in Fig. A8-1. The striking feature of the spectrum is the absence of strong excited states. The differential cross section for the ground state was measured to be 690 ± 140, 810 ± 165, 750 ± 155, 340 ± 75, 90 ± 20, 190 ± 45, 50 ± 15, and 60 ± 20 μb/sr at -5°, 0°, 5°, 10°, 15°, 20°, 25°, and 30°, respectively. While there are indications of transitions corresponding to known states and also to states between 8 and 10 MeV (in the zero degree spectrum), none has a cross section larger than 80 μb/sr. The data at 0° and 15° are summarized in Table A8-1.

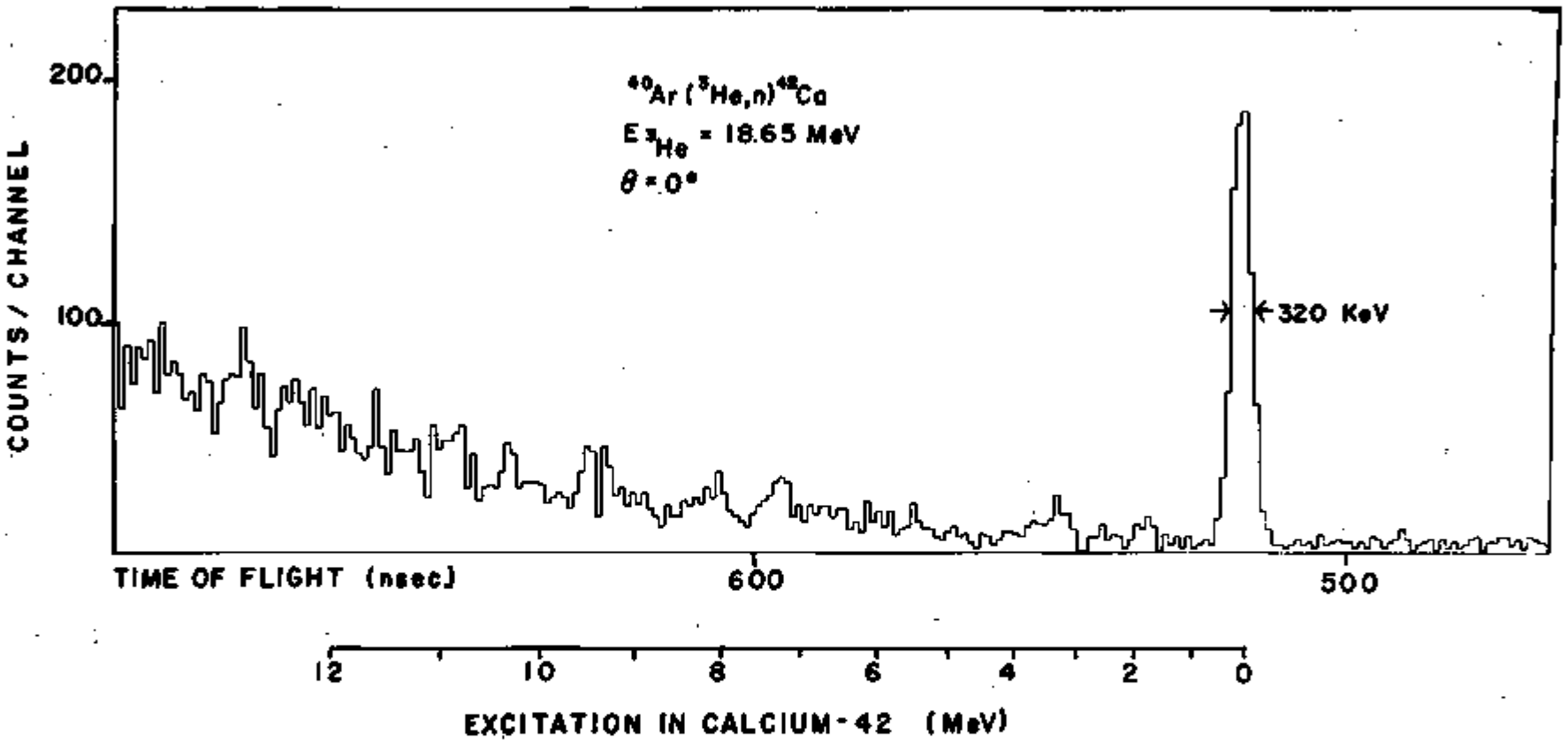
200
100
COUNTS / CHANNEL
$^{40}Ar(^{3}He,n)^{42}Ca$
$E_{^{3}He}$ = 18.65 MeV
$\theta = 0°$
320 KeV
TIME OF FLIGHT (nsec)
600
500
12
10
8
6
4
2
0
EXCITATION IN CALCIUM-42 (MeV)

Fig. A8-1.

TABLE AB-1

$^{40}Ar(^{3}He,n)^{42}Ca$ cross sections at 18.65 MeV incident energy. The uncertainties in the cross sections include a 20% absolute uncertainty as well as the statistical uncertainty. States in ( ) are only tentatively identified.

State	J^{π}	0° $d\sigma/d\Omega$ μb/sr	15° $d\sigma/d\Omega$ μb/sr
g.s.	0^+	813 ± 20%	90 ± 22%
1.52	2^+	≤20	40 ± 45%
1.84	0^+	40 ± 32%	≤20
2.42	2^+	30 ± 40%	40 ± 55%
3.4	2^+	50 ± 28%	50 ± 55%
3.7	2^+	30 ± 55%	30 ± 75%
7.3	2^+	60 ± 28%	50 ± 75%
(8.5)	(0^+)	50 ± 55%	≤30
(9.7)	(0^+)	80 ± 28%	≤30
(10.3)	(0^+)	50 ± 55%	≤30
(10.9)	(0^+)	60 ± 55%	≤30

Because the levels at high excitation are not seen at larger angles, they may be 0^+ states. It is worth noting that because of the high Q value of the $(^{3}He,n)$ reaction (+10.36 MeV), states due to likely contaminants will not appear in the first 10 MeV of excitation. This was verified by back-

ground measurements taken with the gas cell evacuated.

The data show that the transition to the 1.85 MeV 0^+ state is a factor of twenty weaker than the transition to the ground state. To indicate that it is impossible to understand this result in terms of the simplest interpretations of the 4p-2h state, several DWBA calculations using standard optical model parameters have been performed with the two-nucleon transfer option of the computer code DWUCK. The calculations are described in detail in a letter which is in press. [1] The results are that the predicted strength of the 1.84 MeV 0^+ state ranges from 23% to 180% of the ground state strength. The calculations are the most elementary application of the calculated wave functions, but it is felt that they are sophisticated enough to detect a considerable discrepancy between the data and the theoretical treatments.

References

1) J. F. Petersen and W. C. Parkinson, Phys. Lett. B, in press.

A9. Pair Excitations in ^{90}Zr

R. H. Day and W. C. Parkinson

The ground state of ^{90}Zr is a linear superposition of the shell model states $(2p_{1/2})^2$ and $(1g_{9/2})^2$. It has been suggested [1] that in analogy with the ground state a state might exist near 10 MeV excitation which is constructed of a coherent superposition of the L=0 strength of the shell model levels from the next major shell, ($1g_{7/2}$, $2d_{5/2}$, $1h_{11/2}$, $2d_{3/2}$, and $3s_{1/2}$), and with a cross section as large or larger than the ground state.

It is of interest therefore to look for such a state via the (^{3}He,n) two-proton transfer reaction on ^{88}Sr. It is also of interest to compare the excitations with those induced by the two-proton transfer reaction (^{16}O,^{14}C) reported by Christensen et al. [2]

The (^{3}He,n) reaction was studied using The University of Michigan neutron time-of-flight spectrometer. [3] A typical spectrum for an incident ^{3}He energy of 20.59 MeV is shown in Fig. A9-1. The target was 1.8 ± 0.2 mg/cm^2 of Sr enriched to 99.8% in ^{88}Sr sandwiched between two gold backings 2 mg/cm^2 thick. Only two states in ^{90}Zr are visible. The measured cross section for the ground state is 302 ± 60 μb and for the first excited state at 1.76 MeV is 20 ± 10 μb. No other states up to an excitation energy of 12.6 MeV with a cross section as large as 30 μb are visible. The large peaks at the left result from the reactions ^{16}O(^{3}He,n)^{18}Ne and ^{12}C(^{3}He,n)^{14}O due to the carbon and oxygen contaminants which have relatively large cross sections (∿ 3000 μb). At a ^{3}He energy of 20.59 MeV, the ground state of ^{14}O obscures a region of about 400 keV centered at 9.6 MeV excitation in ^{90}Zr. To kinematically shift the ^{14}O peak, the beam energy was changed to 16.86 and to 25.49 MeV. The results are displayed in Fig. A9-2 where the counts due to the ^{14}O ground state for the two incident energies are plotted as a function of excitation energy in ^{90}Zr. The dotted curve is the location of the ^{14}O peak at 20.49 incident ^{3}He energy. The ordinate has been adjusted to equalize the backgrounds for the three spectra. The window between the 16.86 and 25.5 MeV peaks allows an upper limit of 30 μb to be put on the cross section of any state in ^{90}Zr.

In searching the region near 10 MeV, a variety of natural and enriched targets of various thicknesses were used. The measured cross sections,

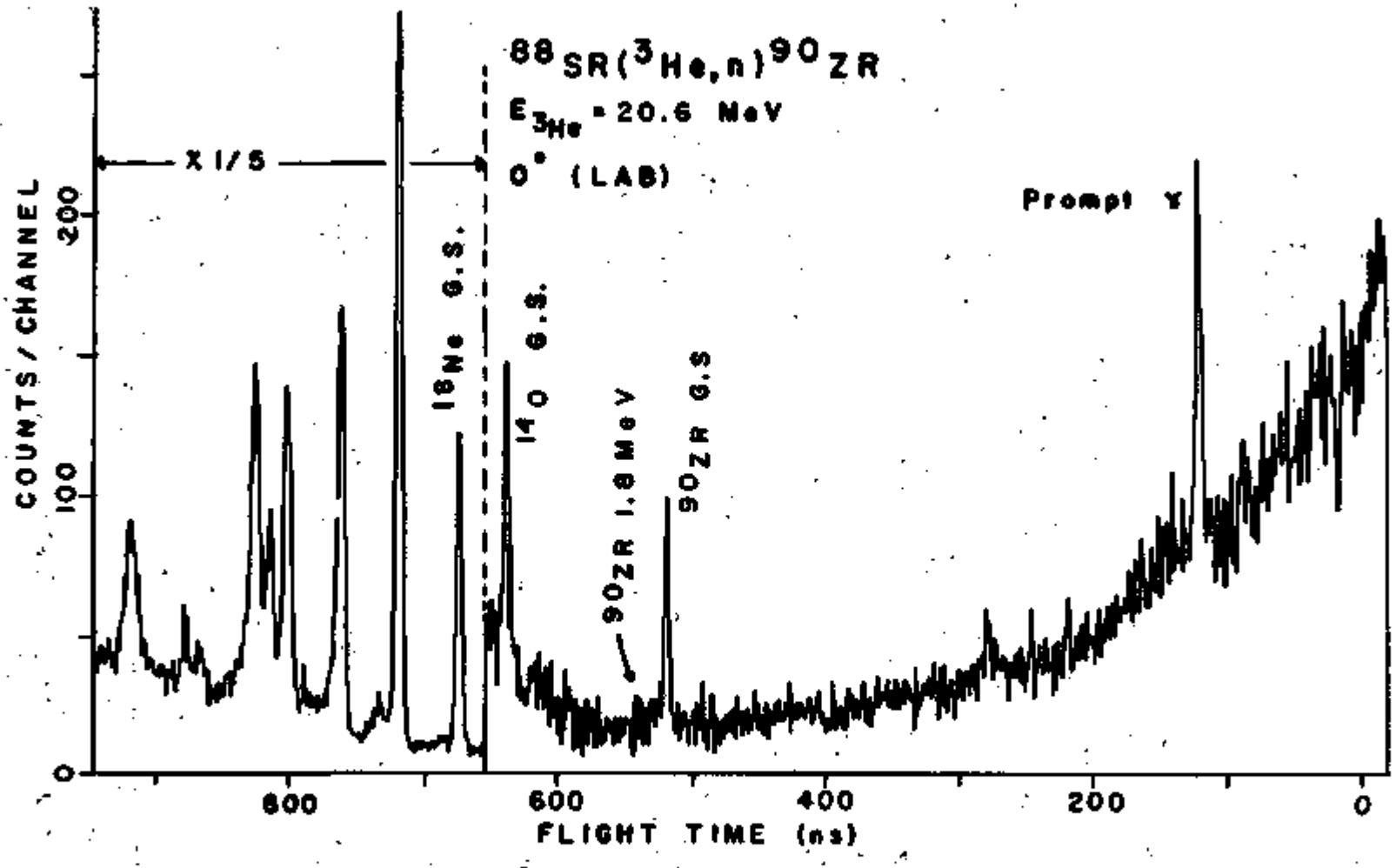

Fig. A9-1. The spectrum of $^{88}Sr(^{3}He,n)^{90}Zr$ at $E_{^{3}He}$ = 20.59 MeV.

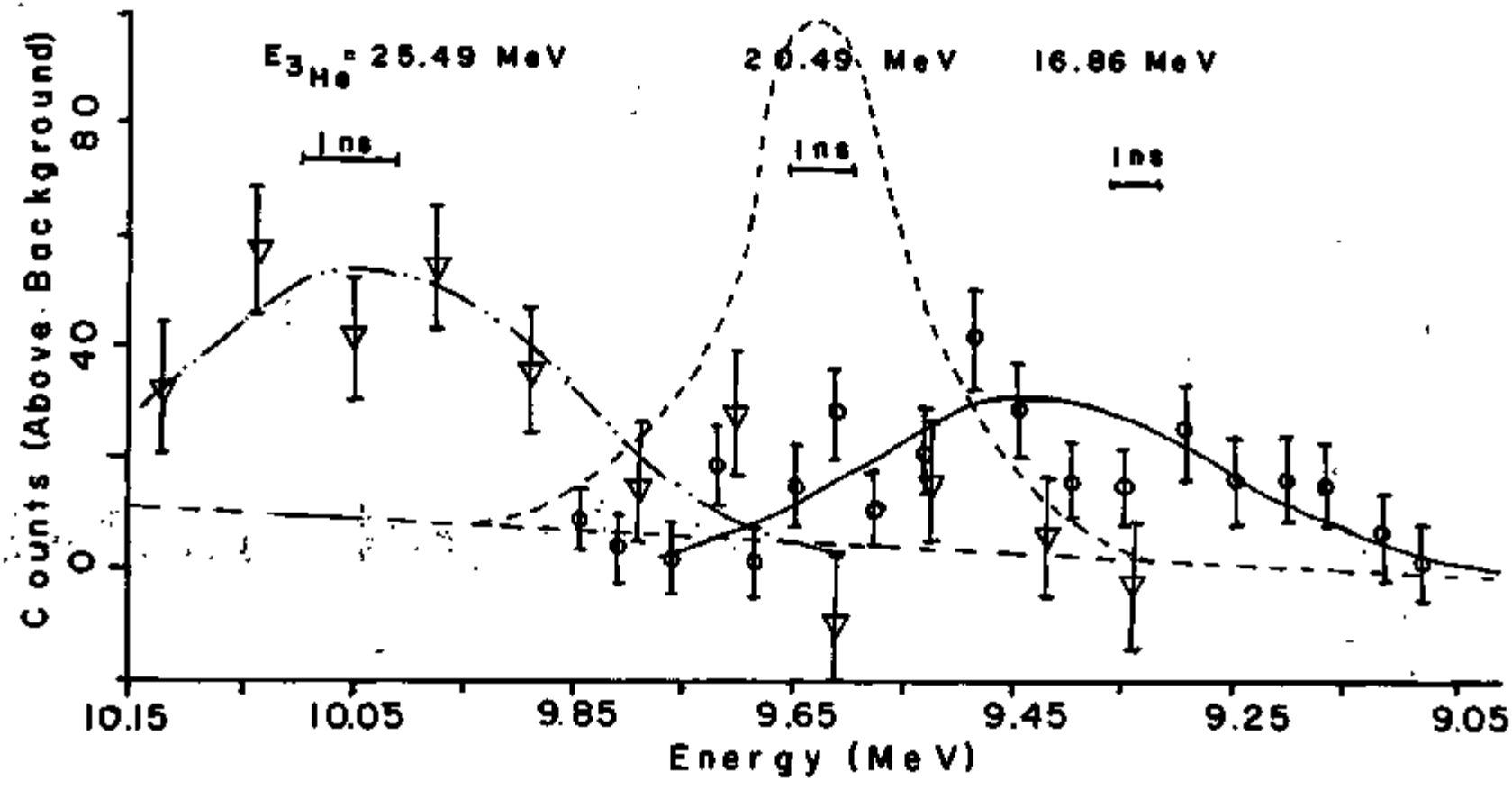

Fig. A9-2. The region of excitation in ^{90}Zr near 10 MeV.

Including the ground states of ^{88}Zr and ^{89}Zr, due to ^{86}Sr and ^{87}Sr present in the natural targets are summarized in Table A9-1. The table includes in parentheses the DWBA predictions of the computer code DWUCK [4] normalized to the measured cross section for the ^{90}Zr ground state for E_{He} = 20.59 MeV.

TABLE A9-1

$Sr(^3He,n)Zr$

$d\sigma/d\Omega$ ($\mu b/_{str}$) at 0°

The DWBA cross section normalized to the data at 19.95 MeV is given in parentheses.

^3He Energy (MeV)	$^{90}Zr_{g.s.}$	$^{90}Zr_{1.76}$	$^{89}Zr_{g.s.}$	$^{88}Zr_{g.s.}$
16.86	123 ± 60 (135)	---	---	120 ± 70
19.95	240 ± 50 (240)	---	301 ± 120	320 ± 150
20.59	302 ± 60	20 ± 10 (9.5)	---	---
25.49*	282 ± 60 (-4.7°) (251)	---	300 ± 150	380 ± 170

*To reduce the background, the measurement at E = 25.49 MeV was made at $\theta = -4.7°$.

The wave functions used for the ground state and first excited state are taken from Gloeckner et al.; [5] the ^{3}He optical potentials are set "B1" of Becchetti et al., [6] and the neutron potentials were those of Becchetti and Greenlees. [7] According to DWUCK, there would be no reduction in cross section due to kinematic effects at 10 MeV excitation.

The ^{90}Zr ground state differential cross sections measured at 0°, 10°, and 15° are 275 ± 60 μb, 220 ± 55 μb, and 27 ± 11 μb, respectively. The cross section at 20° (and beyond) falls below our present limit of detectability. The computed ground state angular distribution, similar to those reported by Baer et al. [4] in their study of (p,t) on the even titanium isotopes, is characterized by a sharp forward peak and is a characteristic of the (^{3}He,n) reaction for 0^+ transitions. The computed and measured distributions are in good agreement.

For the (^{3}He,n) reaction, the two protons are transferred as a spin anti-symmetric pair. This is not assured in a heavy ion reaction such as (^{16}O,^{14}C). The reaction ^{88}Sr(^{16}O,^{14}C)^{90}Zr populates three states in ^{90}Zr; the ground state and first 2^+ state with about equal intensities and a 3^- collective octopole state at 2.75 MeV with 30% of the ground state intensity. No higher states were observed. Evidently (^{3}He,n) is much more selective in populating only that state in the residual nucleus with the lowest lying L=0 strength.

A paper describing these results has been submitted for publication.

References

1) A. Arima, private communication.

2) P. R. Christensen, V. I. Manko, F. D. Becchetti, and R. J. Nickles, Nucl. Phys. A207, 33 (1973).

3) Submitted to Nuclear Instruments and Methods.

4) H. W. Baer, J. J. Kraushaar, C. E. Moss, N. S. P. King, R. E. L. Green, P. D. Kunz, and E. Rost, Ann. of Phys. 76, 437 (1973).

5) D. H. Gloeckner, M. H. Macfarlane, R. D. Lawson, and F. J. D. Serduke, Phys. Lett. 40B, 597 (1972).

6) F. D. Becchetti, W. Makofske, and G. W. Greenlees, Nucl. Phys. A190, 437 (1972).

7) F. D. Becchetti, and G. W. Greenlees, Phys. Rev. C4, 1190 (1969).

A10. Study of Isobaric Analog States in the A>90 Region Using the (^{3}He,t) Reaction

W. S. Gray, R. S. Tickle, J. Janecke, and F. D. Becchetti

A program to study isobaric analog states in heavy nuclei with the (^{3}He,t) reaction has recently been initiated. This reaction has been used for many years to study analog states in light- and medium-weight nuclei, but to our knowledge no data have been published for targets heavier than zirconium. Compared with the (p,n) reaction, (^{3}He,t) has the advantage that better resolution can be achieved, thus permitting more accurate determination of level widths and Q values. In addition, many nuclei are accessible which cannot be reached by proton resonance scattering experiments.

Preliminary measurements have been made on targets of ^{116}Sn, ^{124}Sn, and ^{166}Er. These were made using a position-sensitive detector at the image surface of the first analyzing magnet. This scheme makes possible measurements at 0°, the angle at which the ℓ=0 transition to the isobaric

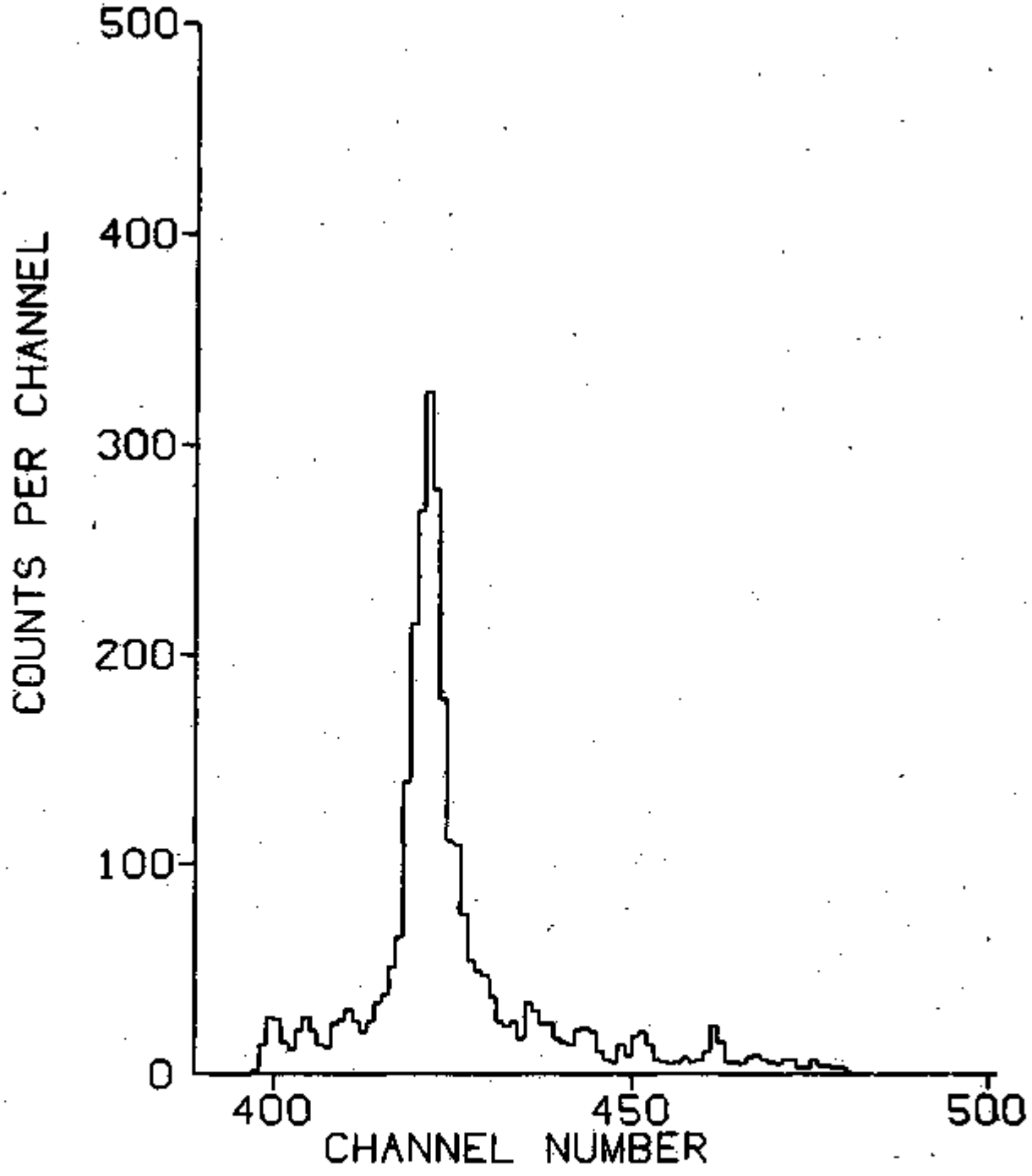

Fig. A10-1. Position spectrum at 0° showing the IAGS peak in ^{116}Sb excited in the $^{116}Sn(^{3}He,t)^{116}Sb$ reaction.

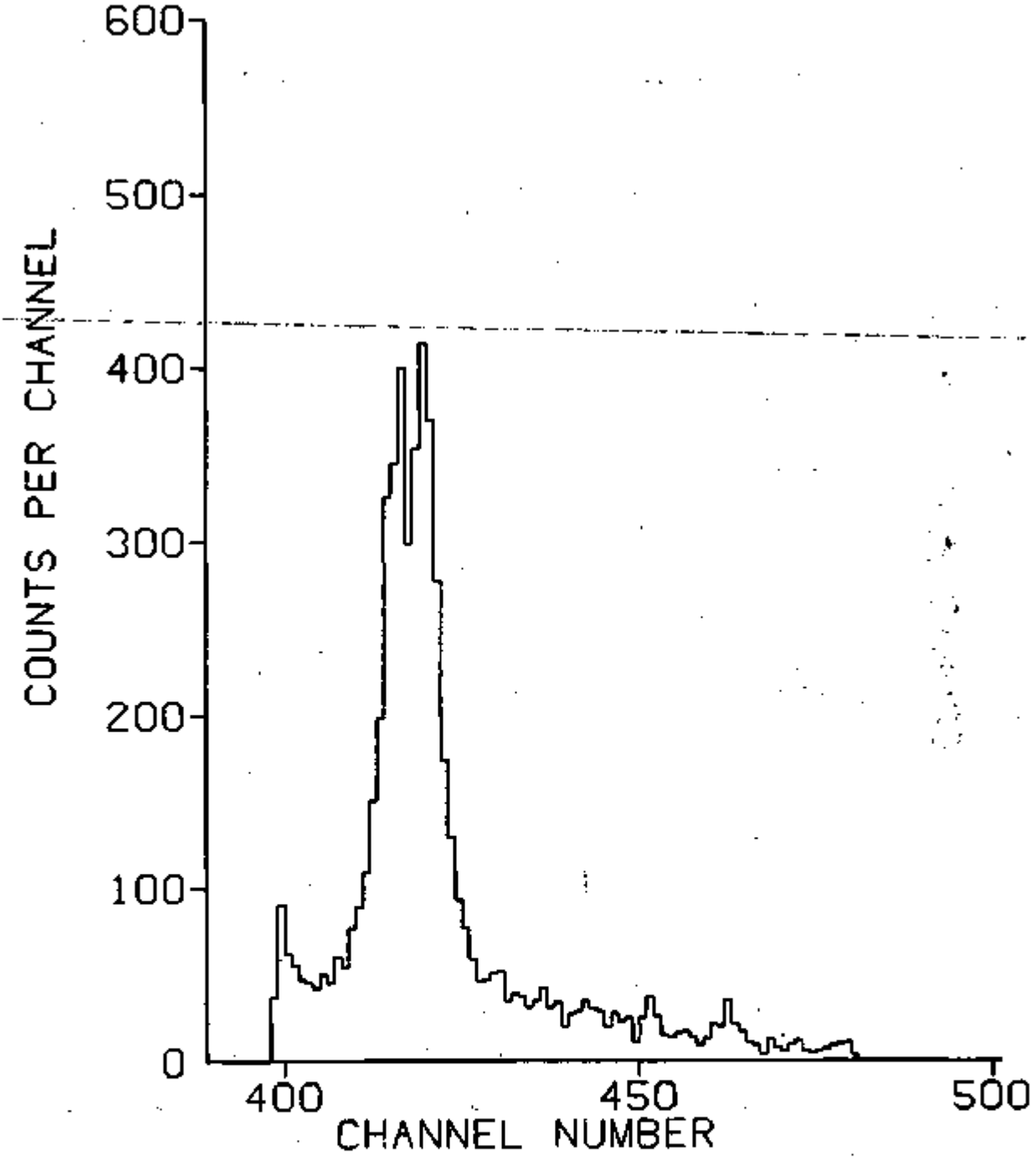

Fig. A10-2. Position spectrum at 0° showing IAGS peak in ^{124}Sb excited in the $^{124}Sn(^{3}He,t)^{124}Sb$ reaction.

analog ground state (IAGS) has its largest cross section. Spectra taken at 0° from ^{116}Sn and ^{124}Sn targets are shown in Figs. A10-1 and A10-2. The bombarding energy was 46.8 MeV. The divided XE/E position spectrum of a single, 50 mm-long detector is plotted. These spectra cover a range of approximately 600 keV of excitation in the residual nucleus. The peaks have been identifed from kinematics as levels in ^{116}Sb and ^{124}Sb which are believed to be the analogs of the ^{116}Sn and ^{124}Sn ground states. Preliminary determinations of the Q values for these transitions are Q = -13.12 and -12.85 MeV, respectively, in agreement with the trend of known Coulomb energies. The prominence of the IAGS peak above the continuous triton background is apparent. At angles other than 0° the peak is not as prominent, but it appears that it will be feasible to measure angular distributions and to search for analogs of excited states of the target.

28773

A11. Structure of ^{159}Tb via Proton Transfer Reactions

J. Splett and W. C. Parkinson

The study of ^{159}Tb via proton transfer reactions continues. ^{159}Tb was selected for scrutiny because of the wealth of unique effects found in the level scheme below ≈ 1.25 MeV of excitation. Early γ-decay work [1] indicated the presence of members of the $7/2^-[523]$ and $5/2^-[532]$ bands, which showed strong coriolis mixing. Early work also indicated the presence of the $1/2^+[411]_\gamma$ vibrational state based on the $3/2^+[411]$ ground state at about 580 keV excitation. The single-particle contribution to the latter was calculated to be approximately 60% by Soloviev and Vogel. [2] In

addition, the positive-parity states showed bandhead angular momenta of 1/2, 3/2, 5/2 and 7/2, indicating the likelihood of strong coriolis mixing. Finally, the $1/2^-[541]$ band, which showed remarkable fragmentation in the holmium experiments performed at this laboratory, appears to be quite distant from any coriolis partners.

In light of these considerations, it was decided that this nucleus should be studied by means of the $^{158}Gd(\alpha,t)^{159}Tb$, $^{158}Gd(^3He,d)^{159}Tb$ and $^{160}Dy(d,^3He)^{159}Tb$ reactions. The first two were to provide energy data and spectroscopic information; the last was to provide a check on the first two as well as a signature of the hole nature of various states (the discrepancy in the Fermi surface makes this a bit tenuous, however).

Angular distributions for the (α,t) reaction at 45.5 MeV and the $(^3He,d)$ reaction at 46.5 MeV have been measured from 0° - 35° and from 0° - 30°, respectively, and have been analyzed by means of J. S. Comfort's peak-fitting program AUTOFIT. The bands present appear to be $3/2^+[411]$, $7/2^-[523]$, $5/2^-[532]$, $5/2^+[413]$, $1/2^+[411]_\gamma$, $7/2^+[404]$, $5/2^+[402]$, $1/2^+[411]$, and $1/2^-[541]$. A comparison between the (α,t) and $(^3He,d)$ angular distributions for the $5/2^+$ member of the $3/2^+[411]$ band yielded an (α,t) normalization of ≈ 44.7 (good to within ≈30%). The (α,t) spectroscopic factors presented in Table AII-1 represent values intermediate between those determined from the Rochester [3] and McMaster [4] data. The $(^3He,d)$ spectroscopic factors will be compared with those given in Table AII-1 to check for reaction discrepancies. In addition, the improved resolution of the $(^3He,d)$ will unfold a number of marginally resolved (α,t) doublets.

$^{160}Dy(d,^3He)^{159}Tb$ spectra were measured at 20°, 25°, and 30° which unfortunately included a high deuteron background because of improper slitting.

TABLE AII-1

^{159}Tb Table of Spectroscopic Information: Experimental Values of $2U^2C^2$.

Level	(^{3}He,d)	(α,t)	Rochester	McMaster[d]
3/2 3/2$^+$[411]	.033	.049	.05	.12
5/2 3/2$^+$[411]	1.37	1.37	1.3	1.98
7/2 3/2$^+$[411]		.15	.11	.24
9/2 3/2$^+$[411]	.32	.12	.31	.16
5/2 5/2$^-$[532]	.015			
5/2 5/2$^+$[413]	.071			.06
7/2 5/2$^-$[532]	.070	.070	.04	.09
7/2 5/2$^+$[413]	.74		.46	.79
9/2 5/2$^-$[532]	.30			.20
11/2 5/2$^-$[532]	1.37	2.66[a]	2.1	2.9
1/2 1/2$^+$[411]$_\gamma$	.08		.05	.07
3/2 1/2$^+$[411]$_\gamma$	.90	1.24	.52	1.05
5/2 1/2$^+$[411]$_\gamma$	.44	.79[b]	.29	.42
7/2 1/2$^+$[411]$_\gamma$	.66			
7/2$^+$[404]	1.68	3.19	1.5	2.3
11/2 7/2$^-$[523]	.63	.94	.43	.86
1/2 1/2$^-$[541]	.20		.09	.18
5/2 1/2$^-$[541]	.83	.70	.47	.79
1/2 1/2$^+$[411]	.18	.22	.02	.5
3/2 1/2$^-$[541]		.03		
3/2 1/2$^+$[411]	.24	.43	.17	.5
5/2$^+$[402]	1.52	3.08[c]	1.9	1.
5/2 1/2$^+$[411]	1.09		.14	
7/2 1/2$^-$[541]	.59			.06
7/2 1/2$^+$[411]	.81	.84	.10	

a) Includes admixed 9/2 5/2$^+$[413] and 1/2 1/2$^+$[411].

b) Includes admixed 7/2 1/2$^+$[411].

c) Includes admixed 3/2 1/2$^+$[411].

d) $2U^2C^2$ was taken as the sum of the experimental values of U^2C^2.

Representative spectra will be remeasured at several angles with no slits in the scattering chamber. These spectra should illustrate the hole nature of the $7/2^-[523]$ and $5/2^+[413]$ bands.

A coriolis plus pairing analysis of the level structure of ^{159}Tb will be performed assuming a pairing gap parameter of 800 keV.[5] The Fermi surface will be adjusted to yield a best fit to the spectroscopic factors.

References

1) G. Winter, L. Funke, K. H. Kaun, P. Kemnita, and H. Sodan, Phys. Lett. 32B, 161 (1970).

2) V. G. Soloviev, S. I. Fedotov, JINR Research Report No. E4-6055, 1971, and related documents.

3) J. S. Boyno, J. R. Huizenga, Phys. Rev. C4, 1411 (1972).

4) D. Burke, (unpublished).

5) E. R. Marshalek, Phys. Rev. 158, 993 (1967).

28774

A12. Study of One-Quasiparticle States in ^{163,165}Ho Observed in the (^{3}He,d) and (α,t) Reactions

D. A. Lewis, A. S. Broad and W. S. Gray

The analysis of the (α,t) and (^{3}He,d) reactions leading to levels in ^{163}Ho and ^{165}Ho, for which some preliminary data were presented in last year's report, is now essentially complete, and the results are being prepared for publication. Angular distributions for the (^{3}He,d) reaction on ^{162}Dy and ^{164}Dy targets were measured over the angular range 0 - 35°, at a bombarding energy of 46.5 MeV. Additional spectra from the (α,t) reactions

on the same targets were also measured. These (α,t) exposures were useful in picking out levels with relatively high spin, since large ℓ transfers are favored by the momentum matching conditions for this reaction.

Several states were observed in both ^{163}Ho and ^{165}Ho which have not been identified in previous work. In particular, these include members of the $5/2^+[402]$ band in ^{163}Ho and the $1/2^-[541]$ band in ^{165}Ho. Also the $K = 5/2$ band beginning at 1056 keV in ^{165}Ho has been identified as the $5/2^+[402]$ band, in contradiction to a tentative assignment of $5/2^-[532]$ from decay work. [1] In addition a few levels appear in both nuclei which could not be identified with any Nilsson state.

The usual procedure for extracting spectroscopic information from stripping reactions on deformed nuclei is to assume that the reaction proceeds by a one-step direct process which can be treated using the DWBA. We have evidence that multistep processes induced by inelastic scattering can have large effects on predicted cross sections. In addition our results suggest that the usual prescription for treating the bound-state wave function is inadequate for stripping reactions on rare-earth targets. These points will be discussed later in this section.

The (^{3}He,d) data were analyzed with the DWBA code DWUCK. The optical parameters used are given in Table A12-1. Members of the $7/2^-[523]$, $3/2^+[411]$, $1/2^+[411]$, $7/2^+[404]$, $1/2^-[541]$, and $5/2^+[402]$ bands were identified in both nuclei. The angular distributions for some of these states are shown in Figs. A12-1 through A12-5. The DWBA curves have been normalized to fit the data. There also were several peaks in the spectra which could not be identified. Usually peak unraveling problems made it impossible to identify ℓ transfers and extract spectroscopic factors for these states.

$^{162}Dy(^{3}He,d)^{163}Ho$

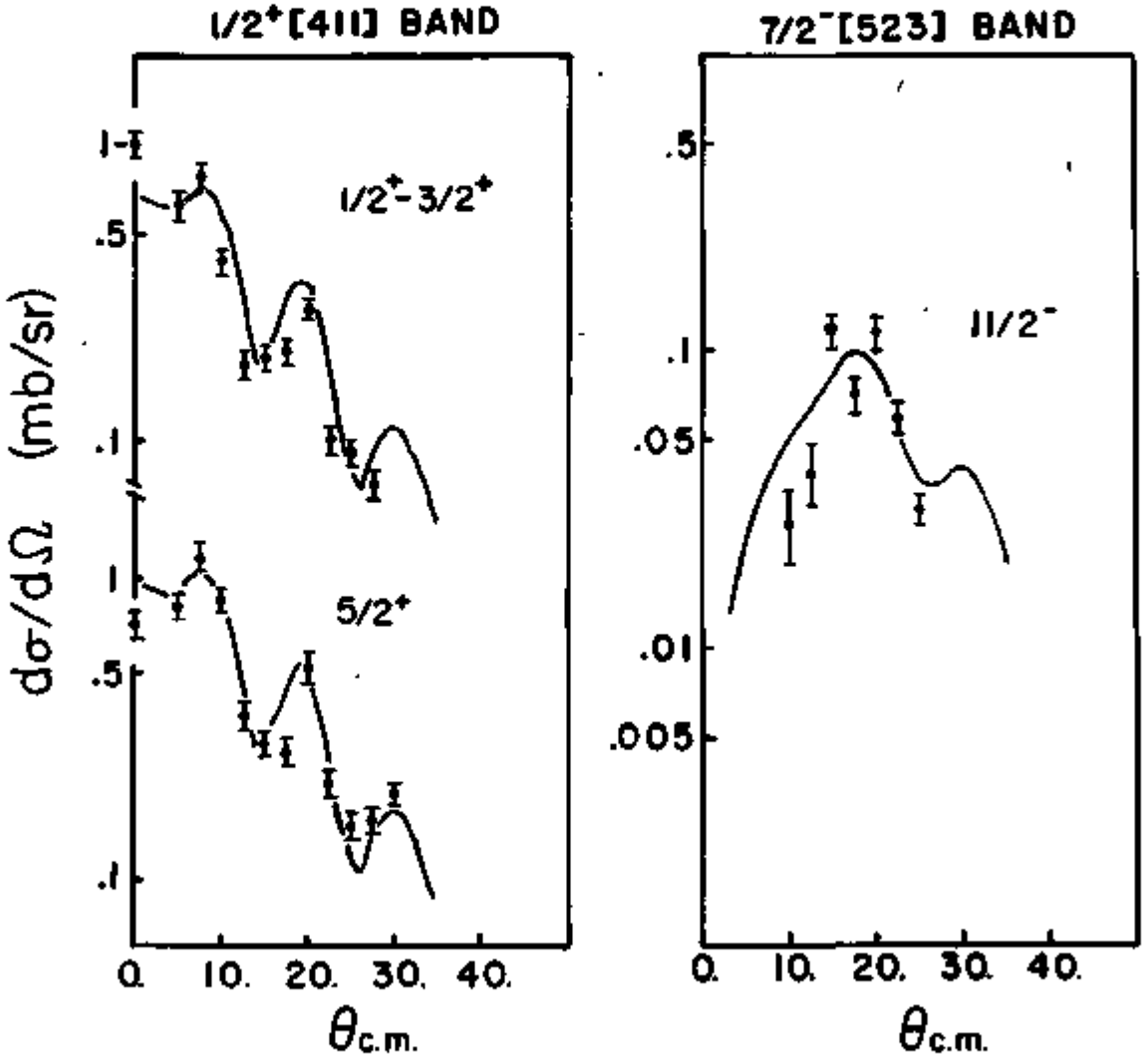

Fig. A12-1.

$^{162}Dy(^{3}He,d)^{163}Ho$

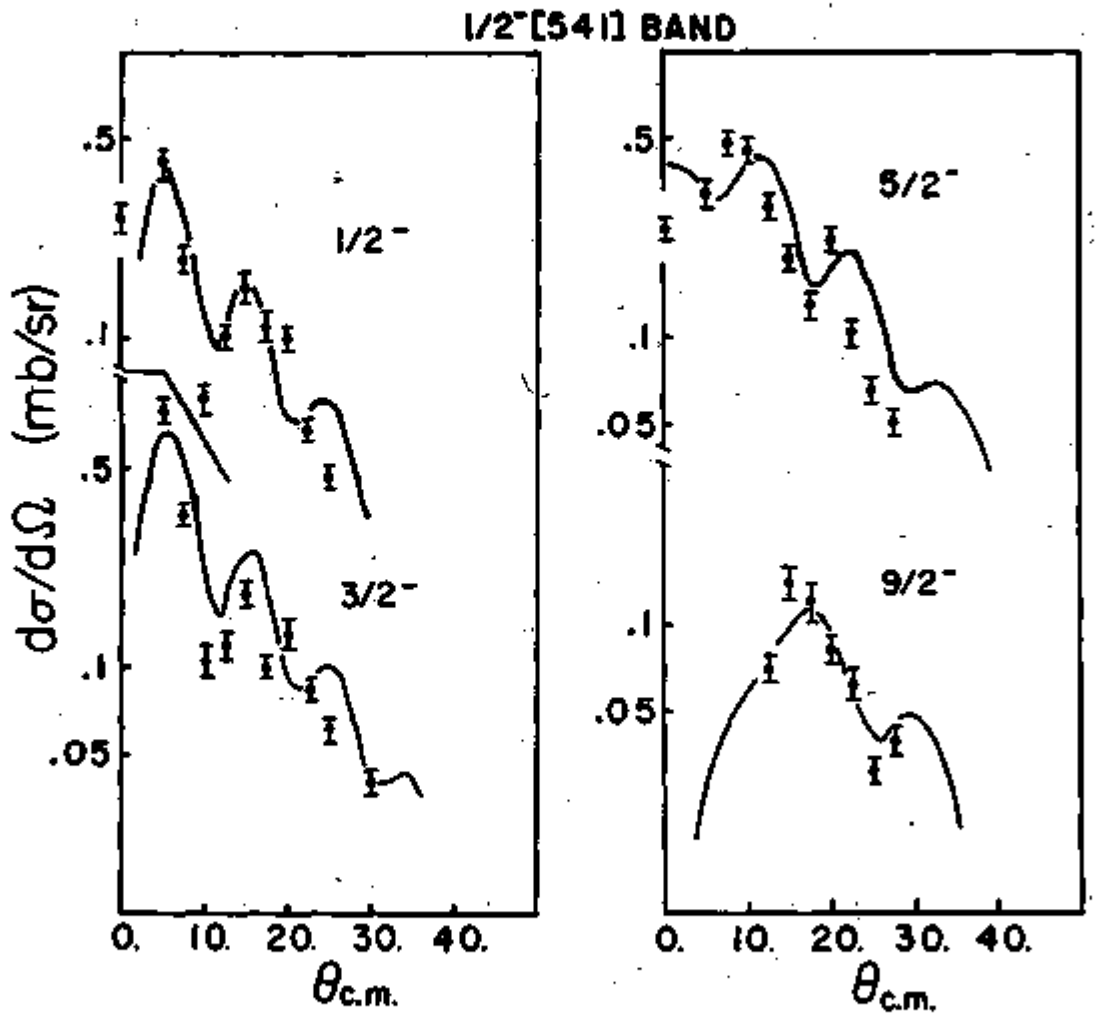

Fig. A12-2.

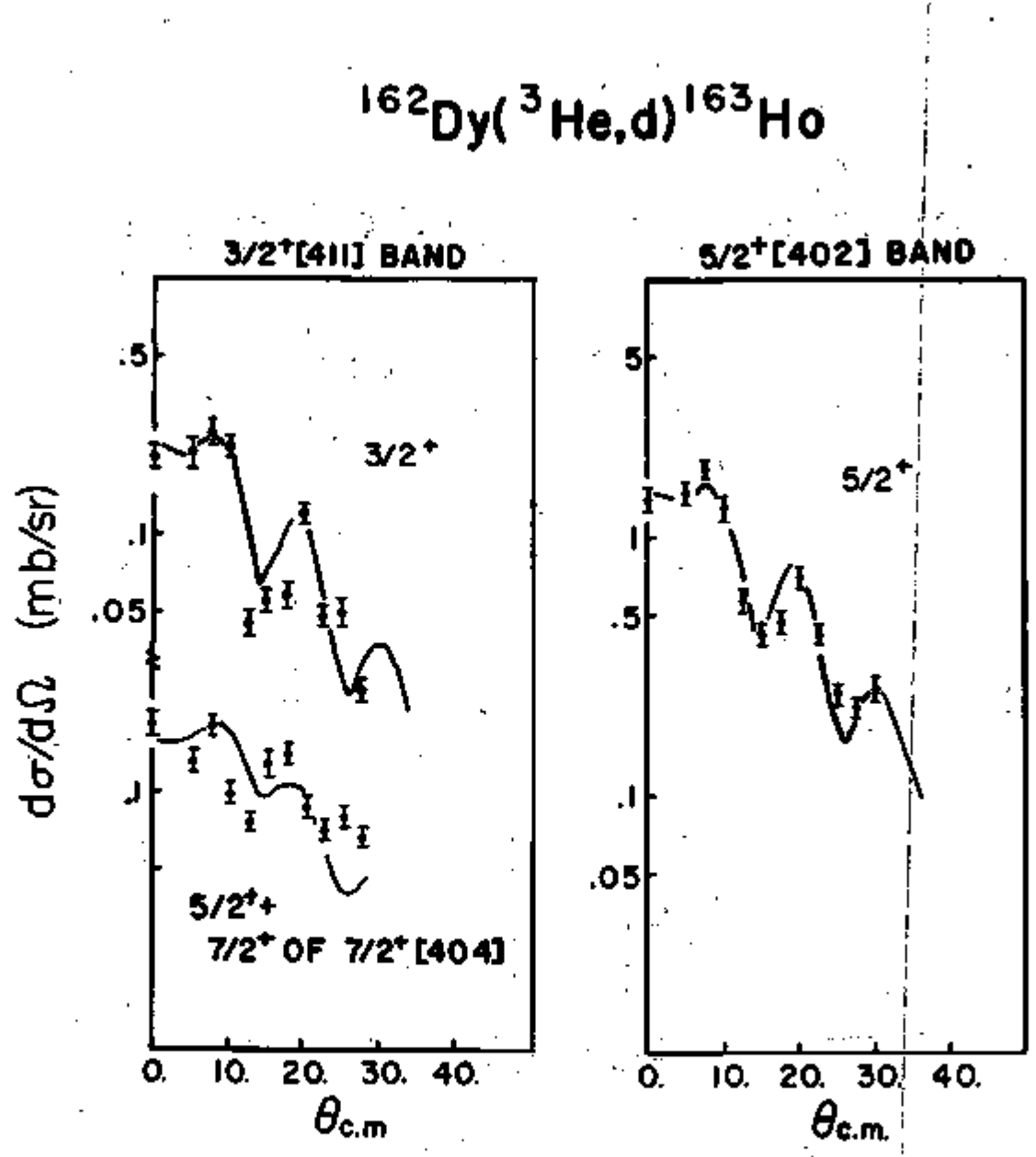
$^{162}Dy(^{3}He,d)^{163}Ho$
3/2⁺[411] BAND
5/2⁺[402] BAND
dσ/dΩ (mb/sr)
.5
.1
.05
.01
3/2⁺
5/2⁺+
7/2⁺ OF 7/2⁺[404]
5
1
.5
.1
.05
5/2⁺
0. 10. 20. 30. 40.
θc.m
0. 10. 20. 30. 40.
θc.m.

Fig. A12-3

$^{164}Dy(^{3}He,d)^{165}Ho$

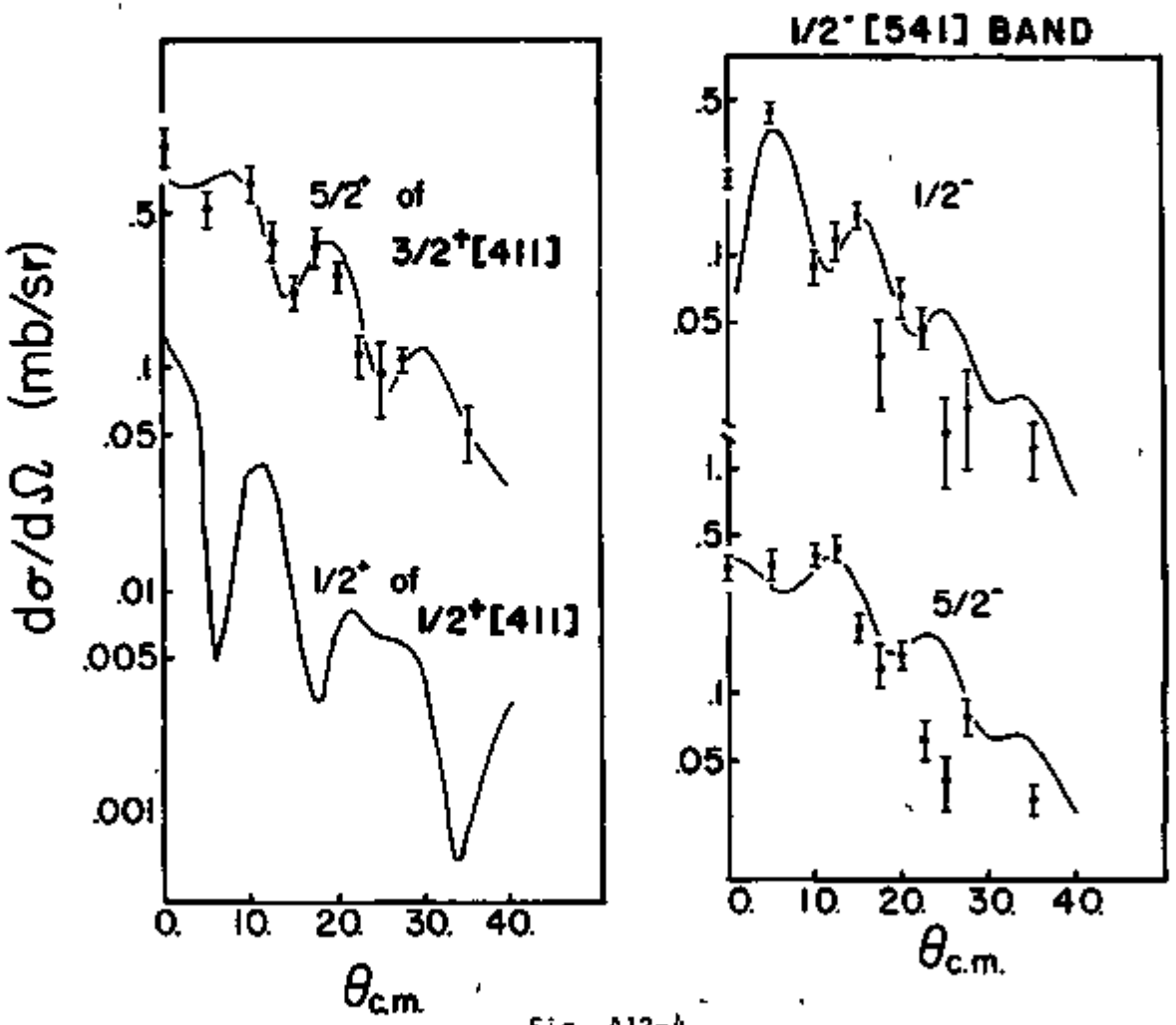

Fig. A12-4.

$^{164}Dy(^{3}He,d)^{165}Ho$

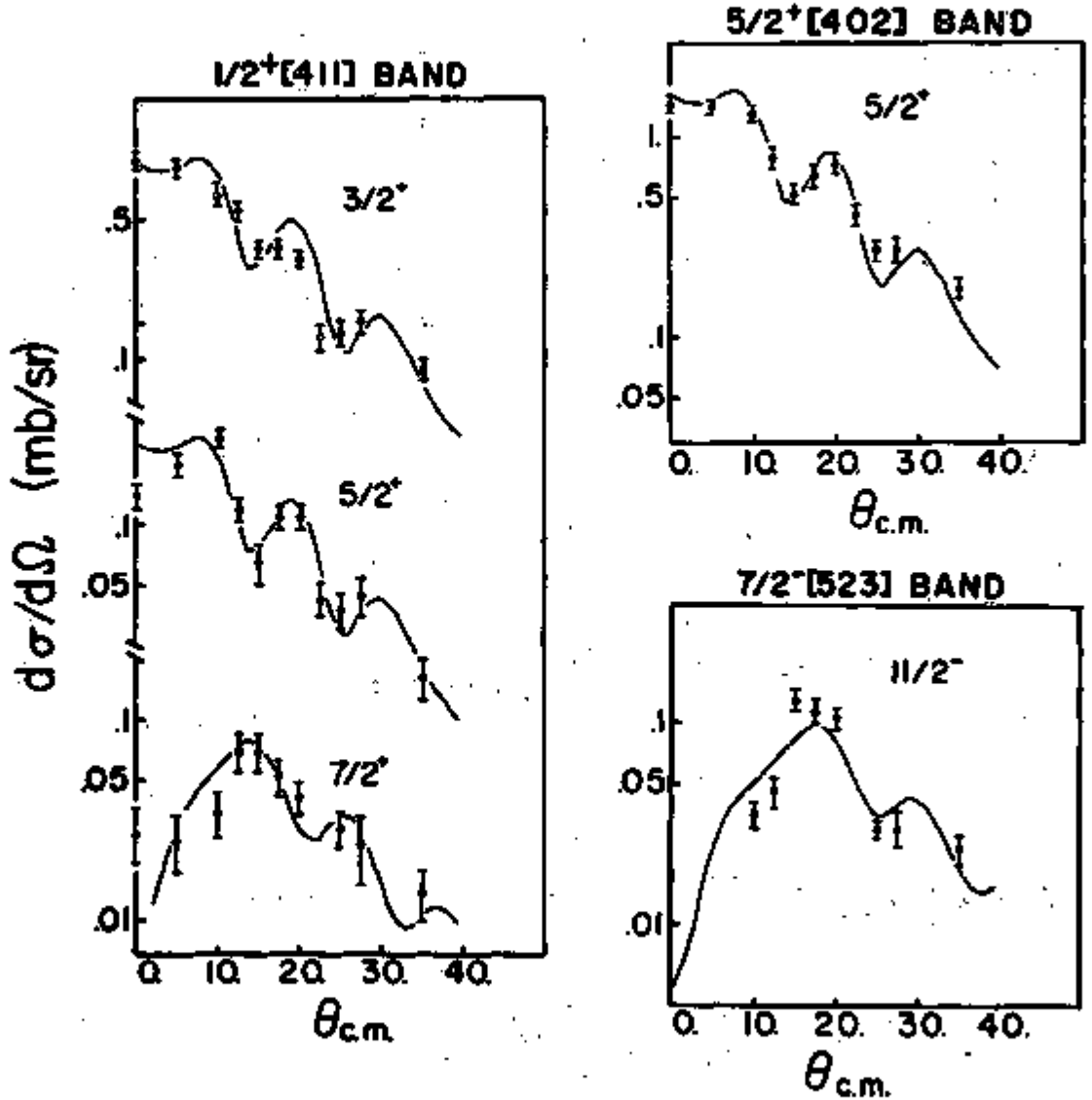

Fig. A12-5.

TABLE A12-1

Particle	V_o (MeV)	r_o (F)	a (F)	W (MeV)	W_D (MeV)	r_o' (F)	a' (F)	r_c (F)	V_{so} (MeV)
d	91	1.16	0.83	0	14.25	1.25	0.90	1.3	0
^{3}He	175	1.14	0.723	17.5	0	1.60	0.90	1.4	0
p	a)	1.25	0.63					1.25	λ=15

a) Adjusted to reproduce the separation energy.

One exception is a fairly well-resolved level with an ℓ transfer of 5 which occurs at about 200 keV of excitation in both ^{163}Ho and ^{165}Ho. From the reaction kinematics and the known percentages of rare-earth impurities in the targets, it has been established that this peak is not due to an impurity.

The spectroscopic factors for the states which were identified are listed in Table A12-2. For deformed nuclei these assume the form $U^2C^2_{\ell j}$ where U^2 is a measure of the emptiness of the level in the target nucleus and $C_{\ell j}$ is the appropriate Nilsson coefficient.

The zero-range approximation was used in the DWBA calculations. Bassel's [2] value of 4.42 was used as an overall normalization for the (^{3}He,d) reaction in order to extract values of $U^2C^2_{\ell j}$.

Along with the experimental values of $U^2C^2_{\ell j}$ in Table A12-2, the predictions of the Nilsson model are given in columns 3 and 8. The coefficients $C_{\ell j}$ were extrapolated from Chi's tables [3] with the parameters δ, κ, μ set equal to 2.5, 0.50, and 0.65, respectively. The value of 2.5 for δ corresponds to β_{20} = 0.30, consistent with the value used in the inelastic

TABLE A12-2

Nilsson State		^{165}Ho Experimental Energy	^{165}Ho Nilsson $U^2C_{\ell j}^2$	^{165}Ho Coriolis $U^2C_{\ell j}^2$	^{165}Ho BOUND $U^2C_{\ell j}^2$	^{165}Ho Experimental $U^2C_{\ell j}^2$	^{163}Ho Experimental Energy	^{163}Ho Nilsson $U^2C_{\ell j}^2$	^{163}Ho Coriolis $U^2C_{\ell j}^2$	^{163}Ho BOUND $U^2C_{\ell j}^2$	^{163}Ho Experimental $U^2C_{\ell j}^2$
$7/2^-[523]$	7/2	0				---	0	.011	.012	.033	.02
	9/2	95				---	100	.008	.009	.05	.08
	11/2	210	.56	.82	.89	.76	222	.56	.83	.88	.79
$3/2^+[411]$	3/2	360	.008	.00	---	<.01	360	.008	.034	.16	.20
	5/2	420	.20	.31	.39	.52	441	.20	.04	.05	---
$1/2^+[411]$	3/2	449	.46	.48	.74	.80	308	.46	.44	.65	.55
	5/2	539	.18	.14	.20	.20	392	.18	.48	.62	.90
	7/2	590	.13	.18	.05	.55	431	.13			---
$1/2^-[541]$	1/2	685	.04	.04	.32	.10	471	.038	.038	.26	.11
	3/2	?	.04	.04	.13	?	578	.041	.043	.13	.17
	5/2	705	.20	.24	1.95	.20	500	.21	.24	1.72	.5
	9/2	?	.57	.82	4.41	?	613	.57	.80	4.05	.95
$7/2^+[404]$		716	.93	1.0	.32	2.0	440	.93	1.1		---
$5/2^+[402]$		1056	.91	.86		1.2	713	.91	.79		1.4

scattering calculation to be discussed below. The emptiness parameter U^2 was calculated using the pairing force treated in the usual BCS approximation. The gap parameter Δ was set equal to 650 keV, the value suggested by the even-odd mass differences. A survey by Ogle et al. [4] suggests that the chemical potential λ should be just below the ground state in the holmium isotopes. It was placed 100 keV below the ground state.

The theoretical predictions for $U^2C^2_{\ell j}$ are significantly improved if the coriolis coupling between particle motion and core rotation is included. This coupling introduces an additional term (H_{RPC}) into the Hamiltonian which mixes all the single-particle bands which originate in a given major oscillator shell. The basis used to diagonalize H_{RPC} should include all of these states. Unfortunately, only the energies of the bands nearest the ground state are known. Usually the energies predicted by the Nilsson model are within about 0.5 MeV of experimentally observed energies. Consequently, H_{RPC} was first diagonalized in a basis in which the states whose energies are not known experimentally were placed at the energies predicted by the Nilsson model. The energy of each of these states was then moved up and down 0.5 MeV to determine what effect this would have on the spectroscopic factors. All states predicted by the Nilsson model to be within 5 MeV of the ground state were included in the calculation. In many cases the presence of these additional states had a significant effect on spectroscopic factors of the low-lying states in the spectrum. However, in every case variations of $\pm$ 0.5 MeV in energies had almost no effect.

No systematic attempt was made to fit experimental energies by varying bandhead energies and moments of inertia. In cases where strong mixing occurred for bands near each other, small changes were made in bandhead

energies to test the sensitivity of the predicted spectroscopic factors to the precise positions of these states. In all cases in these holmium isotopes, small changes in the energies had only negligible effects.

The results of this calculation are given in columns 4 and 9 of Table A12-2. The overall agreement with the experimental values of $U^2C^2_{\ell j}$ is greatly improved. In particular one can understand why the $3/2^+[411]$ bandhead is observed in ^{163}Ho and not in ^{165}Ho. However, the theoretical prediction of $U^2C^2_{\ell j}$ for this state is still a factor six too small for ^{163}Ho.

Some of the remaining discrepancies between theoretical and experimental values of $U^2C^2_{\ell j}$ are due to the use of unrealistic form factors in the reaction calculations. A method for generating improved bound-state wavefunctions was discussed in the progress report of May 1972, and is based on a procedure due to Rost. [5] The wavefunctions are generated in a deformed Woods-Saxon well with $\Delta N=2$ mixing and the effect of continuum states included in a natural way. This is in contrast to the usual procedure in which one assumes the components of the wavefunction are simply $C_{\ell j}\ \phi_{N\ell jr}$ where $\phi_{N\ell jr}$ is the wavefunction of a proton bound in a spherical Woods-Saxon well.

For the components of the wavefunction which have $C_{\ell j} \sim 1$, there is little difference between calculations based on Rost's method and the usual procedure. This is evident from Fig. A12-6 in which the radial part of the $j = 11/2$ component of the $7/2^-[523]$ state in ^{165}Ho is plotted. The curves resulting from the two procedures lie on top of each other. This is not the case for components which have smaller values of $C_{\ell j}$. Figures A12-7 and A12-8 display the results for the $7/2^+$ component of the $1/2^+[411]$ state in ^{165}Ho and the $3/2^+$ component of the $3/2^+[411]$ state in ^{163}Ho. The

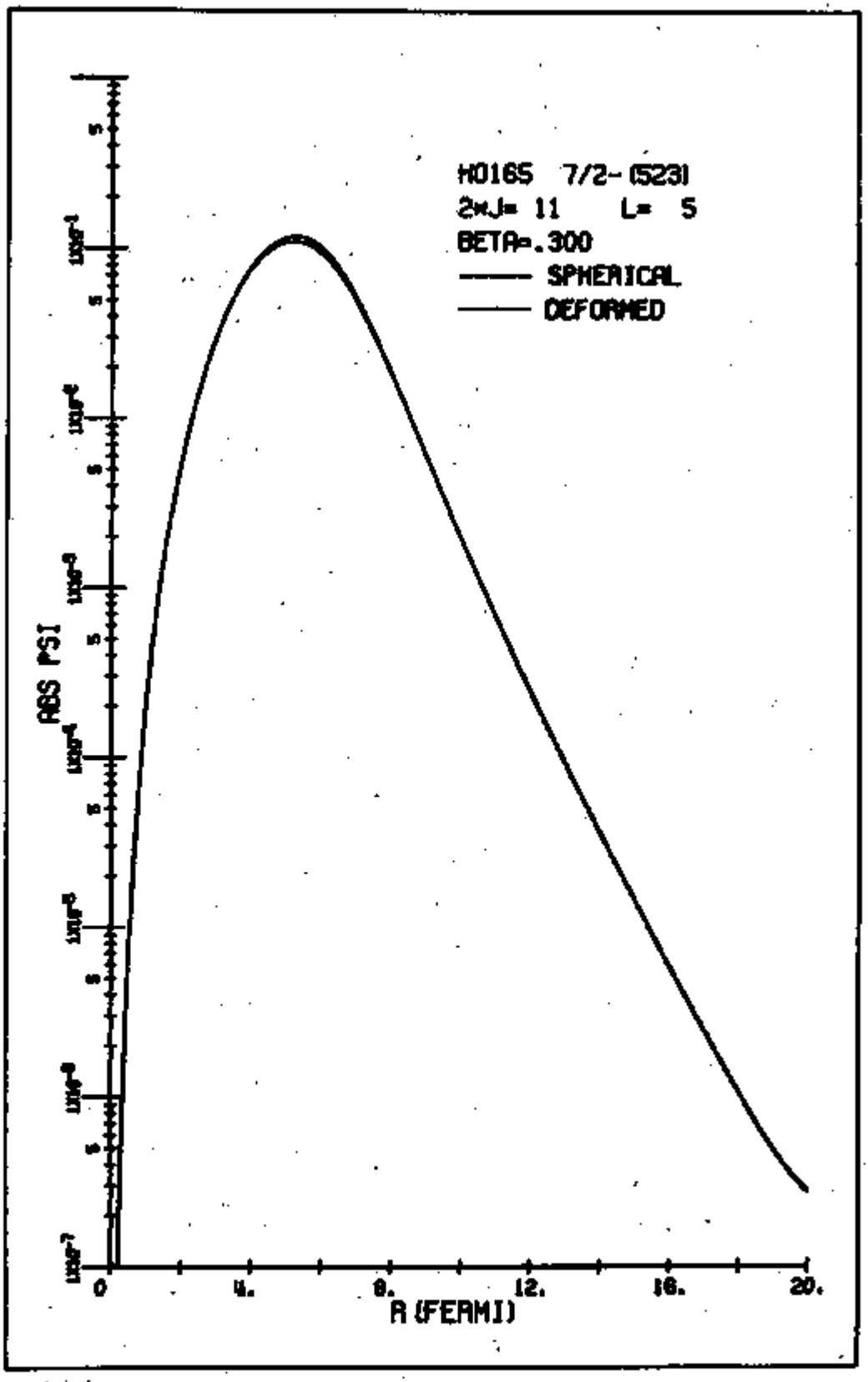
H0165 7/2-[523]
2xJ= 11 L= 5
BETA=.300
SPHERICAL
DEFORMED
ABS PSI
0
4.
8.
12.
16.
20.
R (FERMI)

Fig. A12-6.

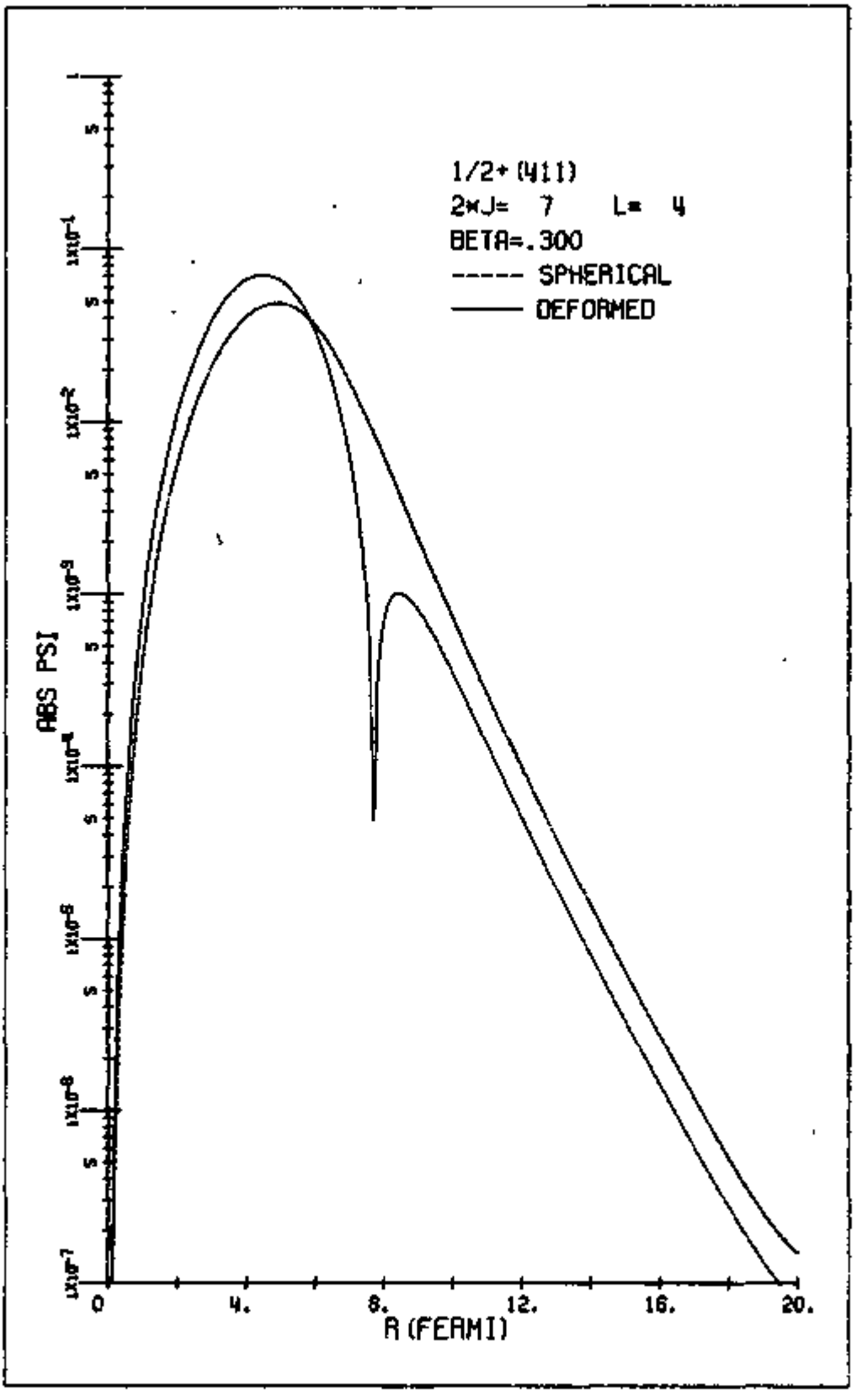
1/2+ (411)
2*J= 7 L= 4
BETA=.300
----- SPHERICAL
—— DEFORMED
ABS PSI
R (FERMI)
0
4.
8.
12.
16.
20.

Fig. A12-7.

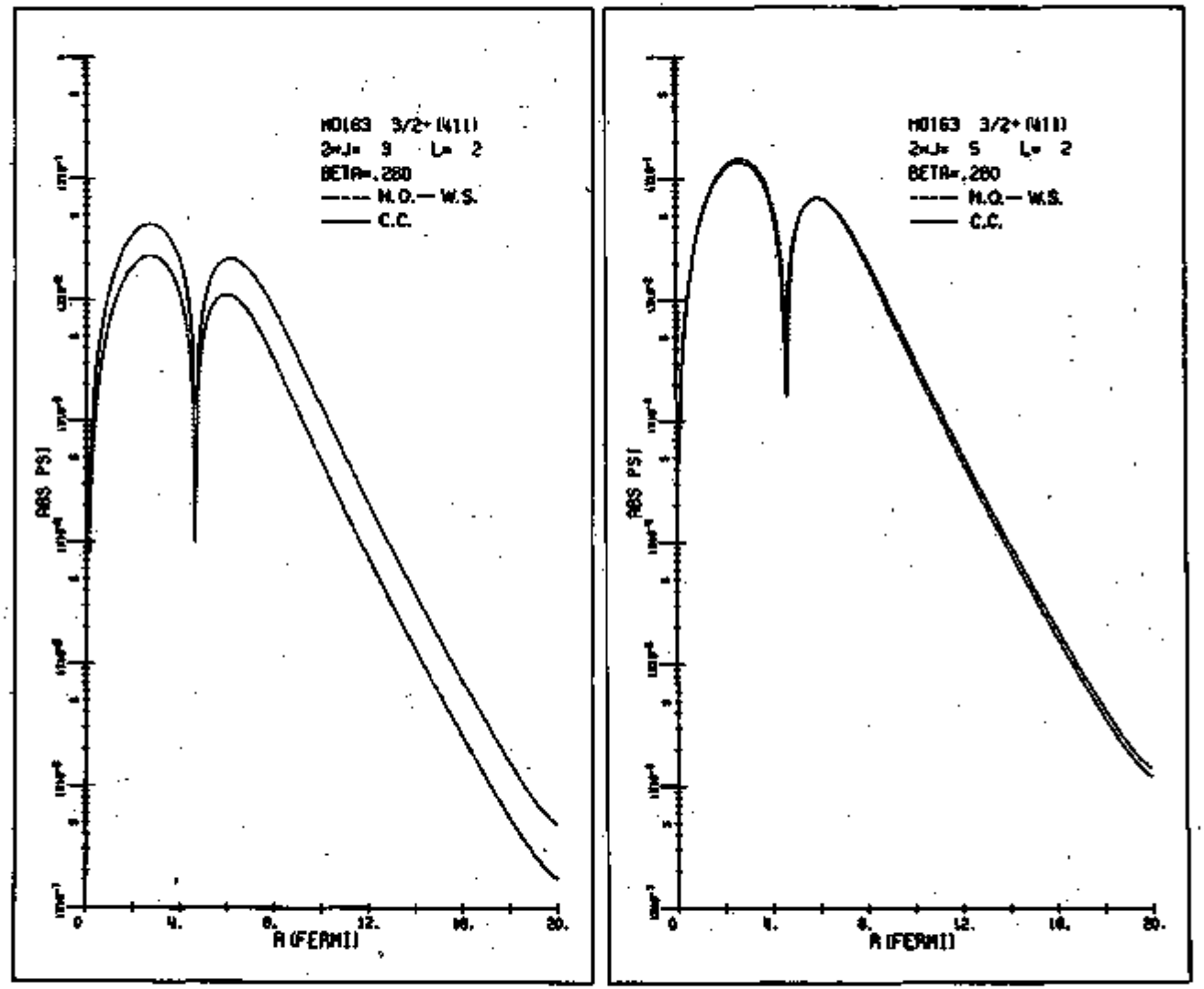
H0163 3/2+ [411]
2*J= 3 L= 2
BETA=.280
---- H.O.— W.S.
—— C.C.
RHS PSI
R (FERMI)
H0163 3/2+ [411]
2*J= 5 L= 2
BETA=.280
---- H.O.— W.S.
—— C.C.
RHS PSI
R (FERMI)

Fig. A12-8.

additional node in the $7/2^+$ component of the $1/2^+[411]$ state is probably due to $\Delta N=2$ mixing with the $1/2^+[660]$ state.

It is apparent from the figures that the slopes of the wavefunctions generated by the two procedures are identical in the tail region. This is a result of adjusting the well depth to reproduce the correct binding energy of the proton. Since the (^{3}He,d) reaction is surface peaked, the shapes of the predicted angular distributions will be about the same for both methods of calculating the form factors, but the magnitudes will differ. If the spectroscopic factors are corrected for this effect, one obtains the results listed in columns 5 and 10 of Table A12-2. The striking difference in the extracted values of $U^2C^2_{\ell j}$ for the $3/2^+[411]$ bandheads in ^{163}Ho and ^{165}Ho can now be understood. The overall agreement for the first three bands is much improved with one exception. The theoretical value of $U^2C^2_{\ell j}$ for the $7/2^+$ member of the $1/2^+[411]$ band is now a factor 10 too small. In addition, the predictions for the $1/2^-[541]$ band are made considerably worse.

Before trying to explain these discouraging results, it is advantageous to first consider the effects of inelastic processes on the proton transfer reaction cross sections. It was noted in last year's progress report that the elastic scattering cross sections for ^{166}Er(d,d), E_d = 29 MeV, and ^{162}Dy(^{3}He,^{3}He), E_{He} = 45 MeV, could not be reproduced by optical model calculations using reasonable parameters. This difficulty was ascribed to the strong coupling expected between the elastic channel and inelastic excitation of low-lying rotational states of the target. Since then the cross sections for the elastic and the inelastic scattering to the first 2^+ state have been measured for ^{166}Er + d at 34.5 MeV and ^{162}Dy + ^{3}He at 46.5 MeV and the data subjected to a coupled-channels analysis. The coupled-channels calculations

were performed with the assistance of P. J. and A. D. Ellis of Oxford University. The ground state, 2^+ state, and 4^+ state were included in the coupled-channels basis, although the cross section for the 4^+ state was not measured. The optical model parameters of Parkinson et al. [6] for the ^{3}He channel and of Hinterberger et al. [7] for the deuteron channel were used in the analysis (see Table A12-1). These parameter sets were derived from experiments in the lead region and the optical model predictions do not reproduce the elastic scattering from Dy and Er. However, it was found that using these parameters and a reasonable value for the deformation parameter β_2 of 0.28, the coupled-channels predictions gave good fits to both the elastic and the inelastic scattering cross sections for each projectile. The coupled-channels and optical model predictions are compared with the data in Figs. A12-9 and A12-10. Including direct hexadecapole excitation of the 4^+ state, with the rather small value of β_4 which has been determined from other experiments for nuclei in the $A \sim 165$ region, was found to have no significant effect on the predicted 0^+ and 2^+ cross sections. However, a reasonable fit to the ^{3}He inelastic scattering was achieved only with a deformed Coulomb potential, a refinement which was not required to reproduce the deuteron scattering.

These results suggest that parameters from the lead region (Table A12-1) are appropriate for analysis of the (^{3}He,d) reaction on rare-earth nuclei, but only on a coupled-channels basis in which the effects of indirect processes are included.

Some preliminary coupled-channels (CCBA) calculations have been made for the (^{3}He,d) reaction at Oxford University, with the help of P. J. and A. D. Ellis. A computer code based on the source-term formalism of Ascuitto

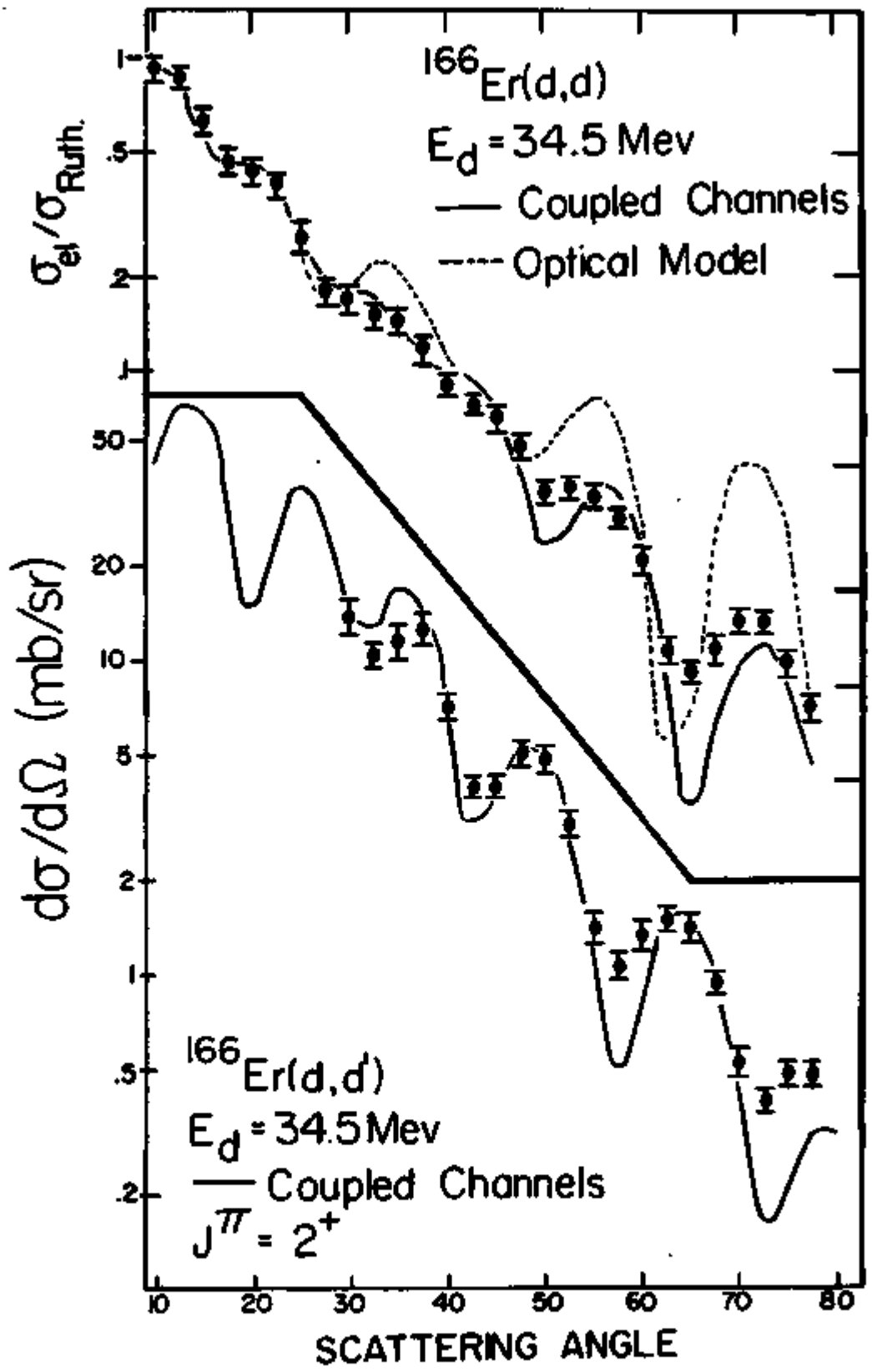
^{166}Er(d,d)
E_d = 34.5 Mev
Coupled Channels
Optical Model
$\sigma_{el}/\sigma_{Ruth.}$
$d\sigma/d\Omega$ (mb/sr)
^{166}Er(d,d')
E_d = 34.5 Mev
Coupled Channels
$J^{\pi} = 2^+$
SCATTERING ANGLE

Fig. A12-9.

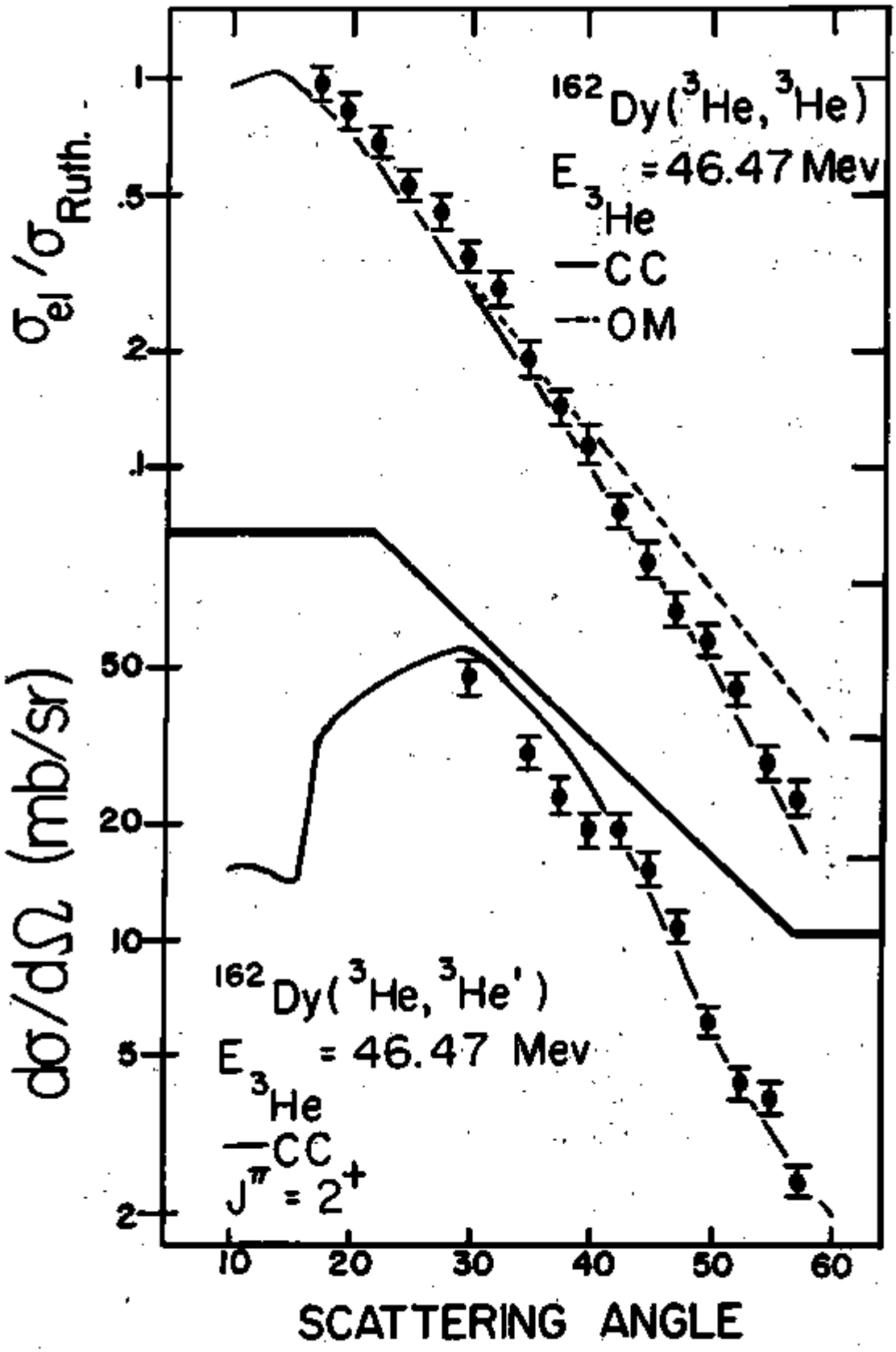
^{162}Dy(^{3}He, ^{3}He)
$E_{^3He}$ = 46.47 Mev
—CC
---OM
$\sigma_{el}/\sigma_{Ruth.}$
1
.5
2
.1
$d\sigma/d\Omega$ (mb/sr)
50
20
10
5
2
^{162}Dy(^{3}He, ^{3}He')
$E_{^3He}$ = 46.47 Mev
—CC
$J^\pi = 2^+$
10
20
30
40
50
60
SCATTERING ANGLE

Fig. A12-10.

and Glendenning [8] was used. Unfortunately, these calculations were made only for reactions leading to states in ^{163}Ho and coriolis effects were not included. Nevertheless the results are quite illuminating. The predicted angular distributions can be divided into three classes:

(a) Those for which CCBA agrees with DWBA if the same form factors are used. This class includes the $11/2^-$ member of the $7/2^-[523]$ band, the $3/2^+$ and $5/2^+$ members of the $3/2^+[411]$ band, and the $3/2^+$ and $5/2^+$ members of the $1/2^+[411]$ band.

(b) Those for which the CCBA angular distributions have the same shape as the DWBA curves, but different magnitudes. This class includes the $7/2^+$ member of the $1/2^+[411]$ band and the $5/2^+[402]$ bandhead.

(c) Those for which the CCBA angular distributions disagree with DWBA in both magnitude and shape. The members of the $1/2^-[541]$ band fall into this class.

The CCBA and DWBA angular distributions predicted for selected levels are plotted along with the data in Figs. A12-11 and A12-12. Rost's procedure was used to generate the form factor for the CCBA calculation, and form factors for the DWBA calculation were made in the usual way. These curves have not been normalized to fit the data, but rather reflect the values of $C^2_{\ell j}$ predicted by the two methods for generating the bound-state wave function.

Because of the strong interference which occurs between competing processes in the transitions of classes (b) and (c), one cannot predict with certainty what the results of a CCBA calculation, with coriolis coupling included, would be for these states. This calculation is planned for the near future. In the meantime certain tentative conclusions can be

$^{162}Dy(^{3}He,d)^{163}Ho$

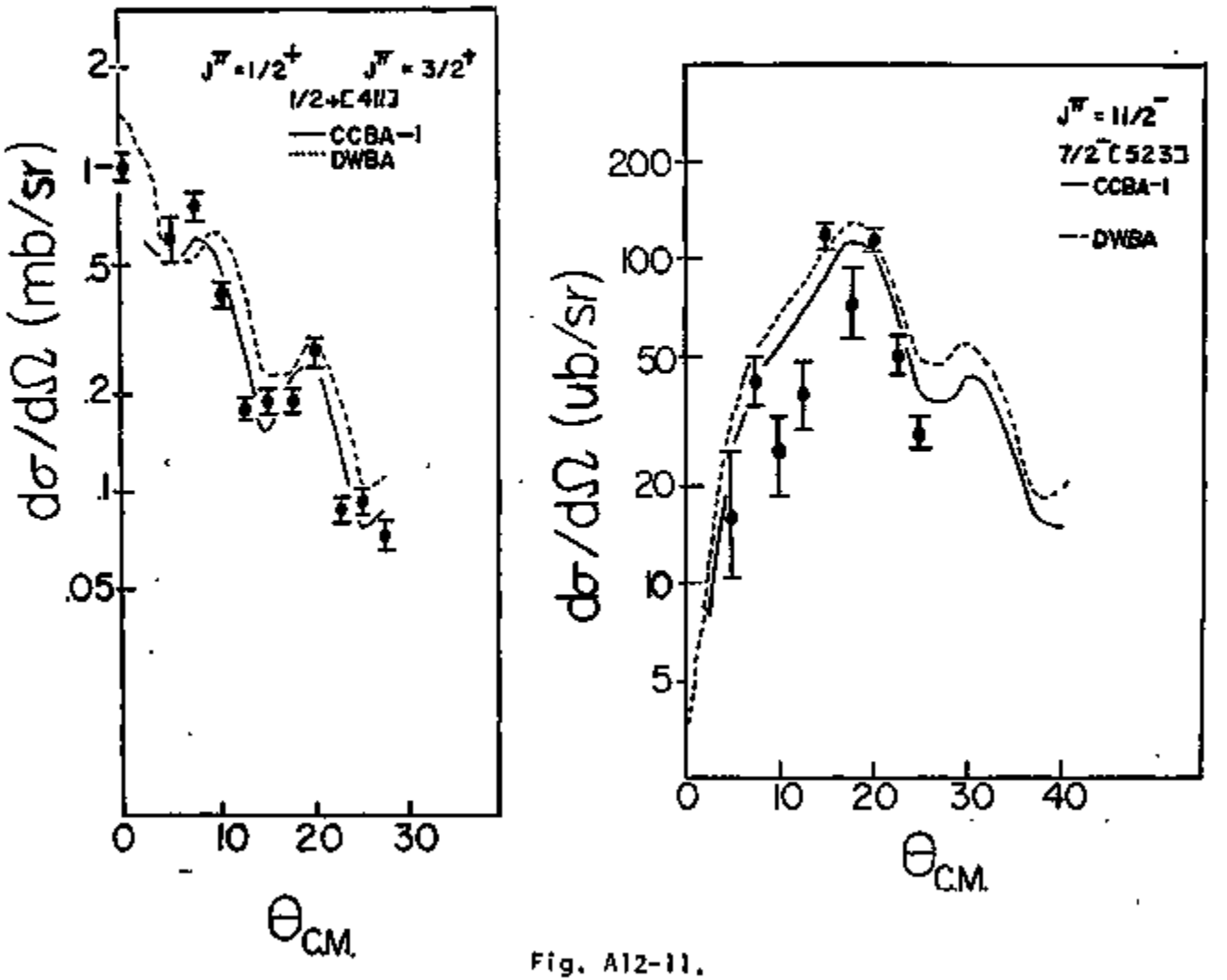

Fig. A12-11.

$^{162}Dy(^{3}He,d)^{163}Ho$

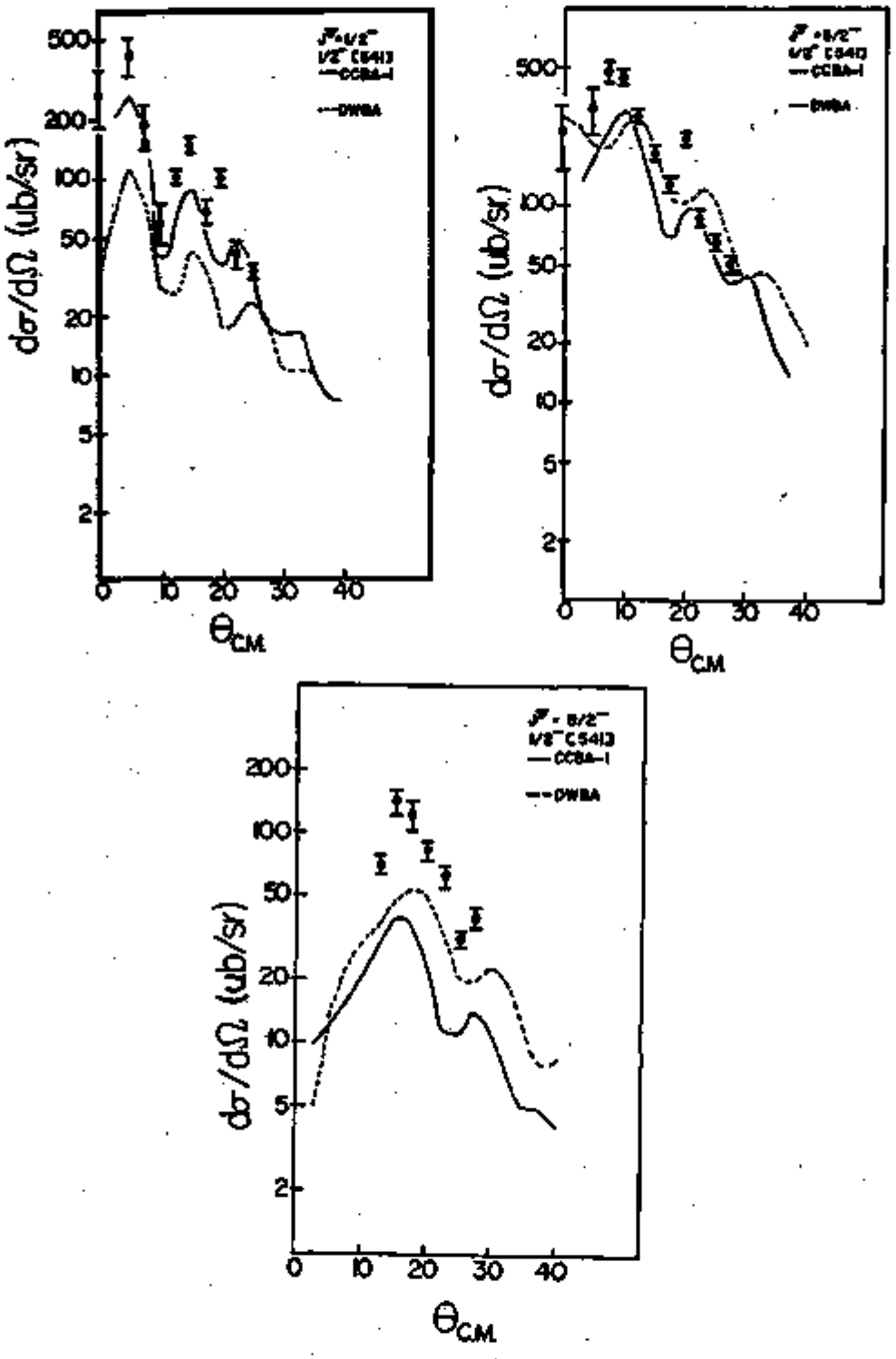

Fig. A12-12.

drawn:

(1) If the CCBA predictions are affected by coriolis mixing in the same way as those of the DWBA (columns 4 and 9 of Table A12-2), the result would be excellent agreement between theory and experiment for the levels of classes (a) and (b). In particular the anomolously large spectroscopic factor obtained for the $3/2^+[411]$ bandhead would be explained by coriolis mixing and form factor effects. Also if calculations from ^{163}Ho are applied to the $7/2^+$ member of the $1/2^+[411]$ band in ^{165}Ho and the CCBA prediction is coriolis shifted, the agreement is again excellent. The order of magnitude discrepancy between columns 4 and 5 (Table A12-2) for this level is removed by constructive interference appearing in the CCBA calculation.

(2) For levels in class (c), i.e., the members of the $1/2^-[541]$ band, if coriolis mixing is taken into account by simply shifting the CCBA predictions, the agreement is still poor but better than that obtained with the DWBA. It is also noteworthy that CCBA angular distributions are much closer in shape to the experimental ones, particularly for the $5/2^-$ and $9/2^-$ levels.

These tentative conclusions can be confirmed only when a full CCBA calculation for both ^{163}Ho and ^{165}Ho, with coriolis effects included in the form factors, is completed. This calculation is planned for the near future.

References

1) G. Mauron, J. Kern, and O. Huber, Nucl. Phys. A181, 489 (1972).

2) R. H. Bassel, Phys. Rev. 149, 791 (1966).

3) B. E. Chi, Nucl. Phys. 83, 87 (1966).

4) W. Ogle, S. Wahlborn, R. Piepenbring, Rev. Mod. Phys. 43, 424 (1971).

5) E. Rost, Phys. Rev. 154, 994 (1967).

6) W. C. Parkinson, D. L. Hendrie, H. H. Duhm, J. Mahoney, and J. Saudinos, Phys. Rev. 178, 1976 (1969).

7) F. Hinterberger, G. Mairle, U. Schmidt-Rohr, G. J. Wagner, and P. Turek, Nucl. Phys. A111, 265 (1968).

8) R. J. Ascultto and Norman K. Glendenning, Phys. Rev. 181, 1396 (1969).

A13. The Ordering of Nucleon Levels for A > 200

F. D. Becchetti

Data from the $^{208}Pb(^{16}O,^{15}O)^{209}Pb$ [1] and $^{208}Pb(^{16}O,^{15}N)^{209}Bi$ reactions [2] have been analyzed with finite range DWBA. [3] Information about the neutron and proton single-particle potentials in heavy nuclei (A > 200) has been deduced. Good agreement between calculated and observed level positions and spectroscopic factors has been obtained with the Batty-Greenlees proton potential [4] and a modified form of the Zaidi-Darmodjo neutron potential [5] having a spin-orbit potential with $r_{so} < r_R$. These potentials have been used to calculate single-particle level spacings near A ≈ 300 and yield the results shown in Fig. A13-1. The magic numbers (defined here as having gaps >1 MeV) occur for Z = 114 and 126, N = 148, 184 and (barely) N = 210. The largest gaps are at Z = 114 and N = 184 (2.5 and 3.5 MeV, respectively). Many of the shell closures predicted by other calculations (see summary in Ref. 6) are not apparent in the present calculations, e.g., those at N = 164, 196, 228 and 236. Also, the predicted gap at N = 184 is much wider (by about 1 MeV) than previous calculations and this suggests that Z = 114 or 126 and N = 184 are the most suitable candidates for stable nuclei near A = 300.

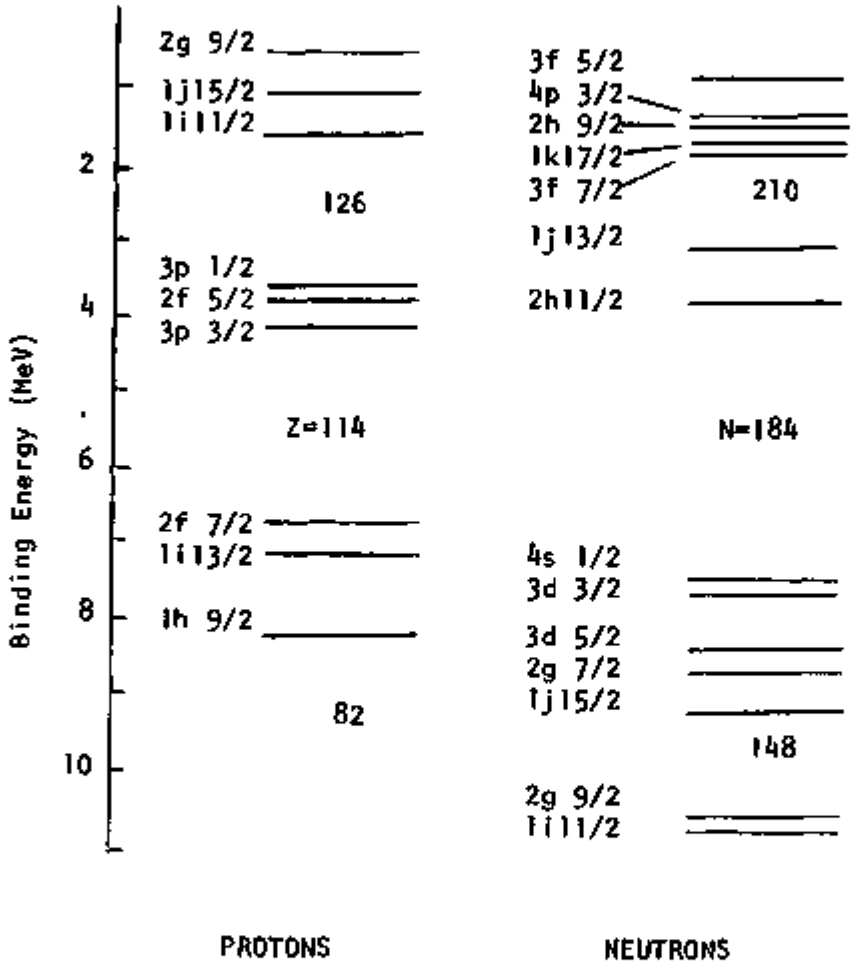

Fig. A13-1. Predicted levels, A $\gtrsim$ 300.

References

1) F. Becchetti, B. G. Harvey, D. Kovar, J. Mahoney, C. Maguire and D. K. Scott, Lawrence Berkeley Laboratory Progress Report (1973, unpublished).

2) D. Kovar, et al., Phys. Rev. Lett. 30, 1075 (1973).

3) Program LOLA, R. DeVries (unpublished).

4) C. J. Batty and G. W. Greenlees, Nucl. Phys. A133, 673 (1969).

5) S. A. A. Zaidi and S. Darmodjo, Phys. Rev. Lett. 19, 1446 (1967).

6) P. E. Nemirovskii and B. N. Vinogradov, Yad. Fiz. 14, 972 (1971) [English translations: Soviet J. Nucl. Phys. 14, 545 (1972)].

28775

A14. High Angular Momentum States in the Lead Isotopes

R. S. Tickle, W. S. Gray, and W. C. Parkinson

Our experimental knowledge of high angular momentum states in the lead region is limited because large orbital angular momentum transfers are required to excite these states. Most of our spectroscopic information has been obtained from single-nucleon transfer reactions such as the (d,p), (d,t), and (^{3}He,d) reactions which transfer only a few units of orbital angular momentum and hence are unsuited for populating high angular momentum states. To study these states, we have used the (α,^{3}He) reaction which has a favored angular momentum transfer of 7 units at the bombarding energy used (58 MeV).

Experimental results from the ^{208}Pb(α,^{3}He)^{209}Pb reaction summarized in an earlier progress report have been augmented by additional measurements. Only three levels in ^{209}Pb are strongly excited by this reaction ($g_{9/2}$ ground

state, $i_{11/2}$ state at 0.78 MeV, and the $j_{15/2}$ state at 1.426 MeV). The angular distributions (see Fig. A14-1) for the $g_{9/2}$ and $j_{15/2}$ states have been measured at the forward scattering angles down to 2.5° (the $i_{11/2}$ state is obscured by an impurity at angles less than 10°). In addition, the $^{208}Pb(\alpha,\alpha)$ elastic scattering at 58 MeV has been measured in the angular range from 10° to 90°.

Of particular interest in this work is the spectroscopic factor for the $j_{15/2}$ level at 1.426 MeV in ^{209}Pb. For this level, Igo et al. [1] have measured a spectroscopic factor of 0.49 using the (t,d) reaction at 20 MeV while Ellegaard et al. [2] measured a spectroscopic factor of 0.53 using the (d,p) reaction at 12 MeV. These small spectroscopic factors imply that approximately 50% of the $j_{15/2}$ strength is to be found in other levels.

Hamamoto [3] has investigated the effects of particle-vibration coupling on the single-neutron states in ^{209}Pb and, in particular, on the fragmentation of the $j_{15/2}$ strength. Based on mixing between the $j_{15/2}$ single-neutron state and the $15/2^-$ members of the $|3^-;g_{9/2}>$ and the $|3^-;i_{11/2}>$ particle-vibration multiplets, Hamamoto's calculations predict the missing $j_{15/2}$ strength is carried in two fragments; one at 3.21 MeV containing 26% of the total strength and the other at 3.50 MeV with 10% of the total strength.

We have measured spectra up to 6 MeV excitation in ^{209}Pb and, contrary to the earlier experimental and theoretical work, find no evidence for appreciable fragmentation of the $j_{15/2}$ strength.

Distorted-wave calculations using the computer code DWUCK have been carried out to determine spectroscopic factors for the three strongly excited levels. Thus far it has not been possible to find a set of optical

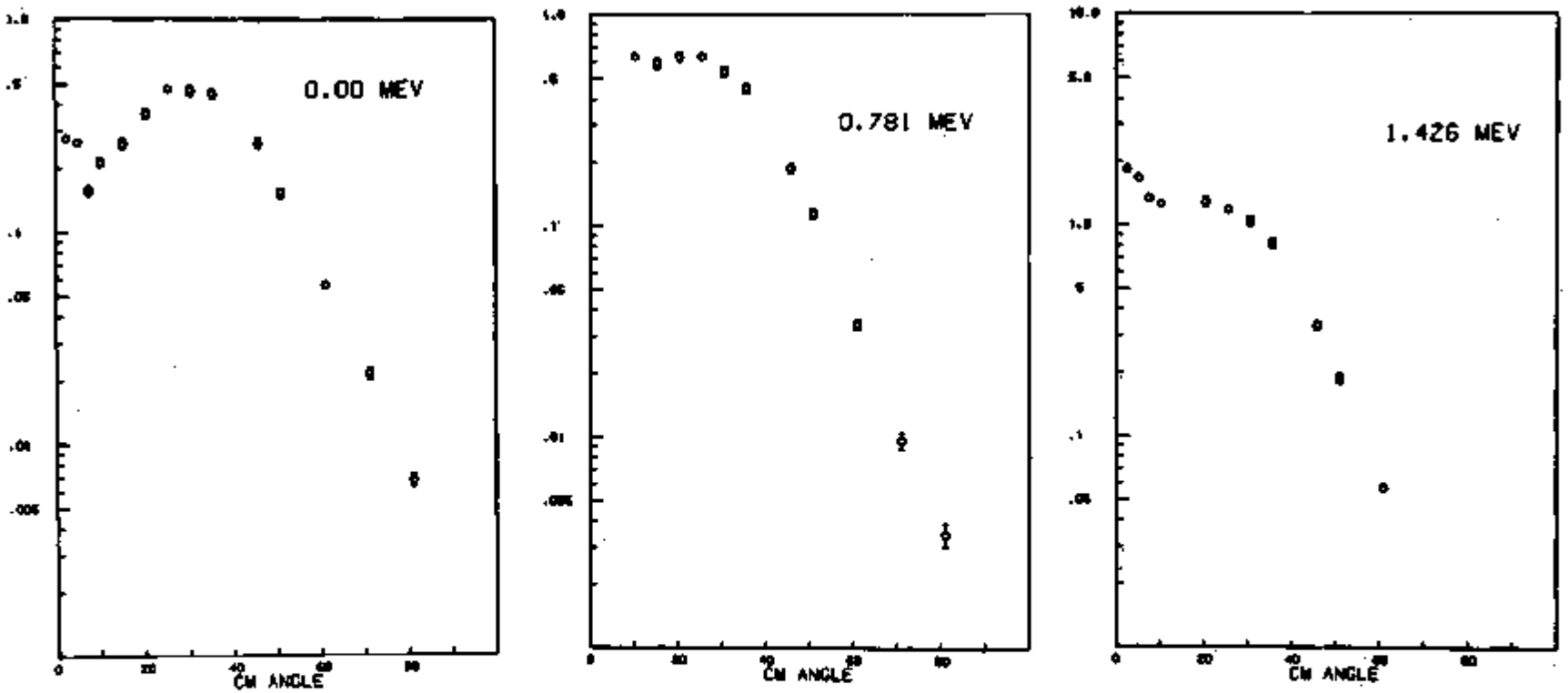

Fig. A14-1. Measured $^{208}Pb(\alpha,^{3}He)$ angular distributions for the $g_{9/2}$ (0.00 MeV), $i_{11/2}$ (0.781 MeV), and $j_{15/2}$ (1.426 MeV) levels in ^{209}Pb.

model parameters which provide good fits to all three of the angular distributions. Generally good fits can be obtained to the $j_{15/2}$ and $i_{11/2}$ angular distributions but not to the $g_{9/2}$ angular distribution.

Spectra for the $^{206,207,208}Pb(\alpha,^3He)$ reactions shown in Fig. A14-2 were recorded at 25° with the identical spectrograph magnetic field. In ^{209}Pb, the three peaks correspond to the $\ell = 4$ $g_{9/2}$, $\ell = 6$ $i_{11/2}$, and $\ell = 7$ $j_{15/2}$ transitions. In ^{208}Pb, the added neutron particle will couple with the $p_{1/2}$-hole of the ^{207}Pb ground state and in lowest approximation one expects the shell model strength for a given orbital to be split into two components. From (d,p) studies, the levels at 3.198 MeV and 3.475 MeV are known to contain a major fraction of the $g_{9/2}$ strength. The two levels at 4.608 MeV and 4.855 MeV almost certainly are $\ell = 7$ transitions. The spin of the level at 4.608 MeV has been tentatively assigned [4] at 8^+. If the intensities of the two peaks follow the 2J+1 rule approximately, the spectrum suggests an assignment of 8^+ for the 4.855 MeV peak and 7^+ for the 4.608 MeV peak. Most of the $\ell = 6$ strength must be contained in the level (possibly a doublet) at 4.186 MeV.

In lowest order, the ^{207}Pb spectrum should resemble that of ^{209}Pb (both targets are even-even nuclei). The energies in the spectrum are computed relative to the energy of the 2.726 MeV level which has been previously determined [5] to contain $g_{9/2}$ strength. Most of the $g_{9/2}$ strength and $j_{15/2}$ strength appears to be contained in the levels at 2.726 MeV and 4.090 MeV. The $i_{11/2}$ strength seems to be fragmented, possibly by mixing with the $11/2^+$ members of the $|2^+;g_{9/2}>$ and $|3^-;f_{5/2}^{-1}>$ multiplets which would be at approximately 3.6 MeV and 3.2 MeV, respectively. Most likely the levels at 3.609, 3.489, and 3.413 MeV contain portions of the $i_{11/2}$ strength.

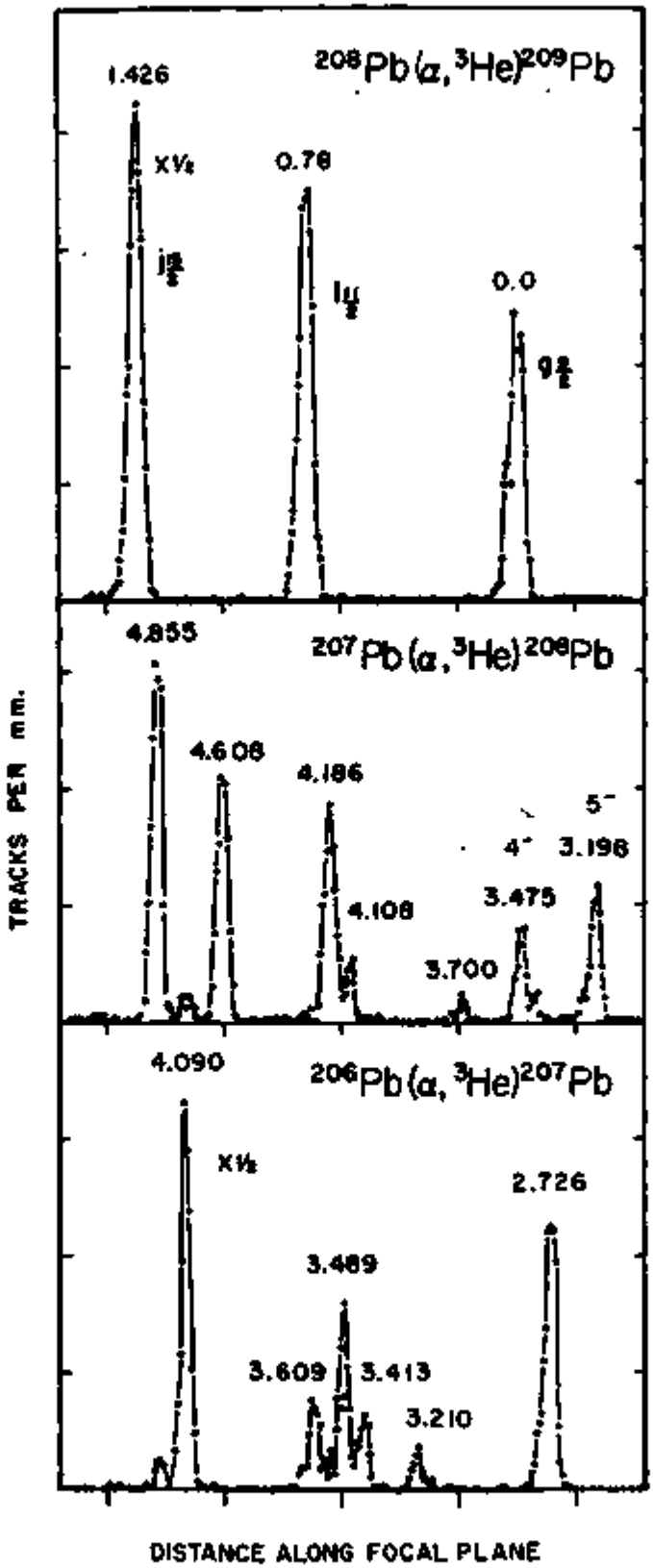
$^{208}Pb(\alpha,{}^3He)^{209}Pb$
1.426
X½
0.78
0.0
$^{207}Pb(\alpha,{}^3He)^{208}Pb$
4.855
4.608
4.186
4.108
3.700
3.475
4⁻
5⁻
3.198
$^{206}Pb(\alpha,{}^3He)^{207}Pb$
4.090
X½
2.726
3.469
3.609
3.413
3.210
TRACKS PER mm.
DISTANCE ALONG FOCAL PLANE

Fig. A14-2.

References

1) G. J. Igo, P. D. Barnes, E. R. Flynn, and D. D. Armstrong, Phys. Rev. 177, 1831 (1969).

2) C. Ellegaard, J. Kantele, and P. Vedelsby, Nucl. Phys. A129, 113 (1969).

3) I. Hamamoto, Nucl. Phys. A126, 545 (1969).

4) Nuclear Data Sheets 5 (1971).

5) R. A. Moyer, B. L. Cohen, and R. C. Diehl, Phys. Rev. C2, 1898 (1970).

A15. Analysis of High-Energy Heavy-Ion Transfer Reactions

F. D. Becchetti

Data [1,2] from the $^{54}Fe^{62}Ni(^{16}O,^{15}N)$ reaction (E_L = 104 MeV) and the $^{54}Fe,^{62}Ni(^{12}C,^{11}B)$ reactions (E_L = 78 MeV) have been analyzed using finite-range DWBA theory. [3] These data are for bombarding energies several times the classical Coulomb barrier and thus provide a stringent test of reaction theories for heavy ions. Previous analyses of these data using no-recoil DWBA indicated serious problems, e.g., the spectroscopic factors deduced for some states were 2 to 200 times larger than accepted values. The present analysis, using DWBA with recoil, however, yields satisfactory results ($C^2S \lesssim 1$). Furthermore, one can now use the pronounced [2] j-dependence of the $(^{16}O,^{15}N)$ and $(^{12}C,^{11}B)$ reactions to make j-assignments for many levels.

References

1) F. Becchetti, et al., Lawrence Berkeley Laboratory progress report (1972, unpublished).

2) D. Kovar, F. D. Becchetti, B. G. Harvey, F. Pühlhofer, J. Mahoney,

D. W. Miller and M. S. Zisman, Phys. Rev. Lett. 29, 1023 (1972).

3) Program LOLA, R. DeVries (unpublished). Calculations performed at Lawrence Berkeley Laboratory.

28776

A16. Nuclidic Mass Relationships, Mass Equations, and the Effective Neutron-Proton Interaction

J. Janecke

Work on nuclidic mass relationships, mass equations and the effective neutron-proton interaction has been continued. [1] Several criteria have been established to test predictions for very neutron-rich and proton-rich nuclei from any given mass equation or procedure for consistency and compatibility with the experimental masses. The effective neutron-proton interaction has been recognized as the quantity which determines the reliability of mass predictions. Solutions of generalized nuclidic mass relationships have been derived.

Numerous numerical applications have become possible. One such application has been completed. The solutions to generalized nuclidic mass relationships generate correction terms for any given mass equation. The corrections ΔM can be written as

$$\Delta M(N,Z) = \eta_1(N-Z)^2 + \eta_2\delta_{\text{odd-odd}} + \eta_3\delta_{\text{even-even}} + F_1(N) + F_2(Z). \quad (1)$$

Here, η_1, η_2 and η_3 are constant parameters, $\delta_{\text{odd-odd}}$ is one for odd-odd nuclei and zero otherwise, $\delta_{\text{even-even}}$ is one for even-even nuclei and zero otherwise, and $F_1(N)$ and $F_2(Z)$ are arbitrary functions of N and Z, respectively.

The above correction term has an analytical form which is related to that of the solutions of the transverse and longitudinal Garvey-Kelson nuclidic mass relationships: [2]

$$\text{GK-T:} \quad M(N,Z)^- = g_1(N) + g_2(Z) + g_3(N+Z) \tag{2}$$

$$\text{GK-L:} \quad M(N,Z) = f_1(N) + f_2(Z) + f_3(N-Z). \tag{3}$$

It should be noted that eqs. (2) and (3) represent mass equations while eq. (1) represents only a correction term. The functions F, g, and f can be obtained in parametric form from a least-squares adjustment to the experimental data.

Correction terms ΔM have been constructed for a variety of liquid-drop model and shell-model mass equations (see Table A16-1). The equations fall essentially into two categories depending on the number of parameters. There are few-parameter equations ($p < 20$) and many-parameter equations ($p > 200$). Clearly, correction terms for the latter (GK-T, GK-L, C2, Z1, Z3) are not appropriate and the results are therefore shown in parenthesis. Since very light nuclei require a special treatment due to pronounced shell effects, only experimental masses with $N,Z \geq 20$ were included in the least-squares adjustments. Table A16-2 shows the results for the standard deviations σ_M and σ_C for the experimental masses and Coulomb displacement energies, respectively. It is interesting to note that the Bethe-Weizsäcker equation <u>with properly adjusted coefficients</u> (BW 1) has the smallest deviation σ_M of all few-parameter equations. Another interesting conclusion from these results is that essentially any mass equation, even the Bethe-Weizsäcker equation (BW 2), can be used to <u>reproduce</u> the experimental masses (> 1000)

TABLE A16-1

List of Mass Equations

GK-T	Garvey-Kelson transverse (ref. 2).
GK-L	Garvey-Kelson longitudinal (ref. 2).
CON	1_{np} = constant.
BW 1	Bethe-Weizsäcker (parameters optimized for minimum σ_M).
BW 2	Bethe-Weizsäcker (a_{sym} and a_{coul} optimized for minimum σ_M').
MS 1	Meyers and Swiatecki; droplet model (ref. 3; parameters of ref. 4; Coulomb exchange term as $c_4 Z 2^{-1/3}$).
MS 2	Meyers and Swiatecki; droplet model (ref. 3; parameters of ref. 4; Coulomb exchange term as $c_4 Z^{4/3} A^{-1/3}$).
MS 3	Meyers and Swiatecki; droplet model (ref. 3; parameters of ref. 5; Coulomb exchange term as $c^4 Z^{4/3} A^{-1/3}$).
C 1	Cameron; liquid drop model (ref. 6).
C 2	Cameron; liquid drop model with shell and pairing corrections (ref. 6).
S	Seeger; liquid drop model (ref. 7).
Z 1	Zeldes et al.; shell model (ref. 8).
Z 2	Liran and Zeldes; shell model, seniority scheme (ref. 9).
Z 3	Liran and Zeldes; shell model, seniority scheme with deformation corrections (ref. 9).

TABLE A16-2

Results of the least-squares analysis for several mass equations and N,Z ≥ 20.*

Equation	Without Correction Terms				With Correction Terms					
	Number of parameters p	Number of exp. masses	Standard deviation σ_M in keV	Standard deviation σ_C in keV	Number of parameters p	Number of exp. masses	Standard deviation σ'_M in keV	Standard deviation σ'_C in keV	η_1 in keV	η_2 in keV
GK-T	484	1040	171	2072	[701	1040	142	2117	1.3	- 11.1]
GK-L	275	1041	268	a	[492	1041	200	a	2.0	- 12.0]
CON	0	1059	---	---	217	1059	662	4719	181.1	-113.0
BW 1	6	1059	2801	963	223	1059	471	2452	-27.3	22.9
BW 2	6	1059	---	---	223	1059	238	865	55.5	24.8
MS 1	10	1059	4441	1406	227	1059	292	726	20.6	-122.4
MS 2	10	1059	3494	1514	227	1059	292	740	21.0	-122.3
MS 3	10	1059	11452	1304	227	1059	307	544	6.8	-123.8
C 1	16	1058	2878	216	233	1058	261	651	8.4	-100.0
C 2	216	1057	316	211	[433	1057	262	630	8.4	-100.0]
S	11	1059	4099	1167	228	1059	260	759	4.1	-110.4
Z 1	~300	1058	188	a	[517	1058	141	a	0.4	- 36.8]
Z 2	90	1053	761	b	307	1053	244	b	- 2.8	- 29.5
Z 3	340	1053	167	b	[557	1053	125	b	- 1.1	- 5.0]
	(144)				(361)					

a Cannot be calculated.

b The standard deviations σ_C and σ'_C are better than 100 keV if discontinuities of several MeV at shell closures are removed.

* Preliminary results.

with a standard deviation σ'_M of 200 - 300 keV if a properly constructed correction term with about 200 parameters is added. This result was expected. [1] The solution of the transverse Garvey-Kelson relationship (GK-T) requires more than twice the number of parameters and leads to only a modest improvement.- The standard deviations σ_C and σ'_C as well as the quantities η_1, $\eta_2 = \eta_3$ and the functions $F_1(N)$ and $F_2(Z)$ provide additional insight into properties of the mass equations but will also not be discussed here.

The standard deviations σ_M and σ'_M for reproducing the experimental masses are not directly related to the accuracy for predicting unknown masses of nuclei far away from the line of beta-stability. The accuracy of predicting such unknown masses with a corrected mass equation depends entirely on how well the effective neutron-proton interaction $V_{np}(N,Z)$ is described by the original mass equation.

References

1) J. Janecke, Phys. Rev. C6, 467 (1972); J. Janecke and H. Behrens, Z. Physik 256, 236 (1972); Proc. Int. Conf. Nucl. Phys., Munich, 1973, p. 321; Phys. Rev. C9, 1276 (1974).

2) G. T. Garvey, W. J. Gerace, R. L. Jaffe, I. Talmi, and I Kelson, Rev. Mod. Phys. 41, S 1 (1969).

3) W. C. Meyers and W. J. Swiatecki, Ann. Phys. (N.Y.) 55, 395 (1969).

4) W. D. Meyers and W. J. Swiatecki, Ann. Phys. (N.Y.) to be published, and report LBL-1957; private communication.

5) S. Ludwig, H. von Groote, E. Hilf, A. G. W. Cameron, and J. Truran, Nucl. Phys. A203, 627 (1973).

6) J. W. Truran, A. G. W. Cameron and E. Hilf, Proc. Int. Conf. Prop. of

Nuclei Far from the Region of Beta-Stability, Leysin, 1970, Vol. 1, p. 275.

7) P. A. Seeger, ibidem, Leysin, 1970, Vol. 1, p. 217.

8) N. Zeldes, A. Grill, and A. Simieric, K. Dan Vidensk. Selsk. Mat.-Fys. Skr. 3, No. 5 (1967).

9) S. Liran and N. Zeldes, Proc. Int. Conf. Nucl. Phys., Munich, 1973, p. 322; S. Liran, Ph.D. thesis, 1973, Hebrew University of Jerusalem; S. Liran, private communication.

A17. Coulomb Energies and Deformed Nuclei

J. Janecke and J. P. Draayer

Extensive experimental Coulomb energy data of deformed nuclei have become available only recently. [1-3] Coulomb displacement energies ΔE_C of deformed nuclei are lower than those of corresponding spherical nuclei, [4-6] an effect clearly seen in plots [3,4] as a function of A of the difference between the measured energies and the predictions based on a spherical shape. The maximum reduction for rare-earth nuclei is 150 - 200 keV. Using recent data, Merrill et al. [3] observed an anomaly of this effect with a local maximum at A = 165 - 170. The authors were unable to explain the effect.

The hexadecapole deformation of the nuclear shape provides a possible explanation of the anomaly. The deformation parameter β_4 changes sign [7] near A = 165. Since in a first-order calculation the energy ΔE_C depends quadratically on β_4, the observed A-dependence can be reproduced. Figure A17-1

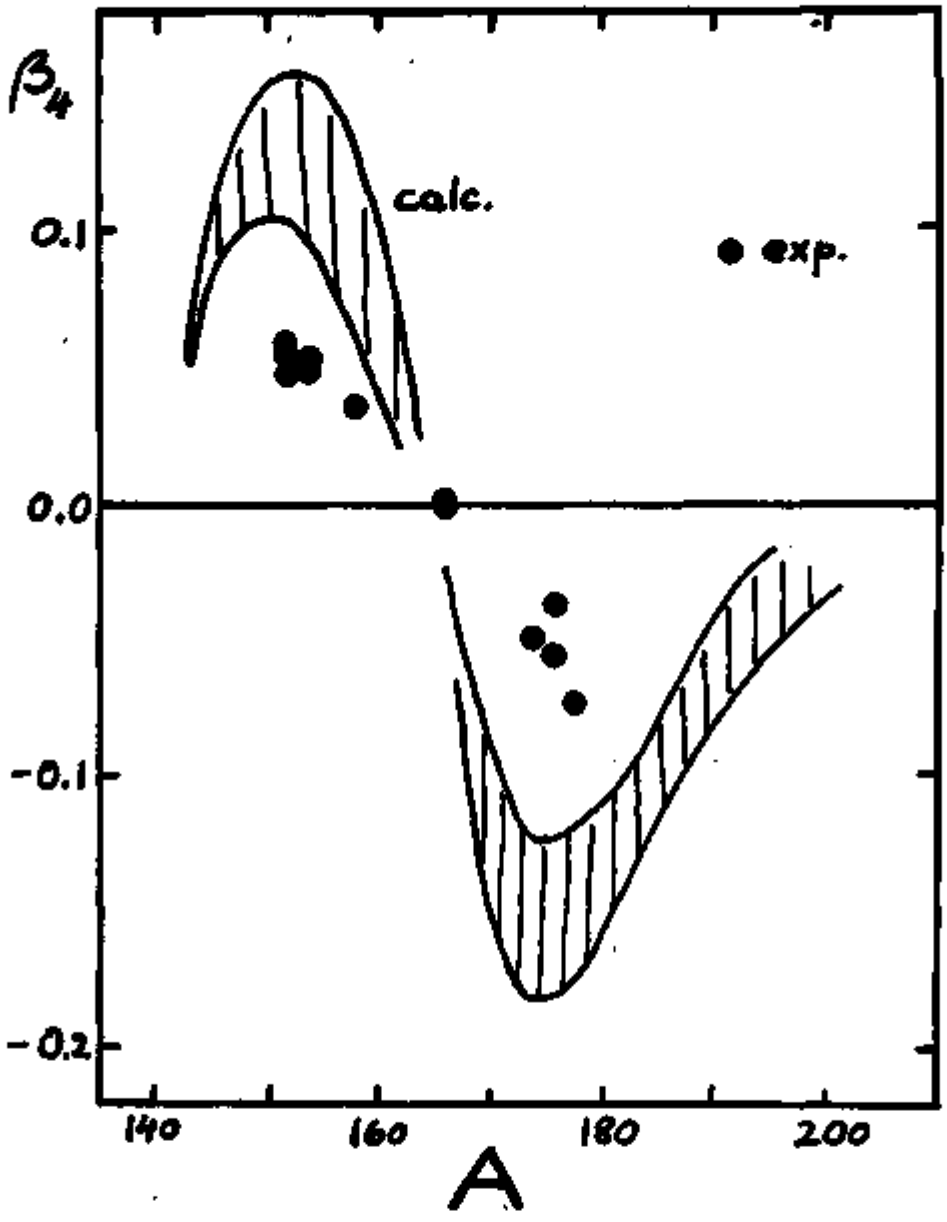

Fig. A17-1.

shows a preliminary comparison between the coefficients β_4 derived from the experimental Coulomb displacement energies (shaded areas) and values derived from other experimental data, mostly from elastic and inelastic α-particle scattering. [7] The agreement in the general dependence on A and particularly the change in sign near A ≈ 165 is quite good. However, the values obtained from ΔE_C are too large in magnitude by a factor of about two. While the deformation parameters for the shapes of the charge distribution and the nuclear potential must not necessarily be the same, it is felt that the above values are probably too big. Calculations based on the Coulomb energy expressions [5] which include deformation and diffuseness corrections to higher orders should clarify the question whether the above anomaly can indeed be explained by hexadecapole deformations.

References

1) P. Foissel, et al., Nucl. Phys. A178, 640 (1972).

2) H. Seitz, Nucl. Phys. A186, 574 (1972).

3) N. H. Merrill, et al., Nucl. Phys. A216, 61 (1973).

4) J. Janecke, in Atomic Masses and Fundamental Constants 4, ed. by J. H. Sanders and A. H. Wapstra, Plenum Press 1972, p. 221.

5) J. Janecke and J. P. Draayer, to be published.

6) J. Janecke, Nucl. Phys. A181, 49 (1972).

7) D. Hendrie, et al., Phys. Lett. 26B, 127 (1968).

B. INSTRUMENTATION

B1. Timing for Neutron Time-of-Flight Spectroscopy

J. F. Petersen, W. C. Parkinson, and D. DuPlantis

Accurate timing in neutron time-of-flight spectroscopy requires two fast time signals -- one corresponding to the production of the neutron, the other to its detection. While ideally the production time signal should be generated by the beam striking the target, any signal may be used which has a fixed time relationship to the beam's arrival at the target.

Two techniques have been used during the past year to generate such a signal. The first uses a capacitive pick-off on one of the cyclotron dee stems to obtain an rf reference voltage which is fed into a conventional constant fraction timing circuit. The output is a negative, fast logic pulse once each rf cycle accurately synchronized with the rf. The pulse train is counted down to the desired mode (f/2, f/3, ...) with standard TTL circuitry. The resulting square wave is used for two purposes. First, it is clipped, amplified, and applied through a transmission line to the control electrode of the gated ion source. Second, it is used to gate the stop input of the time-to-amplitude converter (TAC). While this method provides a stable reference with respect to the rf, the beam itself does not necessarily maintain a fixed time relationship to the rf, especially over the course of hours of operation. Any slow drift in the magnetic field or dee voltage, for example, will result in a slight but appreciable change in the rf phase of the beam.

The timing variations introduced by such drifts can be eliminated if the beam burst itself is used to generate the reference signal, and this is the basis of the new timing system. The optimization of this system is described in detail in a technical letter to be published, and only a general description will be given here. The pick-off device used is a cylindrical capacitance formed by a 3.7 centimeter diameter cylinder coaxial with the 15 centimeter diameter aluminum beam duct. Beam pulses moving along the axis induce a charge on the cylinder and hence a voltage between the cylinder and the grounded beam duct. To maximize the voltage signal, the length of the inner cylinder should be at least as long as the spatial spread of the pulse, and the capacitance should be as low as possible. The capacitance for concentric cylinders is:

$$C = \frac{2\pi\epsilon_o L}{\ln(r_1/r_2)} \quad .$$

where L is the length of the conductor, and r_1 and r_2 are the radii of the inner and outer cylinders, respectively. To minimize the radius of the inner conductor, and thus decrease the capacitance, the device was located just behind the energy defining slits where the beam is focused both vertically and horizontally to a minimal cross sectional area. The length of the inner cylinder is 18 centimeters. For typical pulses of 21 MeV $^3He^+$ ions the pulse width if 4 nanoseconds, corresponding to a spatial spread of 12 centimeters.

To minimize the rise time of the induced voltage signal, a grounded iris is placed 2 centimeters in front of the inner conductor. As a result, the rise time is approximately equal to the time it takes for the beam

pulse to move completely into the inner conductor.

The voltage pulse from the capacitor is amplified by a wide band amplifier (gain-bandwidth product 2000 MHz) with a low shunt capacitance and relatively high input resistance (2 pf||100 kΩ) so that the time constant is long compared to the rise time of the signal. The amplifier is located physically near the pick-off, inside the vacuum duct, to minimize shunt capacitance. The amplifier output is coupled through a 50 Ω line to an ORTEC model 454 timing filter amplifier and ORTEC model 453 constant fraction timing discriminator in the data room. For typical beam currents (200 nanoamperes pulsed at 1 MHz) the voltage induced on the inner conductor is of the order of 0.010 volts.

Figure B1-1 shows the simultaneous time-of-flight spectra from two time-to-amplitude converters (TAC). The start signal for both TAC's was produced by the phase probe with the prompt gamma rays resulting from the beam striking a carbon flag. The right-hand peak is from the TAC using the rf generated stop signal; the left peak is from the TAC using the stop signal generated from the beam pick-off system. For both TACs the time calibration is 4.5 ch/nsec. The data were accumulated over a time span of 10 minutes while the cyclotron dee voltage and frequency were varied over ranges typical for normal operation. The right peak has a FWHM of 2.5 nanoseconds, while the left peak is only 1.5 nanoseconds wide.

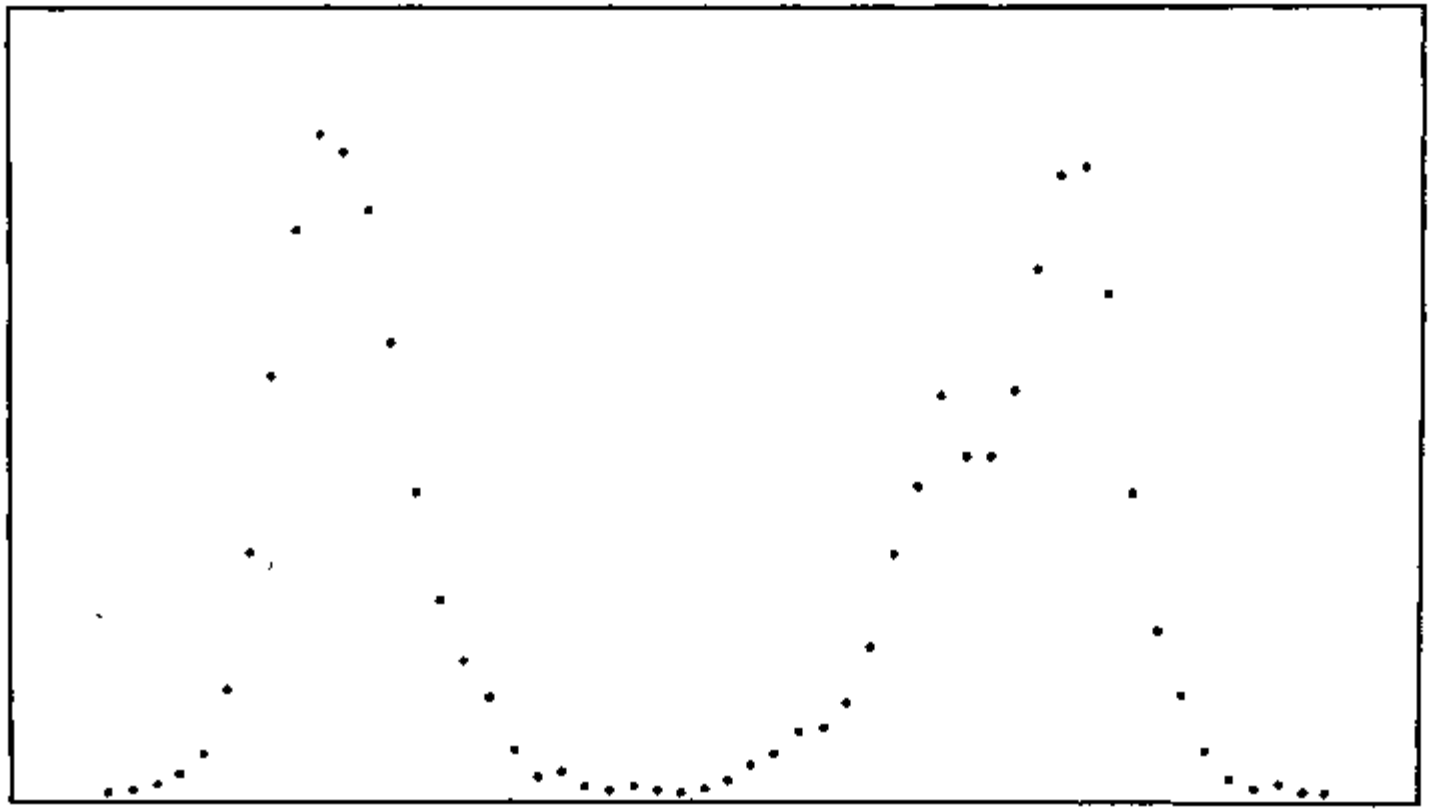

Fig. B1-1. Simultaneous gamma-ray time-of-flight spectra.

B2. Tests of a Position-Sensitive Proportional Counter

F. D. Becchetti

A resistive-wire position-sensitive proportional counter for use in the focal plane of magnetic spectrometers has been constructed and tested. The counter consists of a 25 cm x 5 cm x 1 cm thick position (or ΔE) counter combined with a 2.5 cm thick ΔE counter in a common gas enclosure.

The position counter uses a 1 mil carbon-coated quartz fiber (8 KΩ/mm). Position information is obtained either by charge division or from the pulse rise time. An XE/E vs. position curve is shown in Fig. B2-1 (charge division mode) as obtained using an alpha particle source. The line width (FWHM) is about 2 mm for a 1 mm dia. α-source at $\theta = 90°$. The slight (< 10%) non-linearity observed is comparable to or better than that observed for solid-state detectors and may easily be corrected for. Comparable results have been obtained using the rise time information.

A more serious problem involves the degradation of the ΔE signal when the incident particle enters non-normal, i.e., at an angle θ, and with a finite angular width δθ. Such is the case for operation in the spectrometer focal plane where $\theta = 40°$ and $\delta\theta \approx 4°$. The spread in energy loss due to path differences then becomes non-negligible ($\delta\Delta E/\Delta E \propto \delta\theta/\tan\theta$). The dependence of the ΔE resolution on θ is shown in Fig. B2-2 for an alpha source ($\delta\theta \approx 8°$). The ΔE resolution degrades from 8 - 10% ($\theta = 90°$) to > 20% ($\theta = 40°$). This has been verified using the spectrometer with scattered particles.

One method of improving the ΔE resolution (without reducing δθ and the solid angle) is to measure the particle trajectories with a second counter

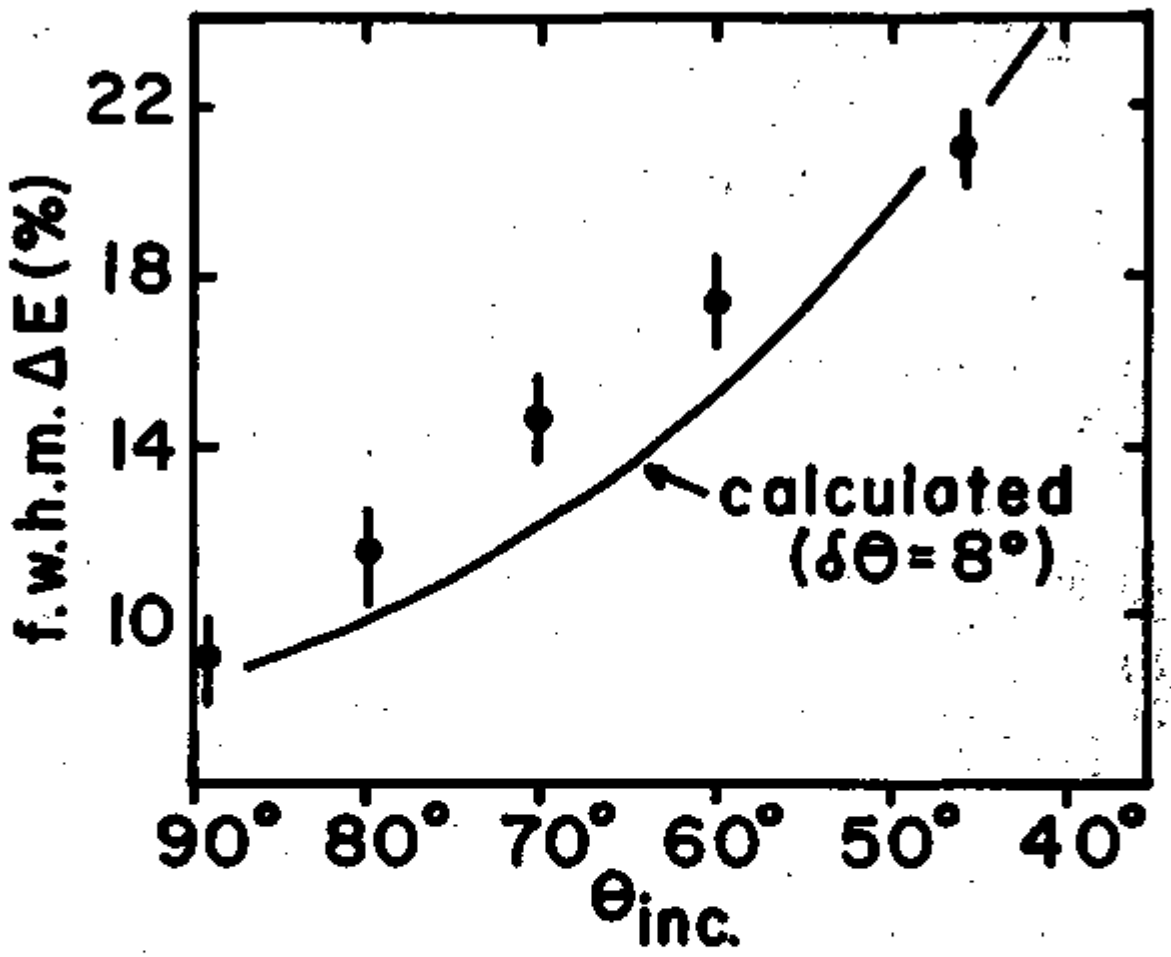

Fig. B2-1. Variation of energy loss resolution vs. angle of incidence ($\delta\theta = 8°$)

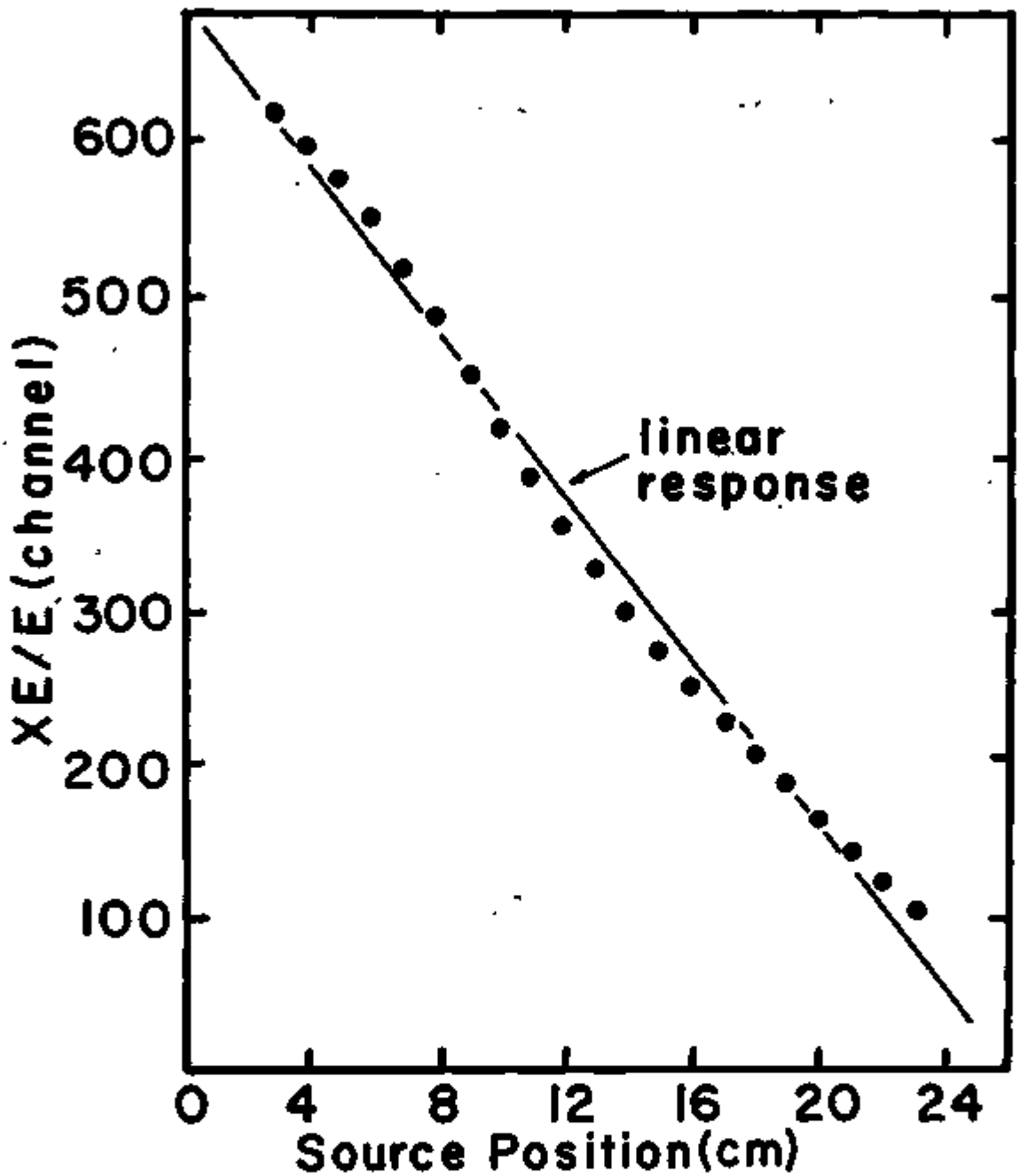

Fig. B2-2. XE/E linearity vs. position (charge division method).

by placing a solid-state position-sensitive detector which provides both a position and an E signal behind the proportional counter or, alternatively, using another position-sensitive proportional counter. Both methods are being investigated.

B3. Particle Identification by Combined Bρ, ΔE and E Measurement

F. D. Becchetti

A position- and trajectory-sensitive counter telescope system has been built and tested as a focal-plane detector for the magnetic spectrometers. The system consists of a double gas proportional counter followed by a 350 μm solid-state position-sensitive detector (or array) (see Fig. B3-1). The gas proportional counter combines a 1 cm thick position-sensitive counter (see Section B2) and a 2.5 cm ΔE counter. The parameters obtained are X1, E1 (or XE1), E2, X3 (or XE3) and E3. The position signals (X1 and X3) determine Bρ while E1 and E2 give ΔE, energy loss, and E3 gives E, the total energy (for stopped particles). The quantities Bρ, ΔE and E permit, in most cases, unambiguous Z and M identification of reaction products. At fixed values of $B\rho (=\sqrt{2ME}/q)$ we have $\Delta E = Z^2M/E = 2(B\rho)^2 Z^2M^2/q^2$, i.e., in the ΔE vs. E spectrum particles are grouped for ZM/q = constant.

The isotope resolution of this system is potentially very high since ΔE and E can be measured to better than ± 5% and ± 2%, respectively; thus $\Delta Z/Z \sim \pm 1/20$ and $\Delta M/M \sim \pm 1/40$ is possible provided the particles of interest are stopped in the E counters. This latter condition is satisfied

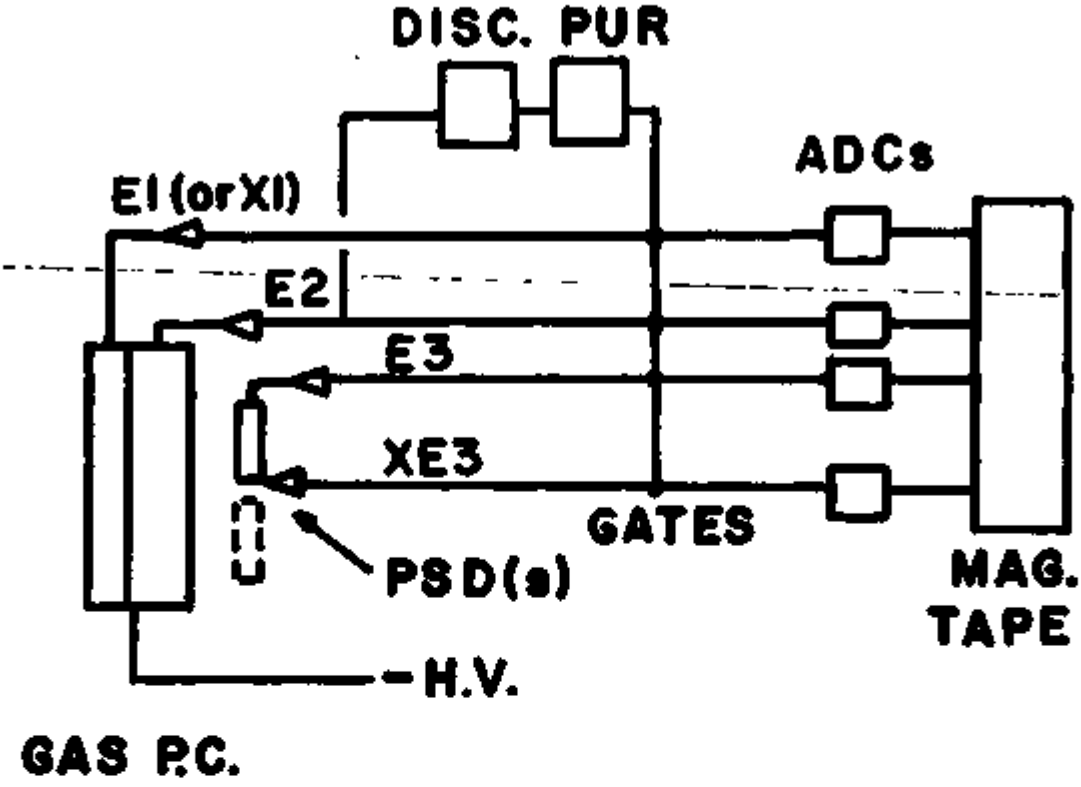

Fig. B3-1.

for most heavy ions, but not for many light ion reaction products. Thus, one observes particle groups also along a line E2 proportional to line E3 corresponding to particles which pass through the E counter. The particles which are not stopped can cause pile-up contamination in the ΔE vs. E spectrum when light ion projectiles are used, e.g., alpha particles. Most pile-up can be eliminated by gating on both E1 and E2, however.

Another feature of the system is the capability of measuring particle trajectories since two position signals are available (X1 and X3). Preliminary tests indicate an angular resolution of ± 2° for the present counter. This allows one to double the spectrometer solid angle without loss in ΔE or Bρ resolution. The increased solid angle then offsets the effect of the "dead" space between PSD detectors which requires double exposures at each magnet setting.

B4. Particle Identifier Counter Telescope

A. VanderMolen

A particle identifier system has been completed and tested in the past year. The acquisition of new electronic components and their integration into a permanent setup has resulted in a more effective use and in improved data. The identifier is of the variable "power law" type developed by Goulding et al. [1] This identifier has the capability of making two independent particle identifications which is important for the isotope resolution of heavy ions. See Fig. B4-1 for the block diagram of the electronic components. The system is presently being used for the study of the

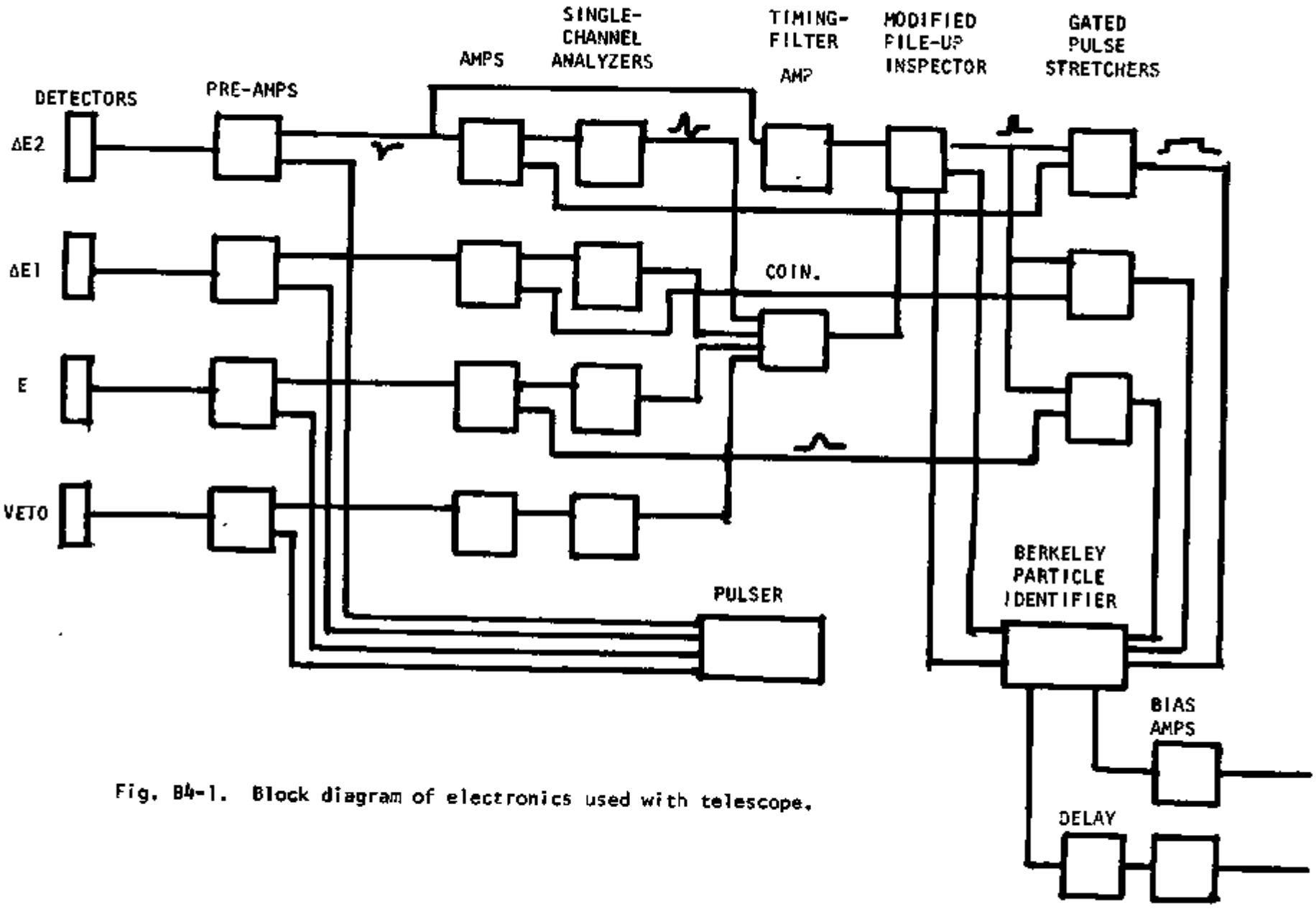

Fig. B4-1. Block diagram of electronics used with telescope.

$(d,{}^{6}Li)$ and $(\alpha,{}^{6}He)$ reactions on several light nuclei.

A new detector mount has been designed and built (see Fig. B4-2). The design is an improvement over previous mounts from both a practical and experimental point of view. The mount accommodates up to four detectors (two ΔE-, one E- and a veto-detector). It is cooled by a thermoelectric cooler backed by a water-cooled copper block. The detector temperature is regulated by the thermoelectric input current. This temperature control is particularly important in the use of thin detectors. The mount subtends an angle of 12° when mounted in the scattering chamber (the large angular width is due mainly to the necessity of providing an rf shield). Data can be recorded at scattering angles as small as 7°.

At present data obtained with the array are stored in a Victoreen 20,000 channel analyzer used in the two-dimensional mode. The data are reduced on an IBM 360 computer via several programs written specifically to read and display them in one and two dimensions as well as to display them isometrically. Other data manipulating options are also available. Now that the capability of our PDP-15 computer has been improved by adding disk and tape units, the identifier system will be integrated with it as soon as the necessary software becomes available.

To facilitate the setup procedure, that is the adjustment of gains, windows, etc., of the system, a conversational-type computer program was written for the PDP-15 that simulates the response of the identifier for various ions (presently from protons to oxygen). Energy losses and ranges are determined by the program from parameterized energy-range relationships of Northcliff and Schilling. [2] Energy straggling is calculated from the results of Tschalär. [3] Also included are such effects as ionization

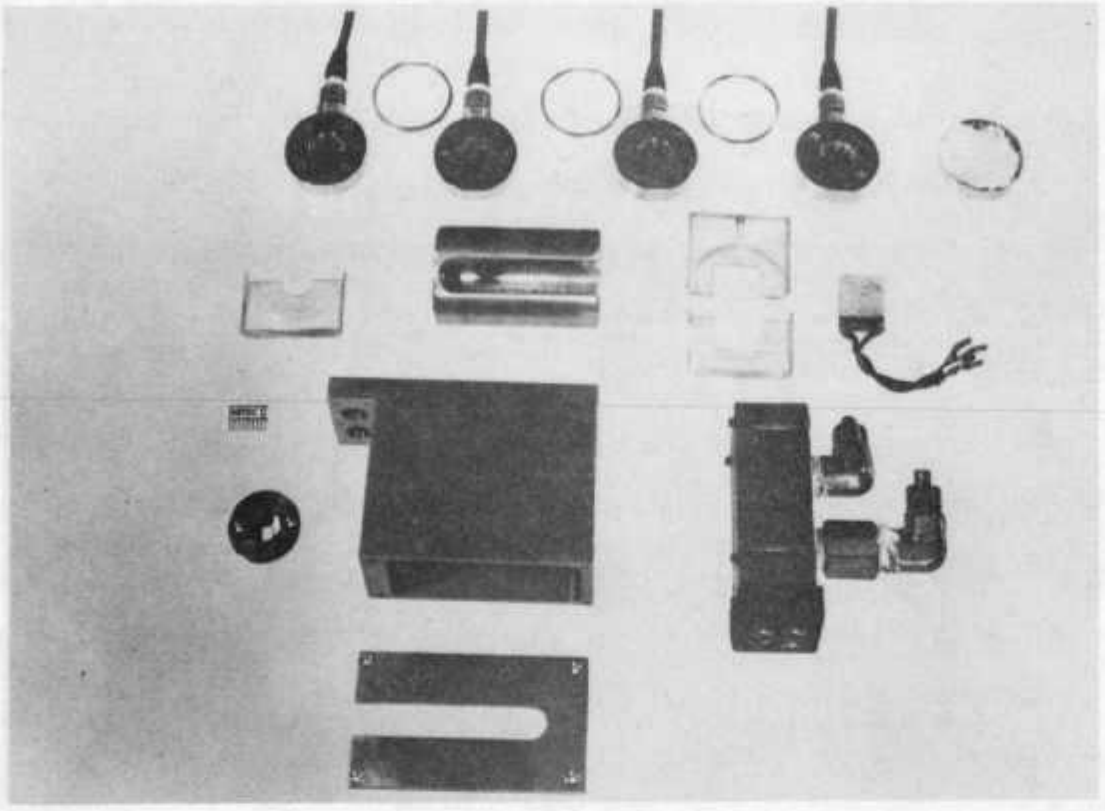

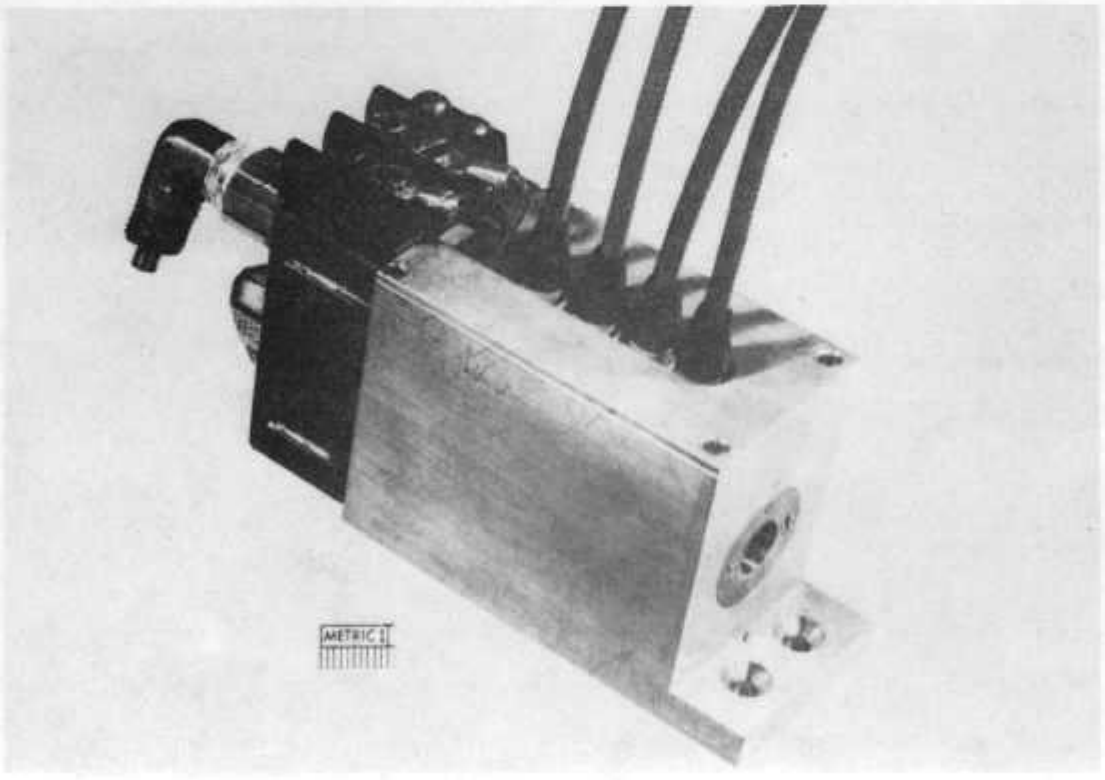

Fig. B4-2. (Top) View exposing the various components of the detector mount. (Bottom) View of mount with components assembled.

fluctuations [4] and nuclear straggling. [5] The program generates relative values for the height of the particle identification signal, its width at half maximum, the energy loss in each of the ΔE detectors, the necessary E detector thickness to stop the respective ion, and the overall energy resolution.

The mass resolution was tested for several ions from protons to carbon. The measured isotope resolution obtained with one ΔE detector agrees well with expected resolution. Figure B4-3 shows an example. The data are displayed with the results predicted by the aforementioned computer program (solid line). Absolute energy measurements have not yet been made. The post amplifier resolution measured with a pulser is 10 - 20 keV/detector. The energy resolution in actual experiments is generally limited by other effects such as kinematic broadening due to the beam divergence.

References

1) F. S. Goulding, D. A. Landis, J. Cerny and R. H. Pehl, UCRL-16711 (Feb. 1966).

2) L. C. Northcliff and R. F. Schilling, Nucl. Data Tables Vol. 7 (3-4), 33 (1970).

3) C. Tschalär, Nucl. Inst. & Meth. 61, 141 (1968) and 64, 237 (1968).

4) G. D. Alkhazov, A. P. Komar and A. A. Vorob'ev, Nucl. Inst. & Meth. 48, 1 (1967).

5) J. Linhard and V. Nielsen, Phys. Lett. 2, 209 (1962).

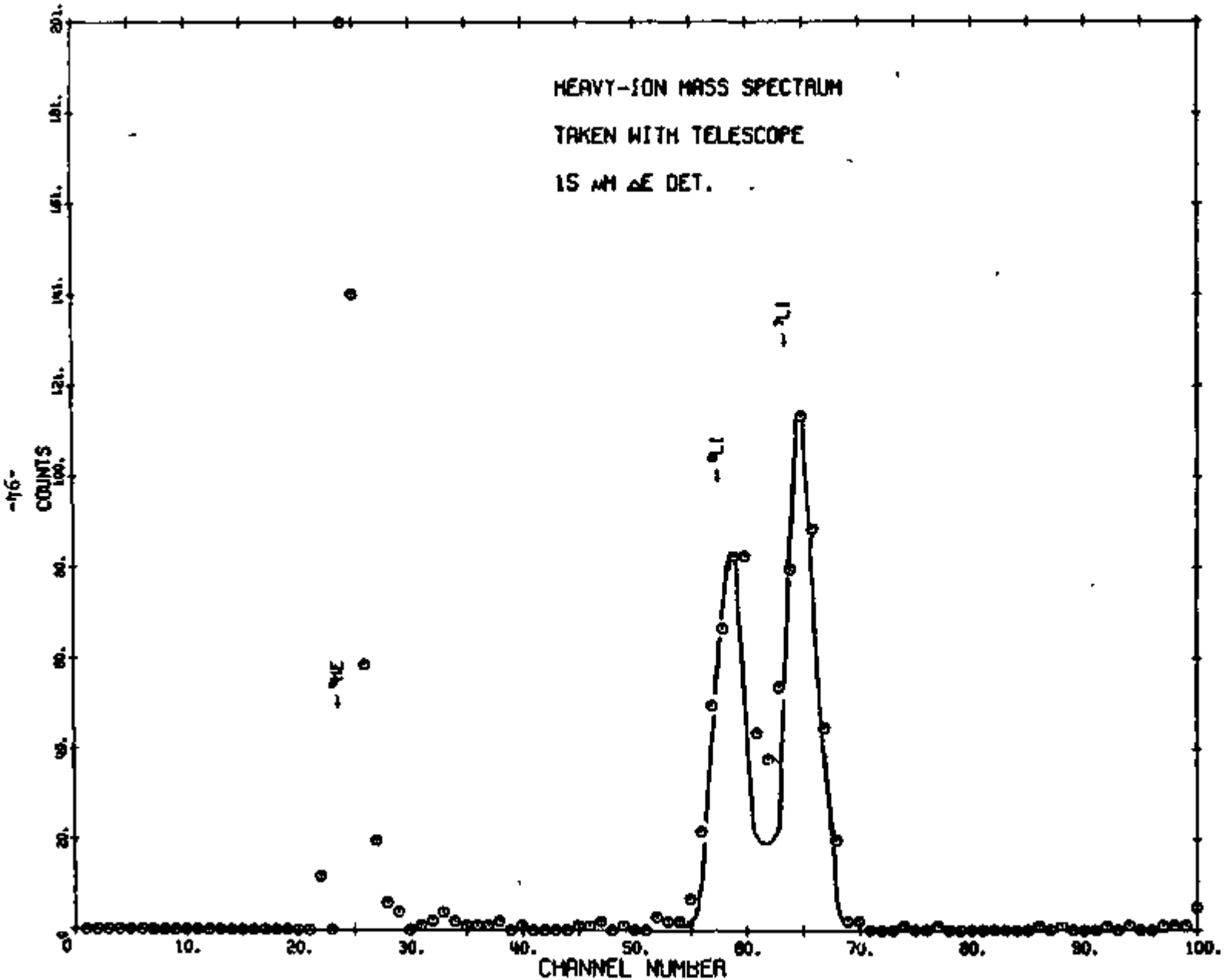
HEAVY-ION MASS SPECTRUM
TAKEN WITH TELESCOPE
15 μM ΔE DET.
COUNTS
CHANNEL NUMBER
0
10.
20.
30.
40.
50.
60.
70.
80.
90.
100.
7Li
6Li
4He

Fig. B4-3.

B5. Gamma-ray Spectroscopy

H. C. Griffin, K. L. Hull, and R. S. Tickle

Previous in-beam studies have indicated the need for more efficient methods of acquisition and analysis of data. Very few useful measurements can be made with single-parameter acquisition, and two-parameter measurements require more "channels" than can be stored in core as a simple matrix. Therefore we have developed improved techniques and have tested them with a variety of off-line studies.

A program was written for the DEC PDP-15/30 computer to allow acquisition of high-resolution two-parameter data. This program permits simultaneous collection of singles spectra from two detectors at a rate of about 50 k sec^{-1} with a maximum size of 13 bits per ADC. These spectra can be used to determine relative intensities for the detectors and to select appropriate digital gates for two-parameter acquisition. Coincidence data (up to 256 gates, 16 k channels of data for gate-related spectra) can be collected at a maximum rate of about 30 k pairs sec^{-1}. These data can be displayed, plotted, or printed as well as stored on and retrieved from Dectape.

The program has been tested with off-line studies of the decay of ^{94}Y, ^{95}Y, ^{146}Pr, and ^{147}Pr. Of these nuclides, ^{95}Y is particularly suitable as a stand-in for in-beam measurements. The short half life (10.5 min) and large number of low intensity γ-ray cascades (see Fig. 85-1) require high efficiency and selectivity in collecting data. For example, gate regions are selected from the self-gate spectrum from one detector. Each gate can correspond to any set of channels, not necessarily adjacent, from one ADC.

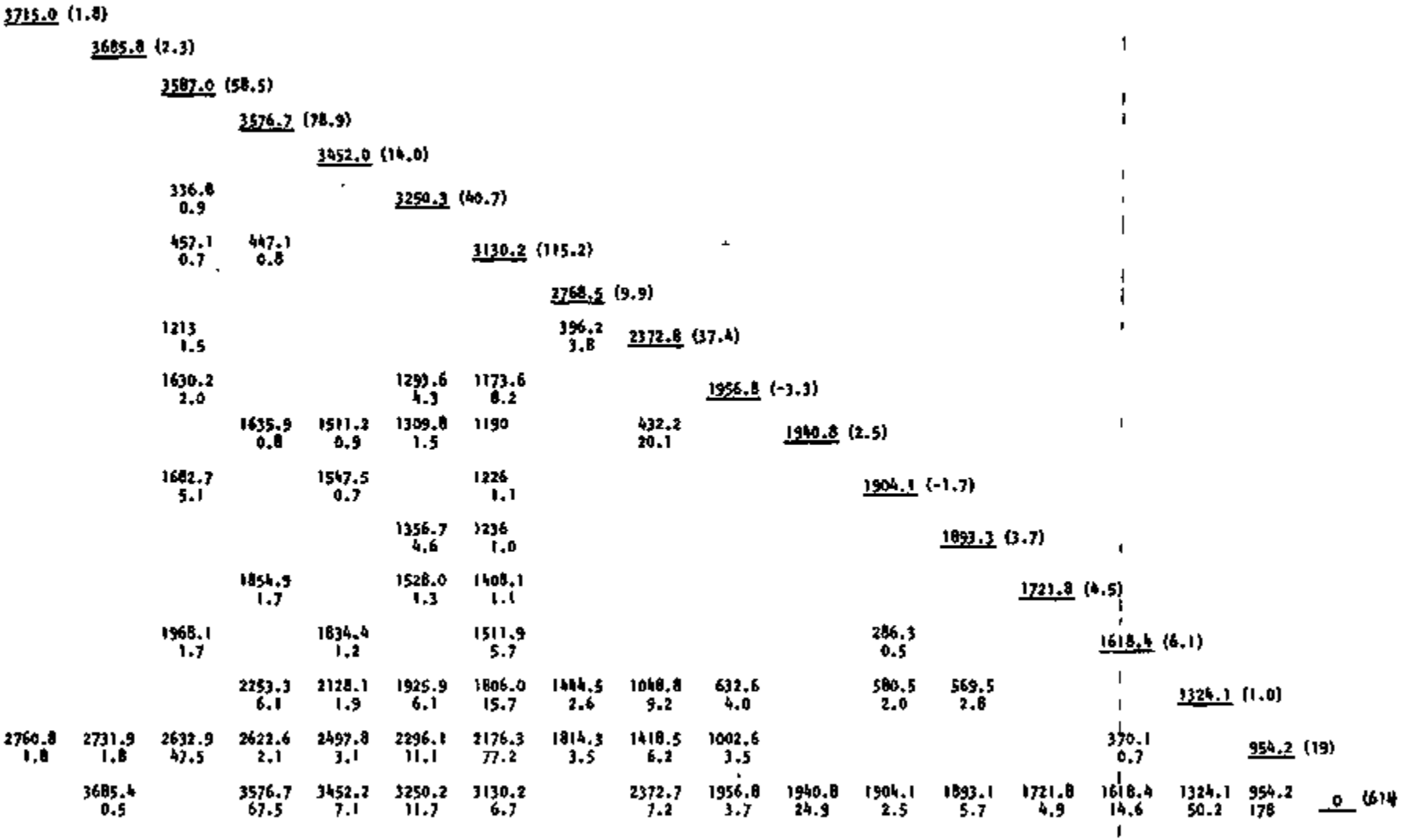

Fig. 85-1. Levels in ^{95}Zr populated in the decay of ^{95}Y. Only levels which are involved in cascades are given. Underlined entries on the diagonal are level energies in keV (β branching per 1000 decays deduced from γ intensities). Matrix entries indicate γ-ray energies and intensities.

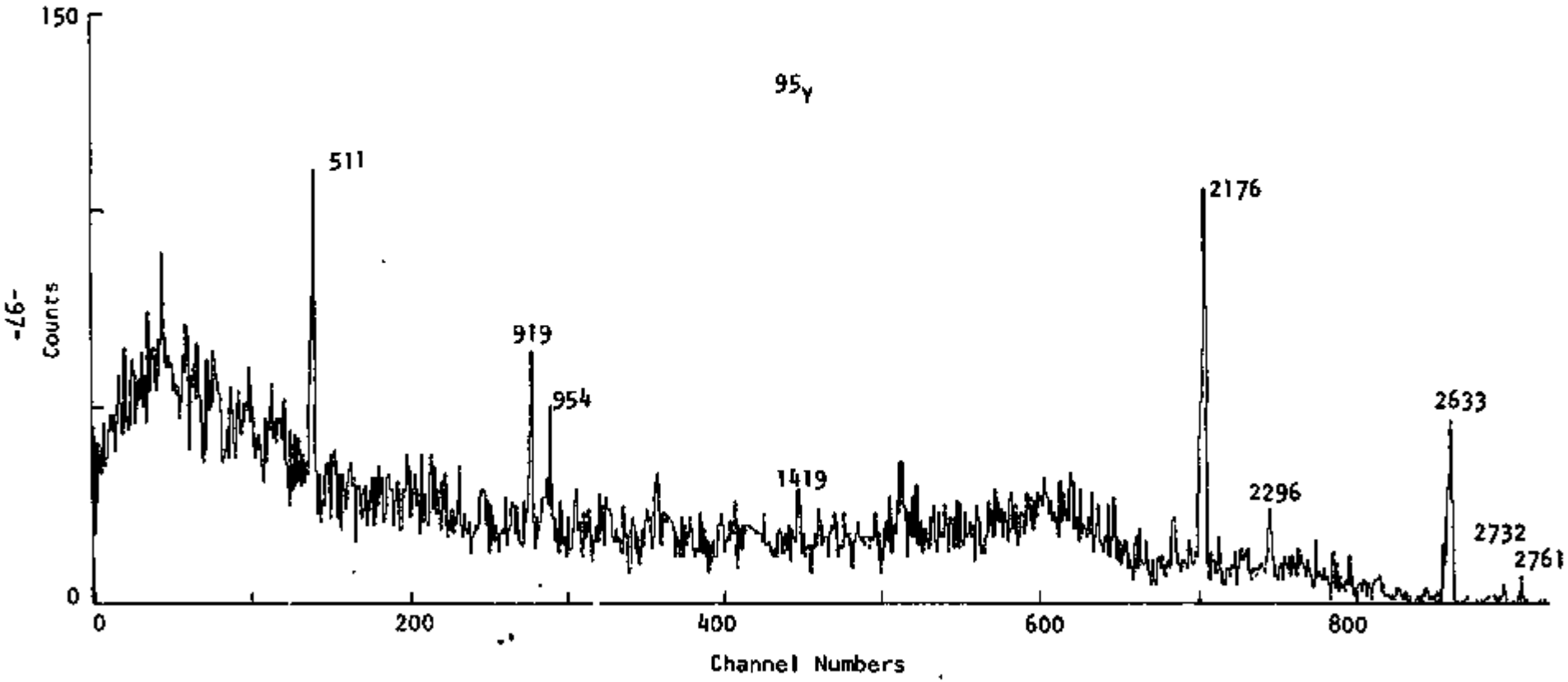

Fig. B5-2. Ge(Li) spectrum coincident with 954 keV (Ge).

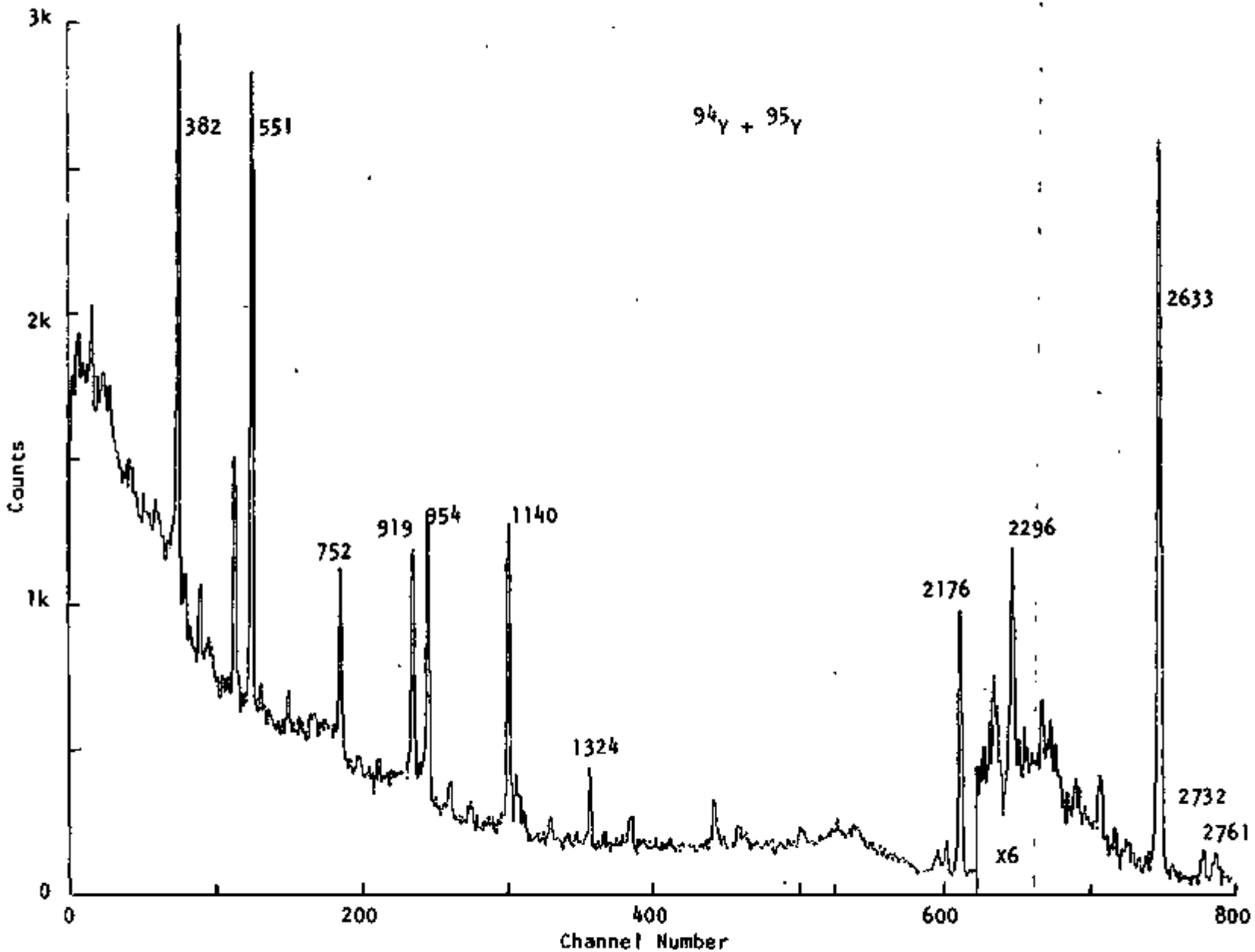

Fig. B5-3. Ge(Li) spectrum coincident with 880-1010 keV (NaI).

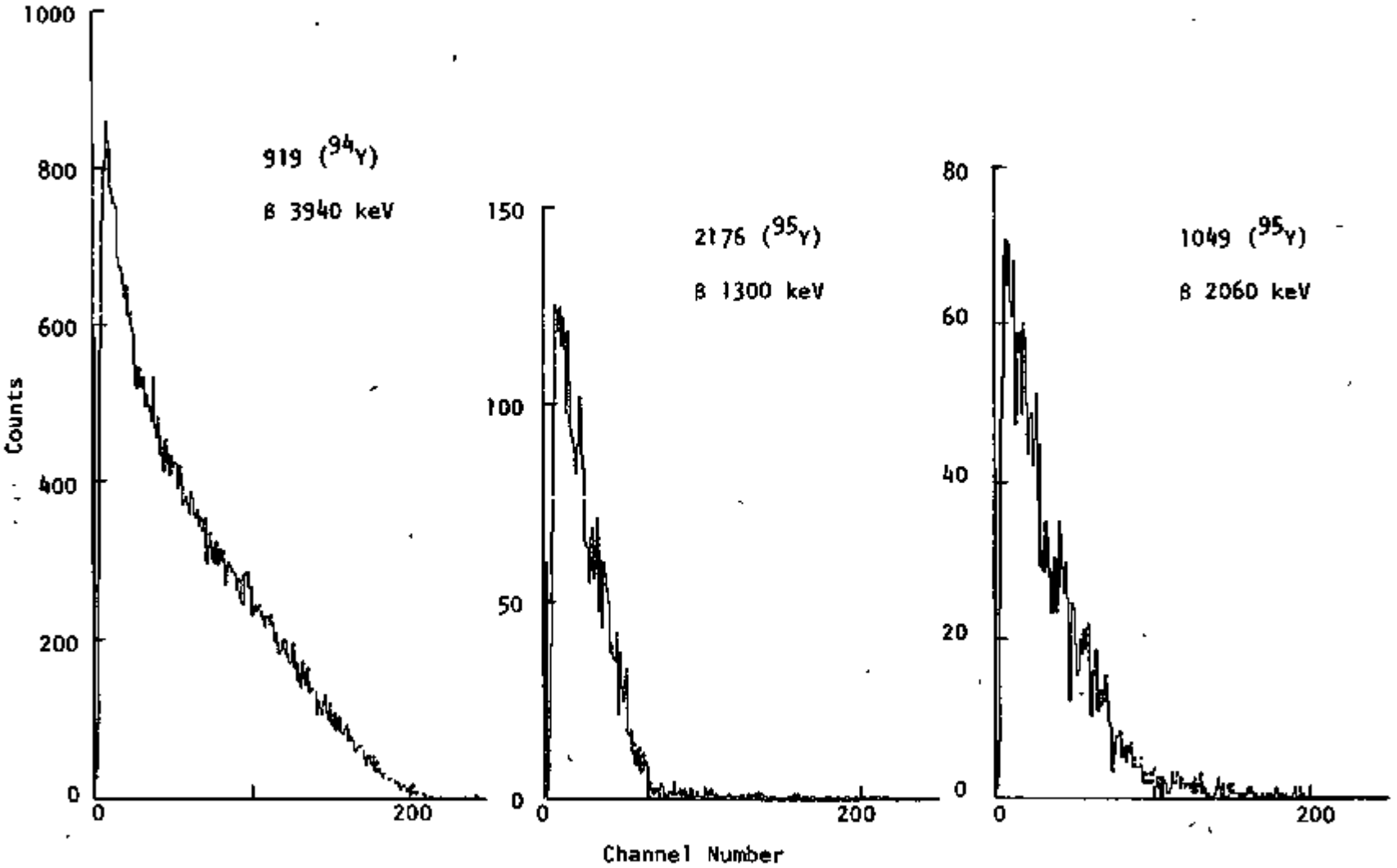

Fig. 85-4. Beta spectra from plastic scintillator coincident with selected ^{94,95}Y γ rays.

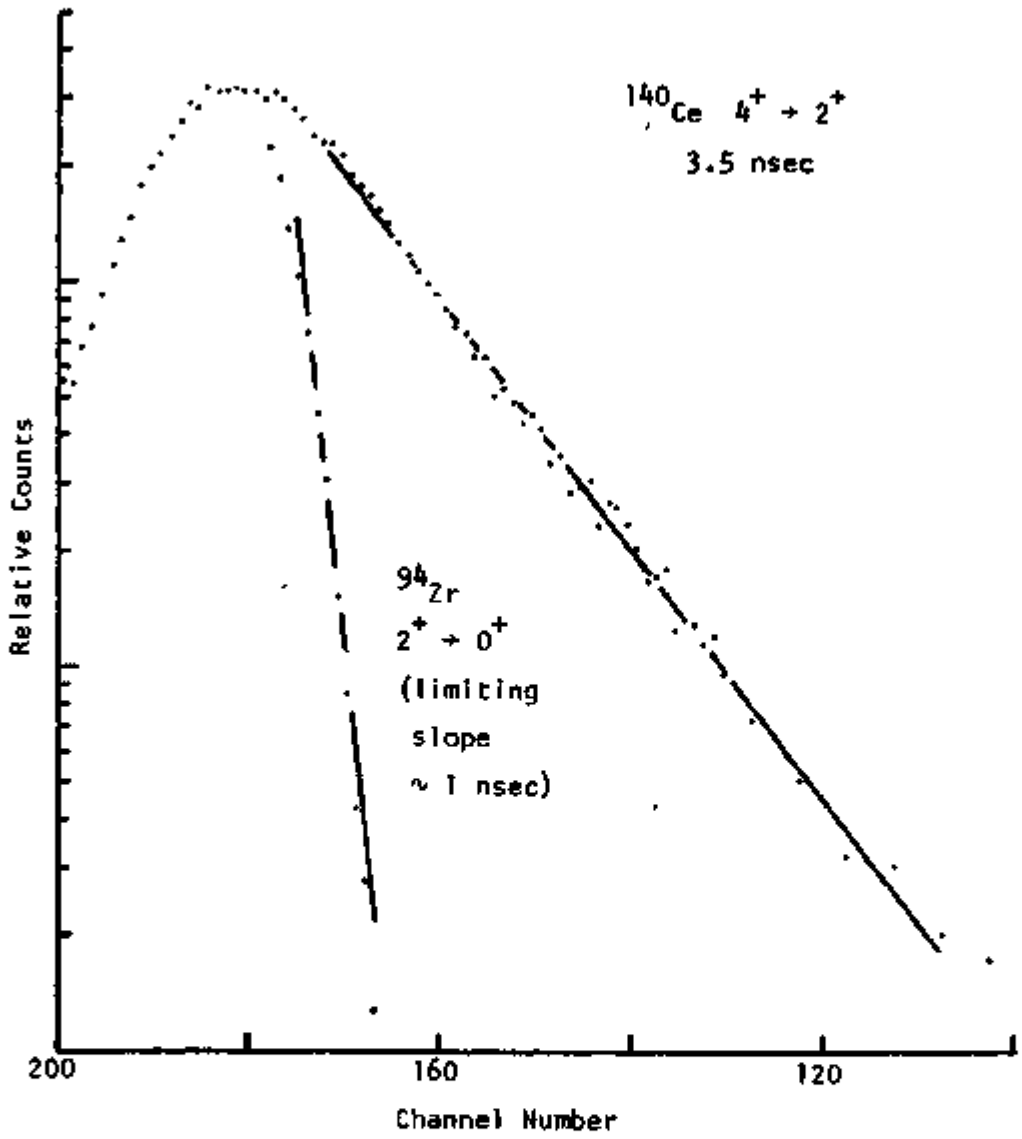

Fig. B5-5. $\beta\gamma(t)$ measurements. The ^{94}Zr data indicate the resolution of the Ge(Li) detector.

Data from the second ADC (Figs. B5-2 through B5-5) are stored in a region assigned to each gate. We have used this program in γ-γ coincidence measurements (high resolution Ge-Ge in Fig. B5-2, low resolution NaI-Ge in Fig. B5-3), γ-β coincidence (Fig. B5-4), and a search for delayed states (Fig. B5-5).

The major limitations imposed by these methods of acquisition are related to the relatively small size of available core and the necessity of using analog restrictions for any parameters other than the basic two. The core limitations will be eliminated when the high-speed magnetic tape is available for list-mode storage of data. Programs which include digital gates for monitoring an experiment and unrestricted list-mode acquisition have been written. Routing in one of the ADCs can be used to extend the usefulness of 2-parameter methods, but installation of the third and fourth ADCs will be required to obtain in-beam data at maximum efficiency.

B6. ^{18}O Target Preparation

L. Chua

An apparatus for the fabrication of ^{18}O targets in the form of NiO has been constructed (Fig. B6-1). The entire assembly is first evacuated using a roughing pump in conjunction with a liquid-nitrogen cold trap. A measured amount of ^{18}O gas is then introduced (usually 6 - 7 mm Hg), and the bell jar isolated from the rest of the system. The Ni foil, which has been sandwiched between two standard (2" x 2") target frames, is heated using a 500-watt projection lamp together with a focusing lens which defines the area to be oxidized (circular spot $\sim$ 1 cm in diameter). Oxidation of

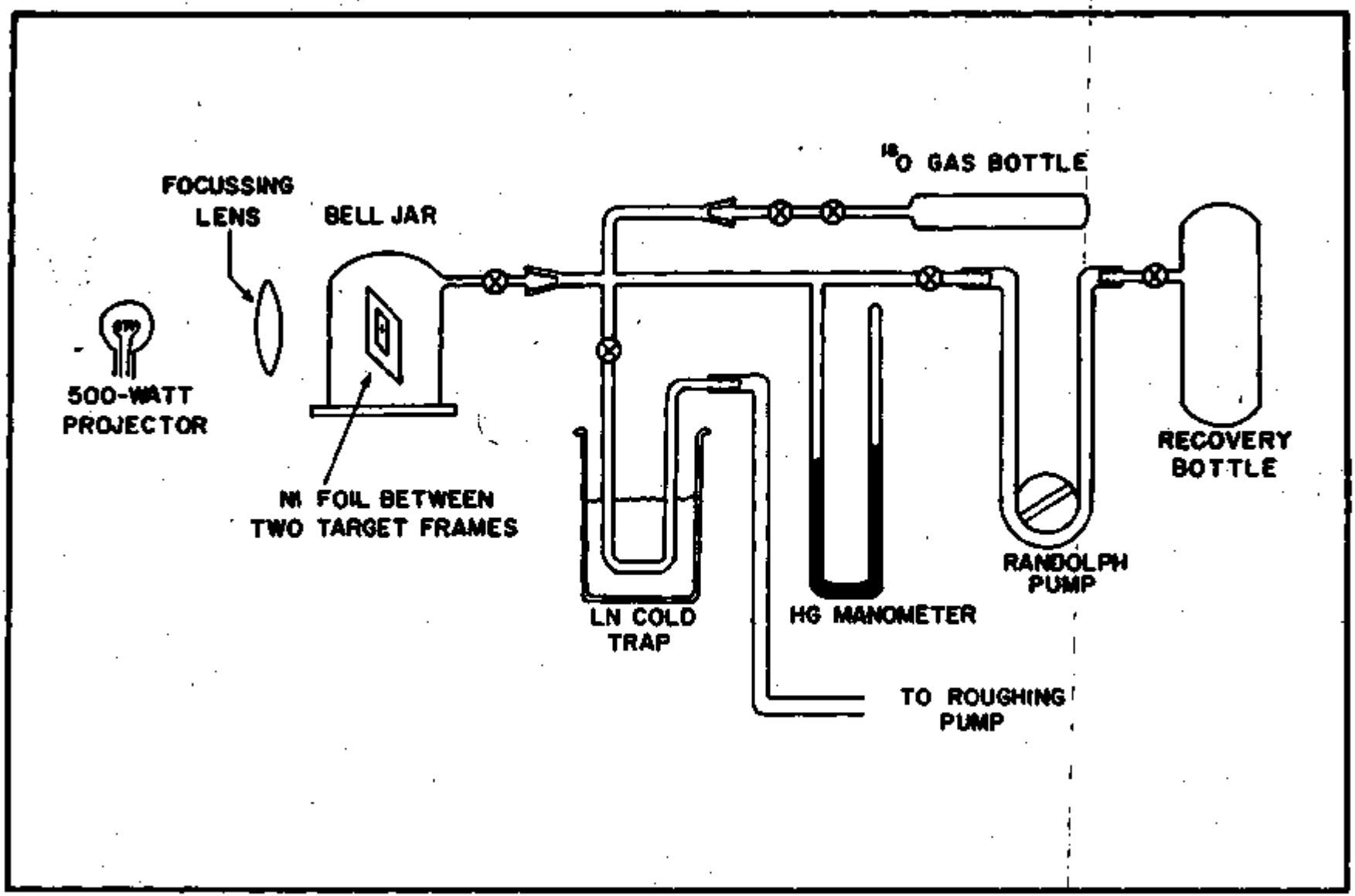
^{18}O GAS BOTTLE
FOCUSSING LENS
BELL JAR
500-WATT PROJECTOR
Ni FOIL BETWEEN TWO TARGET FRAMES
LN COLD TRAP
HG MANOMETER
RANDOLPH PUMP
RECOVERY BOTTLE
TO ROUGHING PUMP

Fig. 86-1.

Ni commences within seconds after heating; the circular spot can be moved over the surface of the foil to produce a NiO target of the desired size. This entire procedure takes from 10 - 15 minutes. The light intensity from the projection lamp must then be reduced gradually to prevent breakage of the target due to unequal thermal stresses on the Ni and the NiO. Ni foils of 1.13 mg/cm^2 and 450 µg/cm^2 have been used and ^{18}O target thicknesses of $\sim$ 100 µg/cm^2 obtained. A major fraction of the ^{18}O gas can be recovered using a Randolph (squeeze) pump. Additional experimentation is required to determine the ^{18}O target thickness dependence on gas pressure and on Ni foil thickness. This apparatus can, with minor modifications, be used to prepare targets by the method of "cracking".

C. FACILITIES IMPROVEMENTS

C1. Cyclotron Stability

Last year, results of an extensive program of orbit studies were reported. This program was undertaken to improve the beam quality from the cyclotron and was in part necessitated by the stringent conditions required for accurate neutron time-of-flight measurements. During the course of this year's operation, it became apparent that some unknown instabilities had developed and were adversely affecting the quality of beams used in the time-of-flight work. As a result a thorough investigation of the stability problem was undertaken. The theoretical considerations, the diagnostic techniques used, and the improvements made are described in a paper which has been accepted for publication (W. C. Parkinson, J. F. Petersen, R. H. Day, D. C. DuPlantis, W. S. Gray, and J. Bardwick; to be published in Nuclear Instruments and Methods).

C2. Development and Tests of a Heavy Ion Source

A cold-cathode Penning Ion gauge (PIG) source has been constructed and tested. The source consists of a water-cooled copper anode body, tantalum anode insert, water-cooled copper cathode holders and tungsten or tantalum cathodes. The source assembly is shown in Fig. C2-1.

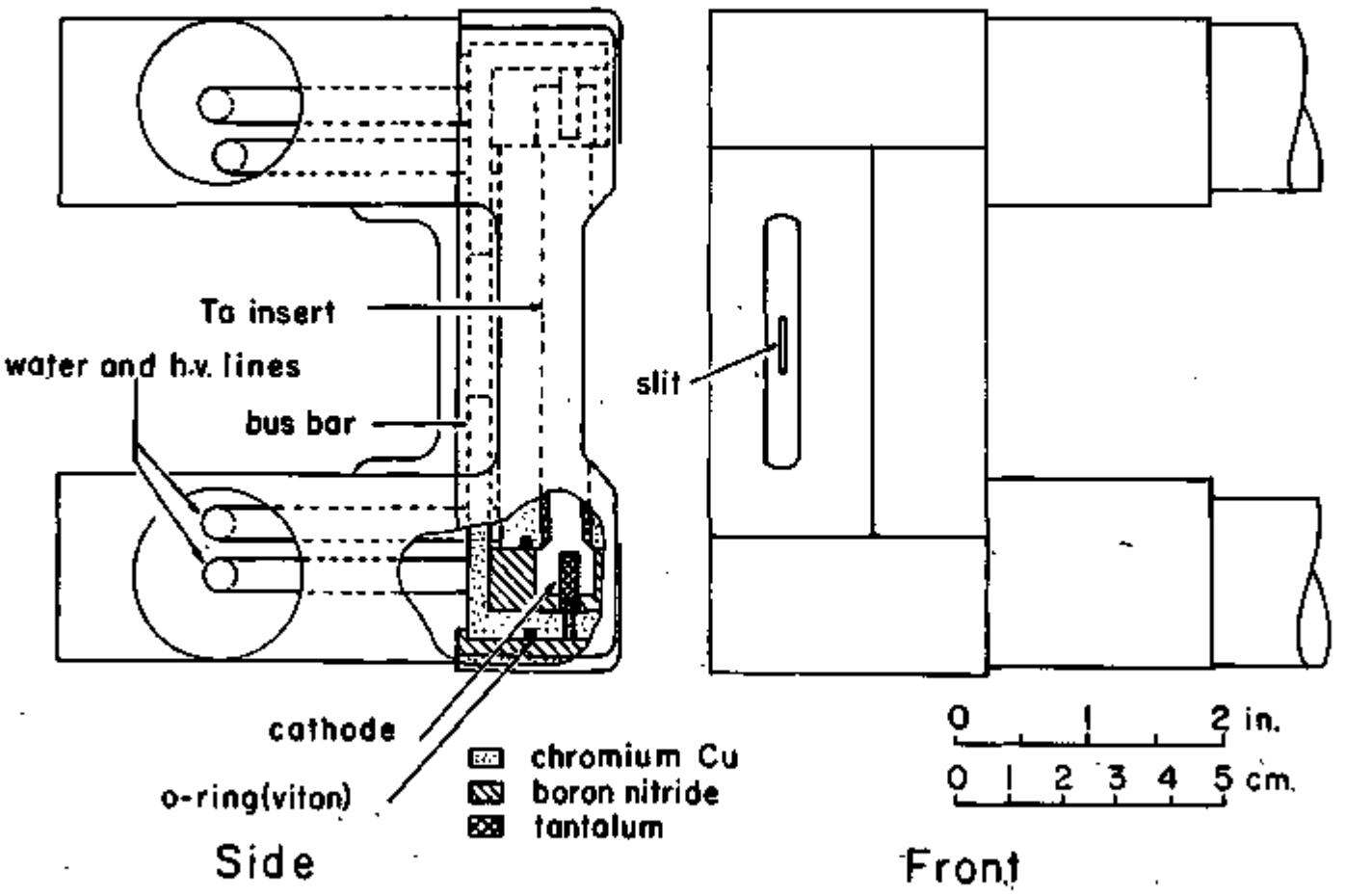
Ta insert
water and h.v. lines
bus bar
cathode
o-ring(viton)
chromium Cu
boron nitride
tantalum
Side
slit
0 1 2 in.
0 1 2 3 4 5 cm.
Front

Fig. C2-1.

Since heavy ion acceleration requires good cyclotron vacuum (to minimize charge exchange) the source is designed to eliminate possible water and gas leaks. All internal water connections are silver-soldered and the anode and cathode bodies are sealed with viton O-rings. The source has a high power capability (> 5 KW) and has provisions for pulsing and gating.

High voltage testing began in January. These tests indicated that the PVC insulator on the cathodes lines was unsuitable due to its tendency to carbonize after arcing. The PVC material has been replaced with Teflon and minimal arcing problems have occurred since. Various cathode-to-anode insulator materials have been tried, but only boron nitride appears to be suitable at high arc powers (> 1/2 KW).

After suitable modifications to the dummy dee, acceleration tests began in April. A very good quality 58 MeV α^{++} beam was soon accelerated and extracted, and testing with heavy ions began. The first heavy-ion beam accelerated and extracted was 80 MeV $^{12}C^{4+}$ (q/m = 1/3), which used an existing $^{3}He^{+}$ tune as an analogue. The q/m = 1/3 beam covers an energy range from 6 to 12 MeV/nucleon, e.g., 70 to 140 MeV $^{12}C^{4+}$. In addition q/m = 1/4 beams ($^{12}C^{3+}$ and $^{16}O^{4+}$) have been accelerated. These use α^{+} tunes as analogues. The q/m = 1/4 tune is extremely valuable in that a wide variety of heavy-ion beams may be accelerated on essentially the same tune by changing the rf frequency slightly. We have accelerated 22 MeV α^{+}, 66 MeV $^{12}C^{3+}$ and 88 MeV $^{16}O^{4+}$ using this procedure. The beam species was identified by scattering from a thin carbon foil and measuring the energy loss of the scattered beam in a gas proportional counter placed in the focal plane of the analyzing magnet. A composite energy loss spectrum is shown in Fig. C2-2, obtained by running He and CO_2 gases in the arc source and then varying the rf frequency

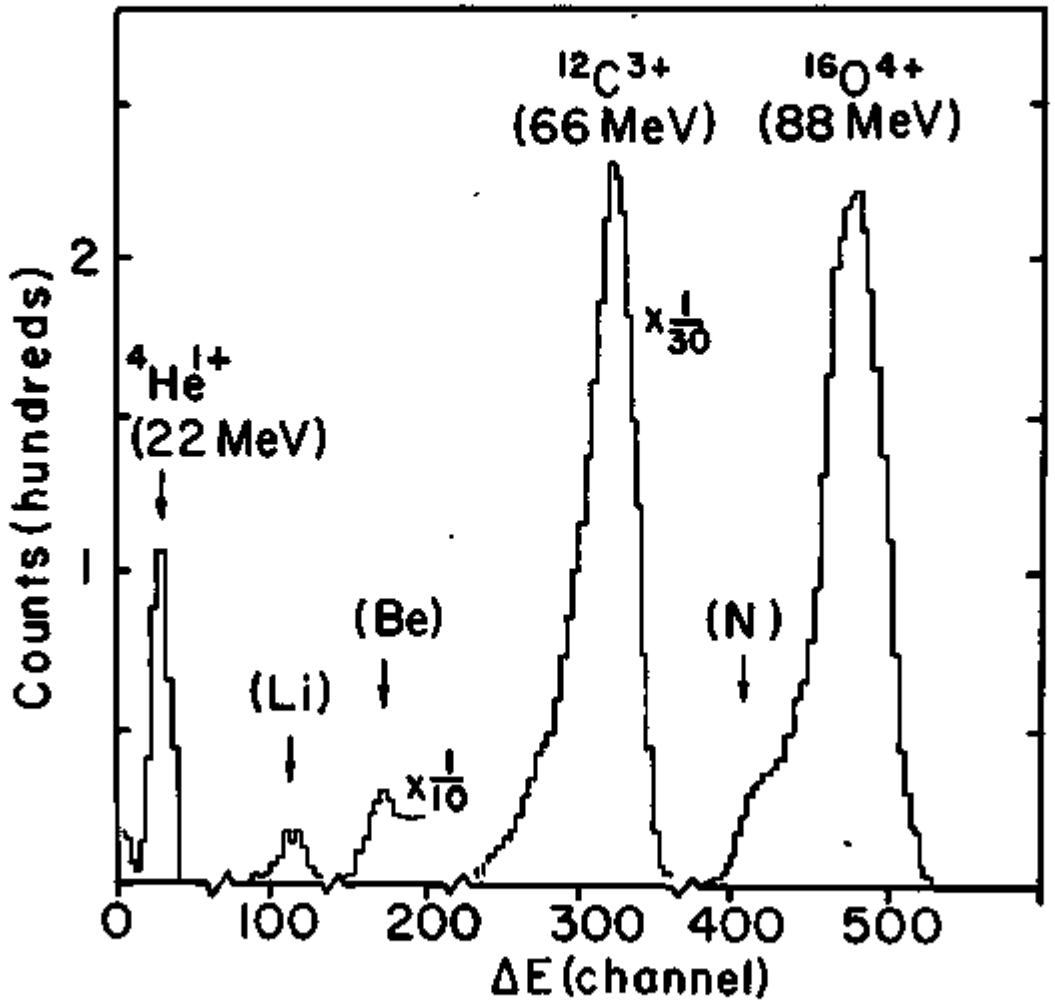
$^{12}C^{3+}$
(66 MeV)
$^{16}O^{4+}$
(88 MeV)
$^{4}He^{1+}$
(22 MeV)
(Li)
(Be)
(N)
$\times\frac{1}{30}$
$\times\frac{1}{10}$
Counts (hundreds)
2
1
0
100
200
300
400
500
ΔE (channel)

Fig. C2-2.

(on-resonance the beams are cleanly separated).

Although initial beam intensities have been modest (50 to 300 na internal, 5 to 100 na external), they will be usable for many experiments. Many parameters remained to be optimized, e.g., slit and puller geometry, etc. so beam intensity should be increased in the near future. An improved ion-source power supply is under construction.

The lifetime of the PIG source is limited when running heavy ions due to the build-up of sputtered metal on insulators, etc., which eventually flakes off and causes cathode-to-anode shorting. Recent modifications of the insulators and cathode holders should extend the source lifetime considerably. Meanwhile, testing with a variety of light and heavy ions continues, and experiments using heavy-ion beams are being initiated.

C3. Modifications to the Extractor System

New tungsten sparking plates have been added to the extraction system with the objective of increasing the maximum breakdown voltage and eliminating pitting of the ground sheets near the deflector due to arcing. Two assemblies, each consisting of four 0.031" thick tungsten sheets clamped to a water-cooled frame, are mounted on the ground sheets above and below the deflector bar. The gap between adjacent tungsten sheets is shielded from the electric field lines by pieces constructed from 3/4" x 1/4" Elkonite bar stock with the corners ground to a 1/8" radius.

In approximately two months of operation, no sign of pitting or permanent scarring of the tungsten or Elkonite surfaces has developed. In addition,

although the breakdown voltage depends upon the condition of the deflector bar, it appears that the maximum sustainable field-voltage product has been increased by approximately 20%, to 1.8×10^4 KV^2/cm.

C4. The Computer System

The cyclotron data acquisition system consists of a Digital Equipment Corporation PDP-15/30 computer with 24K of core memory interfaced with two Northern Scientific analog-to-digital converters. A card reader, storage display, and point plotter facilitate data manipulations in a background stream. A magnetic tape system and a disk cartridge were added this year to provide additional data storage.

The disk system, a CDC model 9425, provides 1.2M words (18 bits) of fixed disk and 1.2M words of removable disk storage. The disk permits faster data collection as well as the use of a disk-based software monitor for ease in programming.

The tape system, a Cipher model 100X, is a 9-track industry compatible magnetic tape transport operating at 45 ips. The tape provides a link to the campus computing center (IBM 360) and serves as a storage medium for multiparameter experiments.

Controllers that are DEC software compatible were furnished for both devices by Peripheral Interface Corporation of California.

An interface for multiparameter experiments has been completed at the laboratory and is presently being debugged. Initially it will provide 4-parameter operation with provisions for future expansion.

D. PERSONNEL

Faculty

J. Bardwick III
(on leave 7/1/73-6/30/74)

F. D. Becchetti
(Appt. Fall 1973)

W. S. Gray

J. W. Janecke

W. C. Parkinson
(on leave 1/1/74-5/31/74)

R. Polichar
(Term. Spring 1974)

R. S. Tickle

H. C. Griffin (Nuclear Chemistry)

A. C. T. Wu
(7/1/73 - 8/31/73)

Research Scholars

L. T. Chua (Appt. 1/1/74)

A. S. Broad (Appt. 12/1/73, Term. 1/31/74)

J. Petersen (Appt. 2/27/74)

Student Assistants

Advanced Graduate

A. S. Broad (Term. 11/30/73)
(see Research Scholars)

R. H. Day (Term. 2/28/74)

M. A. Firestone

D. A. Lewis

F. L. Milder

J. F. Petersen (Term. 2/22/74)
(see Research Scholars)

J. A. Splett

E. R. Sugarbaker (Appt. 1/1/73)

A. M. VanderMolen

K. L. Hull (Nuclear Chemistry--
no financial support)

Graduate

D. P. Duston (Term. 12/31/73)

W. A. Filter (Appt. 5/1/74)

D. J. Overway

Undergraduate and Hourly Assistants

A. H. Bennish (Term. 3/1/74)
P. T. Kolen (Term. 8/31/73)
W. A. Manwaring
M. D. Shane (Appt. 1/15/74)
J. R. Wilson (Appt. 1/8/74)

Engineers

D. DuPlantis - Cyclotron
A. V. Smith - Design

Electronic Technician

J. L. Ferguson

Cyclotron Operations

W. E. Downer - Supervisor
J. A. Koenig - Chief Cyclotron Operator

Instrument Makers

M. W. Prince
D. M. Schleede

Scanners

P. J. Conger (Appt. 9/17/73, Term. 11/30/73)
M. Eaton (Appt. 7/2/73)
N. Hidayet (Term. 7/2/73)
F. Hilberer (Term. 7/2/73)
K. Marcus (Appt. 5/7/74)
C. Pinard (Appt. 8/6/73
J. Rowe (Appt. 5/29/73, Term. 6/18/73)
D. Smith (Appt. 7/31/73, Term. 8/10/73)

Secretary

M. Lammers
G. Petersen (Appt. 2/27/73, Term. 3/25/73)

E. PUBLICATIONS

Abstracts

1. "The Reaction $^{88}Sr(^{3}He,n)^{90}Zr$ by Time of Flight", R. H. Day, J. F. Petersen, and W. C. Parkinson, Bull. Am. Phys. Soc. 18, 1396 (1973).
2. "The Two-Proton Transfer Reaction $^{40}Ar(^{3}He,n)^{42}Ca$", J. F. Petersen, R. H. Day, and W. C. Parkinson, Bull. Am. Phys. Soc. 18, 1396 (1973).
3. "Search for 2.3 Min ^{96}Y", K. Rengan (Eastern Michigan University) and H. C. Griffin, Bull. Am. Phys. Soc. 18, 1417 (1973).
4. "Structure of ^{165}Ho via the $^{164}Dy(^{3}He,d)^{165}Ho$ Reaction", D. A. Lewis, A. S. Broad, and W. S. Gray, Bull. Am. Phys. Soc. 19, 103 (1974).
5. "Coupled Channels Reaction and Form Factor Effects in the $^{162}Dy(^{3}He,d)^{163}Ho$ Reaction at 46.5 MeV", A. S. Broad and W. S. Gray with P. J. Ellis and A. Dudek Ellis (University of Oxford), Bull. Am. Phys. Soc. 19, 104 (1974).
6. "Coupled Channels Analysis of the $^{16}O(d,^{3}He)^{15}N$ Reaction", M. A. Firestone J. Janecke, with A. Dudek Ellis, P. J. Ellis (University of Minnesota) and T. Engeland (University of Oslo), Bull. Am. Phys. Soc. 19, 454 (1974).
7. "Transitions in ^{94}Zr and ^{95}Zr Following the Decay of Y Parents", H. C. Griffin and K. Rengan (Eastern Michigan University), Bull. Am. Phys. Soc. 19, 473 (1974).

Publications

*8. "Studies of ^{205}Bi and ^{207}Bi by Proton-Transfer Reactions", Karl A. Erb and Walter S. Gray, Phys. Rev. C8, 347 (1973).

*9. "A Gated Ion-Source for Time-of-Flight Spectroscopy", R. H. Day and W. C. Parkinson, Nucl. Inst. & Meth. 111, 199 (1973).

*10. "Structure of Alisauakas-Jucys Form of the 9j Coefficients", A. C. T. Wu, Journal of Math. Phys. 14, 1222 (1973).

11. "Generalized Euler-Pochhammer Integral Representation for Single-loop Feynman Amplitudes", Alfred C. T. Wu, Phys. Rev. D9, 370 (1974).

12. "Classical SU(3) Gauge Field Equations", Alfred C. T. Wu and Tai Tsun Wu (Harvard University), Journal Math. Phys. 15, 53 (1974).

13. "Nuclidic Mass Relationships and Mass Equations", J. Janecke and H. Behrens, Proceedings International Conference on Nuclear Physics, Vol. 1, 1973, edited by J. deBoer and H. J. Mang, North-Holland Publ. Co., p. 321.

In Press

14. "Nuclidic Mass Relationships and Mass Equations", J. Janecke and H. Behrens, Phys. Rev. C, in press.

15. "The $^{40}Ar(^{3}He,n)^{42}Ca$ Reaction", J. F. Petersen and W. C. Parkinson, Physics Letters B, in press.

16. "The University of Michigan Neutron Time-of-Flight Facility", W. C. Parkinson, J. F. Petersen, R. H. Day, R. M. Polichar, P. F. Julien, and D. C. DuPlantis, Nucl. Inst. & Meth., in press.

17. "On the Optimization of the Capacitive Beam Pick-off", W. C. Parkinson, J. F. Petersen, and D. C. DuPlantis, Nucl. Inst. & Meth., in press.

18. "The University of Michigan Cyclotron Facility for Research in Nuclear Structure", W. C. Parkinson, J. F. Petersen, R. H. Day, D. C. DuPlantis, W. S. Gray, and John Bardwick, Nucl. Inst. & Meth., in press.

19. "Pair Excitation in ^{90}Zr", R. H. Day and W. C. Parkinson, Physical Review C Communication, in press.

Theses

20. "A Large Scintillation Detector System for Fast Neutron Time of Flight", Paul Frederick Julien, 1973.

21. "Coupled Channels Reaction and Form Factor Effects in Direct Reactions on Strongly Deformed Nuclei", Alan Steven Broad, 1974.

22. "Neutron Time-of-Flight Spectroscopy and the Reaction $^{88}Sr(^{3}He,n)^{90}Zr$", Robert Harlow Day, 1974.

23. "Development of a Time-of-Flight Spectrometer and its Application to the Reaction $^{40}Ar(^{3}He,n)^{42}Ca$", Jay Franklin Petersen, 1974.